UNIVERSITEIT VAN PRETORIA
UNIVERSITY OF PRETORIA
YUNIBESITHI YA PRETORIA

DEVELOPING PET INFECTION IMAGING AGENT FOR VISUALIZING BACTERIAL PEPTIDOGLYCAN ASSEMBLY

PALESA CAROLINE KOATALE

DISSERTATION SUBMITTED FOR THE DEGREE
OF
DOCTOR OF PHILOSOPHY

IN MEDICAL NUCLEAR SCIENCE
FACULTY OF HEALTH SCIENCES
UNIVERSITY OF PRETORIA

SUPERVISOR: PROF. THOMAS EBENHAN
CO-SUPERVISORS: PROF. MIKE MACHABA SATHEKGE
DR AMANDA HENRIETTA MDLOPHANE

JANUARY 2025

THIS DISSERTATION IS PRESENTED IN A PUBLICATION FORMAT

DECLARATION

I, Palesa Caroline Koatale, hereby declare that the dissertation "**Developing PET Infection Imaging Agent for Visualizing Bacterial Peptidoglycan Assembly**" which I hereby submit for the degree of Doctor of Philosophy in Medical Nuclear Science at the University of Pretoria, is my work and has not previously been submitted by me for a degree at this or any other tertiary institution.

ETHICS STATEMENT

The author, whose name appears on the title page of this dissertation, has obtained the applicable research ethics approval (435/2020) for the research described in this work.

The author declares that s/he has observed the ethical standards required in terms of the University of Pretoria's Code of Ethics for Researchers and the Policy guidelines for responsible research.

Student name: Palesa Caroline Koatale

September 2024

DEDICATION

This thesis is dedicated to the memory of my grandparents, Mr Tsie Thomas Koatale, Mrs Mokopi Susan Koatale, Mrs Masennye Rebecca Mogamisi and aunt, Ms Matselane Florence Koatale. Though you are no longer here, your love and wisdom guided me through childhood until adulthood. This accomplishment reflects your sacrifices and unwavering love.

ACKNOWLEDGEMENTS

The success of this project reflects the inspiration, contribution and support I received from my supervisors, mentors, collaborators, colleagues, family, and friends; some of whom are not mentioned by name. I will forever remain grateful and blessed to have every one of you be part of this journey of my life.

Firstly, to my supervisors, Prof Thomas Ebenhan and Prof Mike Sathekge, thank you for allowing me to pursue my PhD in Nuclear Medicine Science and providing valuable guidance, feedback and mentorship throughout the project. Most importantly, I extend my gratitude for all the contributions made towards my personal and professional development.

The project presented many challenges and at some point, it was worth giving up. An immense gratitude to Prof Frederik Cleeren and Prof Mick M. Welling for coming on board and providing your time, expertise, guidance, and support from inception to the end of the project.

Science can only be possible through collaborations with different experts and departments. The success of this project will not be achievable without eternal collaboration. Thank you to Dr Chrisna Durandt, Prof Marleen Kock Prof Iman van den Bout, Prof Duncan Cromarty, Mr Thato Sello and Dr Johan Steyl, for supporting the project by providing equipment, training and valuable expertise.

Mentors are spearheads of every board and I remain grateful to have Dr Ambrose Okem, Dr John Takyi-Williams, Dr Honest Ndlovu, Dr Amanda Mdlophane and Dr Mankgopo Kgatle as mentors. Your wisdom, experience, and friendship gave me strength during difficult times.

To my longstanding friend, Mrs Johncy Mahapane, thank you for your endless support and for seeing me through the hardest seasons. I remain inspired by your strength and courage.

To the staff of Nuclear Medicine Research Infrastructure (NuMeRI) thank you for your endless support, and contribution and for creating a fun working environment.

Lastly, to my family, Mrs Selobelwang, Mr Tebogo and Mr Molebatsi Koatale, you remain the biggest support system. Thank you for always believing and supporting me. Your love motivates me to become the best version of myself and I remain forever grateful for every milestone we celebrated together.

"No eye has seen, no ear has heard, and no mind has imagined what God has prepared for those who love him." **1 Corinthians 2:9**

ABSTRACT

Diagnosis of bacterial infections remains a serious medical challenge making them one of the main causes of mortality and morbidity worldwide. A nuclear imaging modality such as Positron Emission Tomography – Computed Tomography (PET/CT) scanning has been considered one of the better diagnostic alternatives due to its ability to assess anatomical and physiological abnormalities in real-time. Despite excellent pre-clinical studies, specific radiotracers capable of discriminating infection from sterile inflammation or detecting infective foci, especially in the early phases or in deeply seated tissue are lacking in clinical practice. For this reason, the uniqueness of the peptidoglycan cell wall presents an attractive target to improve the specificity and selectivity of PET radiotracers with the potential to identify the causative pathogen (gram-negative vs gram-positive). Many studies have demonstrated the inventiveness of peptidoglycan targeting and imaging using amino acids and glycan core-based radiotracers, however, their prospects in clinical settings are still under development.

As part of the study objectives, diagnostic accuracy, and clinical impact of currently available peptidoglycan-based radiotracers for imaging of bacterial infections were evaluated using QUADAS. The findings revealed that most radiotracers demonstrated high non-target background signals, which might limit their specificity and sensitivity for diagnostic imaging of bacterial infections. Therefore, this warrants further research and development of target-specific radiotracers for infection imaging.

The AeK tripeptide is considered an essential building block of peptidoglycan required by bacteria to proliferate as previously shown by fluorescence imaging *in vitro* using AeK-NBD. In this study, we developed AeK tripeptide radiotracer by replacing the fluorescent tag (NBD) with DOTA chelator to warrant ^{68}Ga-complexation without altering the peptide chain. Given the structural similarity to Aek tripeptide, bacterial uptake of [^{68}Ga]Ga-DOTA-AeK was investigated *in vitro* and *in vivo* for potential infection imaging using PET/CT. An easy-to-implement radiolabeling procedure and SPE purification method were successfully developed for [^{68}Ga]Ga-DOTA-AeK with RCP≥95 %. The radiotracer showed proteolytic stability with limited protein binding. Unlike AeK-NBD, [^{68}Ga]Ga-DOTA-AeK was not successfully taken up by both *E .coli* (gram-negative) and *S.aureus* (gram-positive) bacteria *in vitro* and *in vivo*, ultimately hindering metabolic integration into the peptidoglycan cell wall. Interestingly, the biodistribution data

further revealed inflammatory localization of radiotracer, however, whether this may or may not limit the specificity of AeK tripeptide as a potential radiotracer, needs further investigation.

Based on these findings, it was concluded that the addition of the DOTA hindered the active intracellular transportation of [^{68}Ga]Ga-DOTA-AeK necessary for ultimate metabolic processing and integration into the peptidoglycan. Therefore, alternative radiolabeling strategies without the need for radioisotope chelation, eg. ^{11}C and ^{18}F are recommended to maintain the targeting moiety of AeK tripeptide.

Keywords: Bacteria; infection; peptidoglycan; imaging; precursor; targeting; radioactive; fluorescence; PET/CT; preclinical; tripeptide

TABLE OF CONTENTS

LIST OF TABLES

LIST OF FIGURES

CHAPTER 1GENERAL INTRODUCTION

1.1 BACKGROUND

Bacterial infections continue to pose the greatest threat to the human population today. This is primarily due to the emergence of antibiotic resistance, which has continued to be a global health challenge [1, 2]. It is worth noting that by the year 2050, antibiotic resistance is estimated to be among the leading causes of death, surpassing cancer, resulting in approximately 10 million deaths annually [3]. Consequently, there is an urgent need to prioritize efforts to preserve antibiotics' effectiveness. Achieving this goal necessitates swift action, including the prompt localization and identification of the bacterial pathogen at an early stage is of great importance. Advancements in diagnostic accuracy are crucial in this regard [4]. Microbiological cultures and polymerase chain reaction (PCR) are routine diagnostic tools for detecting infections. However, these methods often face challenges in obtaining clinical samples, especially in the case of deeply localized infections [5]. Furthermore, culturing pathogens is time-consuming, leading to delays in treatment, especially when dealing with pathogens that are difficult to cultivate [6, 7].

1.2 TRENDS IN MOLECULAR IMAGING OF INFECTION

Alternatively, magnetic resonance imaging (MRI) or computed tomography (CT) offer non-invasive methods for the diagnosis of infection, particularly in musculoskeletal infections. However, these imaging techniques primarily detect anatomical abnormalities and may not always reveal the presence of an infection [5, 6]. Moreover, when it comes to early detection of infection, morphologic imaging using ultrasound (US), CT and MRI are not well-suited as these modalities primarily identify tissue architectural distortion that often occurs at an advanced stage of infection [8]. To address the limitations mentioned above, nuclear medicine imaging scans such as positron emission tomography (PET) and single-photon emission computed tomography (SPECT) have been considered promising alternatives, because they can assess early infection-related physiological abnormalities [8, 9]. In hybrid imaging of infection, SPECT and PET are combined with the morphological information afforded by the anatomic imaging with CT or MRI for improved specificity [10-12]. The most recently added imaging modality is the advanced ultrafast large axial field of view (LAFOV)PET/CT, guaranteed to provide high

sensitivity at low radiation doses [13]. Several PET/SPECT radionuclides with different physical and chemical properties including half-life, energies and emission types are available for complexation with a wide range of molecules including peptides, antibiotics, antibodies, aptamers, and glucose [14] (**Table 1-1)**.

Table 1- 1: Properties of commonly used SPECT & PET radioisotopes [15-17].

Isotope	**physical half-life ($t_{1/2}$) (h)**	**Decay mode**	**Decay Energy (MeV)**	**Production**	**Radiolabeling strategy**
^{68}Ga	1.1	β−, EC, γ	1.899	Generator	Chelation
^{64}Cu	12.7	EC, β+	0.653	Cyclotron,	Chelation
^{18}F	1.8	β+, EC	0.634	Cyclotron,	Direct
^{123}I	13.2	γ, EC	0.159	Cyclotron,	Direct
^{11}C	0.3	β+	0.960	Cyclotron,	Direct
^{111}In	67.2	γ, EC	0.245	Cyclotron,	Chelation
^{99m}Tc	6.0	γ	0.141	Generator	Chelation/Direct

EC= Electron capture

1.3 PRIORITIZING RADIOTRACERS SPECIFICITY

PET/CT and SPECT imaging techniques rely on diagnostic radiotracers, with the most commonly used infection imaging agents being radiolabeled white blood cells, [$^{67/68}$Ga]citrate, [^{111}In]oxine/[^{99m}Tc]-hexamethylproplyleneamine oxime (HMPAO), and 2-deoxy-2-[^{18}F]-fluoro-D-glucose ([^{18}F]FDG). However, despite their wide application in infection imaging, these radiotracers have limitations in differentiating infection from inflammation, which can lead to ambiguity in diagnosis [12, 18, 19].

The lack of specificity in these radiotracers indicates that there is still an unmet need in clinically differentiating inflammation from infection. This limitation restricts the diagnostic potential that nuclear imaging tools can provide for effectively diagnosing infection [20]. Nuclear medicine imaging technology is rapidly advancing, and improving the selectivity of bacteria-specific radiotracers will revolutionize how infections are diagnosed and treated in clinical settings [20, 21]. The ability to detect infections early offers numerous advantages, including patient-tailored antibiotic treatment, treatment response evaluation, and non-responder identification. These capabilities are challenging but crucial in tackling anti-bacterial resistance [19]. To realize these possibilities, efforts have been undertaken to improve imaging specificity by developing radiotracers that target bacteria-specific biological structures and biochemical processes unique to bacteria. Some examples of these radiotracers are [^{18}F]-fluorodeoxysorbitol for carbohydrate metabolism, [^{68}Ga]Ga-triacetylfusarinine C for iron transportation, and 1-(2-deoxy-2-fluoro-β-d-arabinofuranosyl)-5-[^{125}I]-iodouracil for nucleic acids [8, 22-24]. Another promising radiotracer is the ^{99m}Tc- or ^{68}Ga-labeled ubiquicidin fragment UBI$_{(29–41)}$ which binds to negatively charged bacterial cell membranes and has shown specificity and effectiveness in clinical applications [25].

1.4 PEPTIDOGLYCAN: TARGET OF CHOICE FOR INFECTION IMAGING

Over the years, the bacterial cell wall's distinctive structure has garnered significant interest, as it is absent in mammalian cells. The bacterial cell wall plays a role in the virulence and invasiveness of different bacterial strains [26]. The gram-negative bacterial cell wall consists of a thinner sheet of peptidoglycan meshed in the middle of the cytoplasmic and an outer membrane compared to gram-positive bacteria. This includes the attachment of lipopolysaccharides and lipoproteins to the outer membrane. On the other hand, in gram-positive bacteria, the cell wall consists of a thicker envelope of peptidoglycan harboring teichoic acids and lipoteichoic acids [27-30] (**Figure 1**). Therefore, the uniqueness of the bacterial cell wall offers several potential targets that can be used to improve the specificity and selectivity of SPECT and PET radiotracers. For example, antibiotic-based radiotracers such as [^{99m}Tc]vancomycin inhibiting the peptidoglycan biosynthesis has been studied for the selective imaging of gram-positive bacteria. However, the issues of high background activity and low sensitivity have hampered successful translation into the clinical management of infections [31].

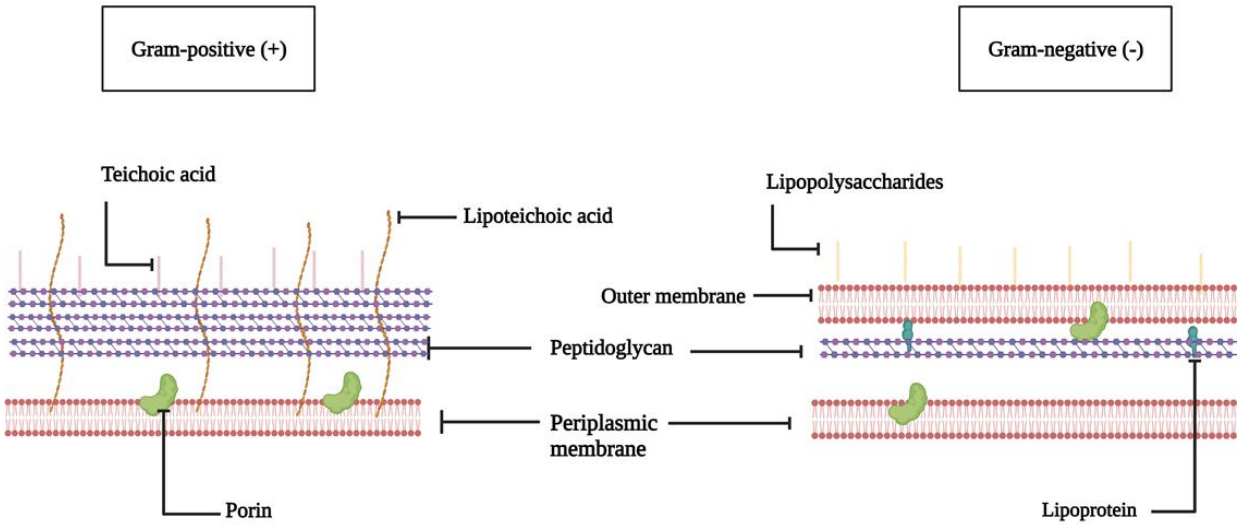

Figure 1- 1: Structural architecture of gram-positive and gram-negative bacteria. Adapted with permission from Auer et al. [28] . Copyright © 2017, American Chemical Society. Created with BioRender.com.

1.5 PROJECT OBJECTIVES AND OVERVIEW OF THE THESIS

The many possibilities of peptidoglycan biosynthesis targeting for bacteria-specific imaging have been vastly demonstrated with fluorescence-based peptidoglycan precursors with recent advancement in development approaches outlined in exceptionally detailed reviews [32-35]. These reviews introduce peptidoglycan precursors as a new target of molecular imaging probes for the bacterial cell wall. **Chapter 2** presents a summary of radiolabeled peptidoglycan precursors developed for SPECT and PET imaging with examples from fluorescent-based probes to highlight unexplored peptidoglycan biochemical processes with potential for specific targeting.

The potential of current radiotracers developed to image peptidoglycan processes in bacteria needs to be systematically reviewed. **Chapter 3** is presented to validate the findings of the selected independent research studies summarized in **Chapter 2** in a non-biased, and analytical way. A qualitative systematic analysis was conducted to assess and generalise the findings of the selected independent studies for diagnostic accuracy of peptidoglycan targeting radiotracers in bacterial infection imaging.

Research question: Can a qualitative analysis provide the required results to justify the clinical performance and usefulness of radiolabeled peptidoglycan precursors in molecular imaging of bacteria-related infections?

From the previous studies highlighted in **Chapters 2-3,** it is evident that bacteria can metabolically incorporate and re-use exogenous peptidoglycan precursors including amino acids, dipeptides, oligopeptides and amino sugars for peptidoglycan biosynthesis allowing possible imaging and localization of bacterial infections. Of particular interest, L-alanyl-D-glutamyl-L-lysine (Aek) tripeptide tagged with the fluorescent nitro-2,1,3-benzoxadiazol-4-yl (AeK–NBD) was successfully taken up by bacteria and incorporated into the existing peptidoglycan layer. In **Chapter4,** as proof of concept we developed a new Aek tripeptide compound conjugated to DOTA chelator to allow complexation with ^{68}Ga isotope for bacterial infection imaging using PET/CT. A manual radiolabeling procedure and purification of [^{68}Ga]Ga-DOTA-AeK was successfully developed and the physiochemical properties including stability and protein binding were established under physiological conditions. The bacterial uptake studies of [^{68}Ga]Ga-DOTA-AeK and its fluorescent analog were performed with gram-negative *(E .coli)* and gram-positive (*S. aureus)* bacterial strains. PET/CT studies and *ex vivo* biodistribution studies of intramuscular dual-animal model of infection and inflammation were performed to evaluate the pharmacokinetics and specificity of the [^{68}Ga]Ga-DOTA-AeK.

Finally, the overall discussion of this dissertation and the future directions of the research project are discussed in **Chapter 5**.

1.6 REFERENCES

1. Jernigan JA, Hatfield KM, Wolford H, Nelson RE, Olubajo B, Reddy SC, McCarthy N, Paul P, McDonald LC, Kallen A, Fiore A, Craig M, Baggs J. Multidrug-Resistant Bacterial Infections in U.S. Hospitalized Patients, 2012–2017. New England Journal of Medicine. 2020;382(14):1309-19.

2. Rao KU, Henderson DI, Krishnan N, Puthia M, Glegola-Madejska I, Brive L, Bjarnemark F, Millqvist Fureby A, Hjort K, Andersson DI, Tenland E, Sturegård E, Robertson BD, Godaly G. A broad spectrum anti-bacterial peptide with an adjunct potential for tuberculosis chemotherapy. Scientific Reports. 2021;11(1):4201.

3. O'neill J. Antimicrobial resistance: tackling a crisis for the health and wealth of nations. The Review on Antimicrobial Resistance. London2014. p. 1-20.

4. O'Neill J. Review on antimicrobial resistance: tackling drug-resistant infections globally: final report and recommendations. 2016. p. 1-20.

5. Jain SK. The promise of molecular imaging in the study and treatment of infectious diseases. Mol Imaging Biol. 2017;19(3):341-7.

6. Rak M, Barlič-Maganja D, Kavčič M, Trebše R, Cőr A. Comparison of molecular and culture method in diagnosis of prosthetic joint infection. FEMS Microbiol Lett. 2013;343(1):42-8.

7. Pongsachareonnont P, Honglertnapakul W, Chatsuwan T. Comparison of methods for identifying causative bacterial microorganisms in presumed acute endophthalmitis: conventional culture, blood culture, and PCR. BMC Infectious Diseases. 2017;17(1):165.

8. Polvoy I, Flavell RR, Rosenberg OS, Ohliger MA, Wilson DM. Nuclear Imaging of Bacterial Infection: The State of the Art and Future Directions. Journal of Nuclear Medicine. 2020;61(12):1708-16.

9. Becker W, Meller J. The role of nuclear medicine in infection and inflammation. The Lancet infectious diseases. 2001;1(5):326-33.

10. Cuocolo A, Petretta M. PET and SPECT Specialty Grand Challenge. When Knowledge Travels at the Speed of Light, Photons Take to the Field. Frontiers in Nuclear Medicine. 2021;1.

11. Alqahtani FF. SPECT/CT and PET/CT, related radiopharmaceuticals, and areas of application and comparison. Saudi Pharmaceutical Journal. 2023;31(2):312-28.

12. van der Bruggen W, Bleeker-Rovers CP, Boerman OC, Gotthardt M, Oyen WJG. PET and SPECT in Osteomyelitis and Prosthetic Bone and Joint Infections: A Systematic Review. Semin Nucl Med. 2010;40(1):3-15.

13. Glaudemans AWJM, Gheysens O. Expert opinions in nuclear medicine: Finding the “holy grail” in infection imaging. Frontiers in Medicine. 2023;10.

14. Crișan G, Moldovean-Cioroianu NS, Timaru DG, Andrieș G, Căinap C, Chiș V. Radiopharmaceuticals for PET and SPECT Imaging: A Literature Review over the Last Decade. International Journal of Molecular Sciences. 2022;23(9).

15. Liu D, Xia Q, Ding D, Tan W. Radiolabeling of functional oligonucleotides for molecular imaging. Frontiers in Bioengineering and Biotechnology. 2022;10.

16. Northrup JD, Mach RH, Sellmyer MA. Radiochemical Approaches to Imaging Bacterial Infections: Intracellular versus Extracellular Targets. Int J Mol Sci. 2019;20(22).

17. Fani M, Maecke HR. Radiopharmaceutical development of radiolabelled peptides. Eur J Nucl Med Mol Imaging. 2012;39(1):11-30.

18. Pimlott SL, Sutherland A. Molecular tracers for the PET and SPECT imaging of disease. Chemical Society Reviews. 2011;40(1):149-62.

19. Jiemy WF, Heeringa P, Kamps JAAM, van der Laken CJ, Slart RHJA, Brouwer E. Positron emission tomography (PET) and single photon emission computed tomography (SPECT) imaging of macrophages in large vessel vasculitis: Current status and future prospects. Autoimmunity Reviews. 2018;17(7):715-26.

20. Ferro-Flores G, Ocampo-Garcia BE, Melendez-Alafort L. Development of specific radiopharmaceuticals for infection imaging by targeting infectious micro-organisms. Curr Pharm Des. 2012;18(8):1098-106.

21. Fazli A, Salouti M. Targeting molecular imaging approach for detection of infection and inflammation by diagnostic nuclear medicine techniques. Current Medical Imaging. 2014;10(3):215-33.

22. Kleynhans J, Sathekge MM, Ebenhan T. Preclinical Research Highlighting Contemporary Targeting Mechanisms of Radiolabelled Compounds for PET Based Infection Imaging. Semin Nucl Med. 2023.

23. Welling MM, Hensbergen AW, Bunschoten A, Velders AH, Roestenberg M, van Leeuwen FWB. An update on radiotracer development for molecular imaging of bacterial infections. Clinical and Translational Imaging. 2019;7(2):105-24.

24. Ordonez AA, Jain SK. Pathogen-Specific Bacterial Imaging in Nuclear Medicine. Semin Nucl Med. 2018;48(2):182-94.

25. Akhtar MS, Imran MB, Nadeem MA, Shahid A. Antimicrobial Peptides as Infection Imaging Agents: Better Than Radiolabeled Antibiotics. International Journal of Peptides. 2012;2012:965238.

26. Parker MFL, Flavell RR, Luu JM, Rosenberg OS, Ohliger MA, Wilson DM. Small Molecule Sensors Targeting the Bacterial Cell Wall. ACS Infectious Diseases. 2020;6(7):1587-98.

27. Silhavy TJ, Kahne D, Walker S. The bacterial cell envelope. Cold Spring Harb Perspect Biol. 2010;2(5):a000414-a.

28. Auer GK, Weibel DB. Bacterial cell mechanics. Biochemistry. 2017;56(29):3710-24.

29. Cabeen MT, Jacobs-Wagner C. Bacterial cell shape. Nature Reviews Microbiology. 2005;3(8):601-10.

30. Meroueh SO, Bencze KZ, Hesek D, Lee M, Fisher JF, Stemmler TL, Mobashery S. Three-dimensional structure of the bacterial cell wall peptidoglycan. Proc Natl Acad Sci U S A. 2006;103(12):4404-9.

31. Signore A, Artiko V, Conserva M, Ferro-Flores G, Welling MM, Jain SK, Hess S, Sathekge M. Imaging Bacteria with Radiolabelled Probes: Is It Feasible? Journal of Clinical Medicine. 2020;9(8):2372.

32. Lin H, Yang C, Wang W. Imitate to illuminate: labeling of bacterial peptidoglycan with fluorescent and bio-orthogonal stem peptide-mimicking probes. RSC Chemical Biology. 2022;3(10):1198-208.

33. Parker MFL, Flavell RR, Luu JM, Rosenberg OS, Ohliger MA, Wilson DM. Small Molecule Sensors Targeting the Bacterial Cell Wall. ACS Infect Dis. 2020;6(7):1587-98.

34. Banahene N, Kavunja HW, Swarts BM. Chemical Reporters for Bacterial Glycans: Development and Applications. Chemical Reviews. 2022;122(3):3336-413.

35. Gale RT, Brown ED. New chemical tools to probe cell wall biosynthesis in bacteria. Current Opinion in Microbiology. 2015;27:69-77.

CHAPTER 2INSIGHTS INTO PEPTIDOGLYCAN-TARGETING RADIOTRACERS FOR IMAGING BACTERIAL INFECTIONS

Palesa. C. Koatale[a, b], Mick. M. Welling[c *], Honest Ndlovu[a, b], Mankgopo Kgatle [a, b], Sipho Mdanda[a, b], Amanda Mdlophane[a, b], Ambrose Okem[d], John Takyi-Williams[e], Mike .M. Sathekge [a,b], Thomas Ebenhan[a, b, f *]

a. Department of Nuclear Medicine, University of Pretoria, 0001 Pretoria, South Africa

b. Nuclear Medicine Research Infrastructure (NuMeRI) NPC, 0001 Pretoria, South Africa

c. Interventional Molecular Imaging Laboratory, Department of Radiology, Leiden University Medical Center, 2333 ZA Leiden, The Netherlands

d.Department of Anaesthesia, School of Clinical Medicine, University of Witwatersrand, 2050 Johannesburg, South Africa

e. Pharmacokinetic and Mass Spectrometry Core, College of Pharmacy, University of Michigan, 48109 Ann Arbor, Michigan, United States of America

f. DSI/NWU Pre-clinical Drug Development Platform, North West University, 2520 Potchefstroom, South Africa

Corresponding author

*) Authors to whom correspondence should be addressed.

Thomas.Ebenhan@up.co.za | m.m.welling@lumc.nl

ACS Infect Dis. **2024** Feb 9;10(2):270-286.

ABSTRACT

The unique structural architecture of the peptidoglycan allows for the stratification of bacteria as either gram-negative or positive, which is distinguishable from mammalian cells. This classification has received attention as a potential target for diagnostic and therapeutic purposes. The bacteria's ability to metabolically integrate peptidoglycan precursors during cell wall biosynthesis and recycling offers an opportunity to target and image the pathogens in their biological state. This review explores the peptidoglycan biosynthesis for bacteria-specific targeting for infection imaging. Current and potential radiolabeled peptidoglycan precursors for bacterial infection imaging, their development status, and performance *in vitro* and/or *in vivo* are highlighted.

Keywords: peptidoglycan, bacteria, precursor, infection, tracer development, nuclear medicine, molecular imaging

2.1 INTRODUCTION

The peptidoglycan layer is a key distinctive feature of the cell wall used to identify bacteria as either gram-negative or positive using gram-staining. Furthermore, it continues to serve as a cornerstone in developing target-based antibiotics [1-4]. The heterogeneity of peptidoglycan offers the advantage of establishing whether gram-negative or gram-positive bacterial strains caused the infection. For this reason, it presents as an attractive target for designing radiotracers capable of accurately detecting infection with possible identification of the causative pathogen, especially for pathogens difficult to cultivate or target, such as those hiding in biofilms [5-9]. This is critical in conditions where multiple species of pathogens are present after initial anti-microbial therapy, as the infection may become more complex. Trying to image and treat all strains simultaneously can lead to challenges in determining the most effective treatment regimen. Hence, targeting specific strains helps simplify the approach and allows for patient-tailored antibiotic therapy, a highly advocated strategy for addressing the continuing rise of antibiotic resistance [10].

2.2 OVERVIEW OF PEPTIDOGLYCAN BIOSYNTHESIS AND RECYCLING PATHWAY AS A POTENTIAL TARGET

The biochemical process of the peptidoglycan biosynthesis begins in the bacterial cytoplasm (**Figure 2-1**), where uridine diphosphate-N-acetylglucosamine (UDP-GlcNAc) is enzymatically transformed to UDP-N-acetylmuramic acid (UDP-MurNAc) by UDP-N-acetylglucosamine enolpyruvyl transferase (MurA) and UDP-N-acetylenolpyruvoyl glucosamine reductase (MurB). This reaction is followed by the sequential addition of amino acids to the UDP-MurNAc to form a peptide stem of the peptidoglycan facilitated by Mur ligases. Firstly, L-alanine (L-Ala) is covalently attached to the UDP-MurNAc via UDP-N-acetylmuramoyl-L-Ala ligase (MurC), followed by addition of D-glutamate (D-Glu) in position 2 via UDP-N-acetylmuramoyl-L-alanine-D-glutamate ligase (MurD). Subsequently, position 3 is then occupied by either meso-diaminopimelate (A2pm or DAP) or L-lysine (L-Lys) facilitated by UDP-N-acetylmuramoyl-Lalanyl-D-glutamate-2,6-diaminopimelate ligase (MurE). The addition of a D-Ala-D-Ala dipeptide substrate in positions 4 and 5 of the UDP-MurNAc-tripeptide is catalysed by UDP-N-acetylmuramoyl-tripeptide-D-alanyl-D-alanine ligase (MurF) and results in the formation of

UDP-MurNAc-pentapeptide (L-Ala-γ-D-Glu-meso-A2pm/L-Lys-D-Ala-D-Ala) precursor [11-13].

The second step occurs in the periplasmic membrane, where the phospho-N-acetylmuramoyl-pentapeptide-transferase (MraY) attaches the UDP-MurNAc-pentapeptide to the membrane-embedded undecaprenyl phosphate carrier lipid (C55-P) resulting in the formation of C55-pyrophosphoryl(PP)-MurNAc-pentapeptide (lipid I) [14, 15]. Thereafter, lipid I is further processed by N-acetylglucosaminyl transferase (MurG), adding a GlcNAc moiety to form a C55-PP–GlcNAc-MurNAc-pentapeptide (lipid II) followed by a subsequent flippase (MraJ) transportation to the periplasmic space [16-18]. The third step occurs in the periplasmic space catalyzed by bifunctional penicillin-binding proteins (PBP). The glycosyltransferases (GTases) and transpeptidases (TPs) add lipid II to the growing peptidoglycan strand by polymerization of alternating sugar moieties [13, 19] to form a rigid peptidoglycan macromolecular layer [12, 20].

During cell elongation and proliferation, the bacteria rearrange the cell membrane by enzymatic decomposition of the peptidoglycan chain using transglycosylases and endopeptidases [21, 22]. The primary by-products of this process include GlcNAc-anhMurNAc-tetrapeptides, which enters the cytoplasmic area using AmpG permease for re-use in peptidoglycan synthesis [23, 24]. Once inside the cytoplasm, the N-acetylmuramyl-L-alanine amidase (AmpD) hydrolyses the tetrapeptide from the glycan strand [25, 26]. Subsequently, LD-carboxypeptidase (LdcA) cleaves the terminal D-ala in position 4, resulting in tripeptide [27, 28]. The tripeptide is then enzymatically linked to GlcNAc by murein peptide ligase (Mpl), forming a UDP-MurNAc-tripeptide [29, 30]. Alternatively, the tripeptide precursor is further digested into single amino acids by murein peptide amidase (MpaA), which then re-enters the peptidoglycan biosynthesis pathway [31, 32].

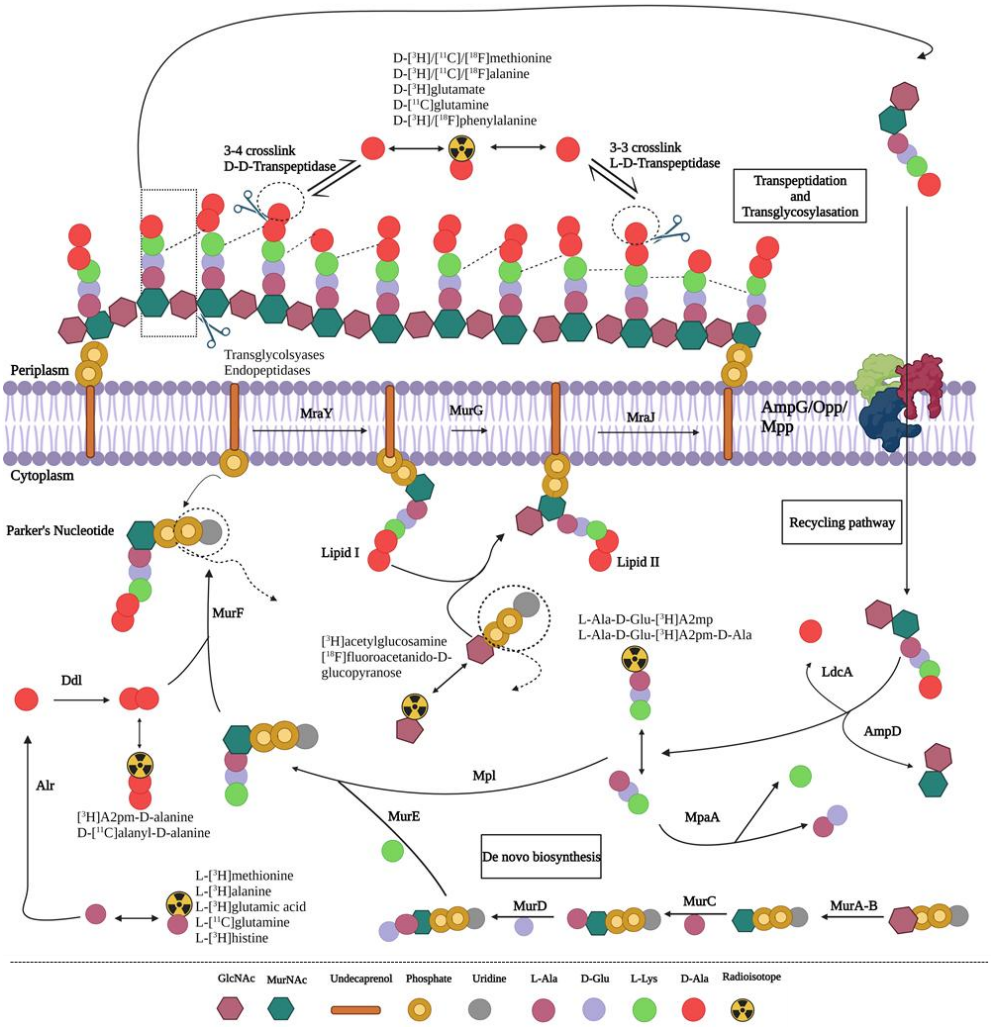

92

93 **Figure 2- 1:** The proposed pathways of peptidoglycan biosynthesis and potential precursors for
94 designing radiotracers or probes for imaging. Adapted from Lin et al. [33] with permission from
95 the Royal Society of Chemistry. Created with BioRender.com.

96

97 Since the heterogeneity and complexity of the peptidoglycan biosynthesis and its recycling
98 pathway involve multiple steps facilitated by the interaction of numerous precursors and
99 enzymes, multiple strategies may be followed to develop the tools for specifically targeting
100 bacterial cell walls. In particular, the possibility for peptidoglycan precursors-based probes using
101 different fluorophores for cell wall studies and diagnostic purposes using modern molecular
102 techniques should be emphasized. The next part of the review will provide an overview of
103 radiolabeled peptidoglycan-based precursors for infection imaging and highlight potential
104 precursors or derivatives with examples from fluorescence imaging.

2.3 EMERGING RADIOTRACERS TARGETING PEPTIDOGLYCAN BIOSYNTHESIS

Table 1-1 summarizes the mechanism of action-based characteristics of relevant radiotracers, discussed in detail in the following sections, including their *in vitro* and *in vivo* evaluation.

2.3.1 Amino acids-based probes

Amino acids are required for several biochemical processes in mammalian and bacterial cells, with the latter showing more preference for D-amino acids than L-amino acids [34]. A decade of research has been dedicated to demonstrating the capability of the bacteria to utilize exogenous D-amino acids for peptidoglycan biosynthesis [35]. This process takes place either in the periplasm by an exchange of D-amino acid at the terminal D-Ala of the peptide stem or cytoplasmic *de novo* synthesis of peptide precursors facilitated by LD-transpeptidase and D-alanine- D-alanine ligase (Ddl) activity, respectively [32, 36-39] (**Figure 2-1**).

Neumann et al. [40] characterized *in vitro* bacterial uptake of D-[^{14}C]methionine (D-Met), D-[^{14}C]valine (D-Val) and D-[^{14}C]phenylalanine (D-Phe), and the significantly more cell incorporation was seen with D-[^{14}C]Met for both *E. coli* (gram-negative) and *S. aureus* (gram-positive) bacteria. These results concord with those observed in another study by Kwak [41]. The possible explanation for the 6-10 fold higher accumulation over D-Val/D-Phe might be because the metabolism of D-Met is independent of the bacterial growth rate [37]. Based on this finding, the group further explored D-Met synthesized by reacting [^{11}C]CH_3I with a D-homocysteine thiolactone precursor, for PET/CT imaging using mice bearing *E. coli* and *S. aureus* [40] (**Figure 2-2**). High uptake of D-methyl-[^{11}C]methionine (D-[^{11}C]Met) was reported in both gram-positive (0.96 %ID/cc) and negative bacteria (0.78 %ID/cc) strains, with significant reduction obtained by co-incubation with unlabeled D-Met, suggesting that incorporation was specific to activate the metabolic pathway. The PET/CT imaging of D-[^{11}C]Met showed >2.5-fold higher counts and selectivity for infection over inflammation using murine myositis model in comparison to L-[methyl-^{11}C]methionine (L-[^{11}C]Met). Non-specific D-[^{11}C]Met accumulation was observed in the lungs, respiratory and gastrointestinal tract [40].

Subsequently, the group by Stewart et al. [42] optimized the radiosynthesis yield of D-[^{11}C]Met using D-homocysteine precursor, and specific uptake was observed in various gram-negative and positive pathogens. Similarly, Muranaka et al. [43] showed superior detection sensitivity of S-methyl-[^{3}H]-D-methionine (D-[^{3}H]Met) with >2-fold higher infection/background ratio over [^{18}F]FDG using a lung-infection-model in mice. Based on these findings, Polvoy et al. [44] successfully reported the first clinical translation of D-[^{11}C]Met in prosthetic joint infections (PJI), and the data indicated significant ($p < 0.0001$) focal infection localization with low background signal using PET/MRI scan (**Figure 2-3**). Although the results are promising, the probe application might be limited to musculoskeletal infections due to the high background signal observed in soft tissues. Following the positive prospects of D-[^{11}C]Met in a clinical setting, D-[^{18}F-CF_3]-methionine was developed to mitigate the logistics challenges associated with the shorter half-life of the [^{11}C]. Despite the bacterial uptake assays not being performed, the low radiochemical yield obtained necessitates further optimization [45].

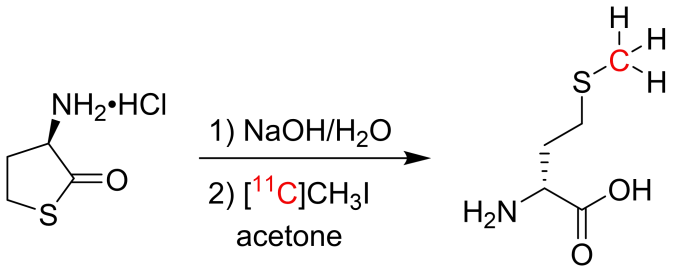

Figure 2- 2: Radiosynthesis of D-methyl-[^{11}C]methionine. Reproduced with permission from Ref [40], published 2017 under a Creative Commons Attribution 4.0 International License.

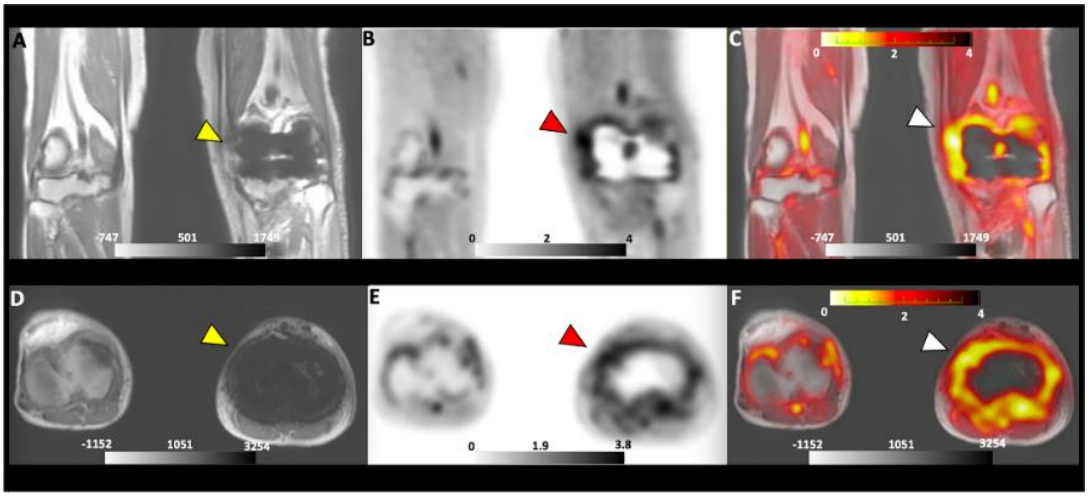

Figure 2- 3: PET/MRI images of D-[^{11}C]Met of a patient with suspected PJI. The yellow arrow indicates the MRI scan (A and D). Red and white arrows indicate the localization of D-[^{11}C]Met in the infected joint area using PET (B and E) and PET/MRI (C and F), respectively. Reprinted with permission ref [44], published under a Creative Commons Attribution 4.0 International License.

The same group synthesized D-3-[^{11}C]alanine (D-[^{11}C]Ala) through alkylation of a glycine-derived Schiff-base precursor with [^{11}C]methyl iodide (**Figure 2-4**). Bacterial metabolism of D-[^{11}C]Ala was reported in different gram-negative and positive bacterial strains with high *in vivo* sensitivity and selectivity (>3.5-fold %ID/g) obtained in comparison to [^{18}F]FDG and [^{68}Ga]citrate [46] (**Figure 2-5**). The study further reported possible applications in detecting spinal infections, pneumonia, and infections with antibiotic-resistant strains, which is currently challenging in the clinical setting. Similar *in vitro* results were obtained using D-2, 3-[^{3}H]-Ala. However, the group did not further pursue the *in vivo* bio-distribution investigations of the probe [41, 43]. Based on these promising results, for the first time, ^{18}F-labeled alanine derivative (D-[^{18}F-CF_3]-alanine) was reported for infection imaging. Unfortunately, the probe performed less than expected, with low specific activity and bacterial incorporation [45].

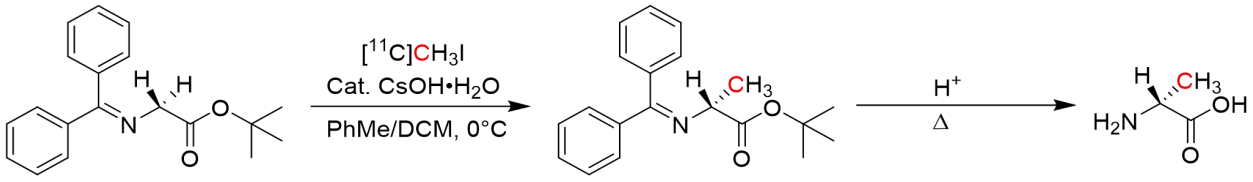

Figure 2-4: Radiosynthesis of D-3-[^{11}C]alanine. Reproduced with permission from ref [46]. Copyright 2020 American Chemical Society.

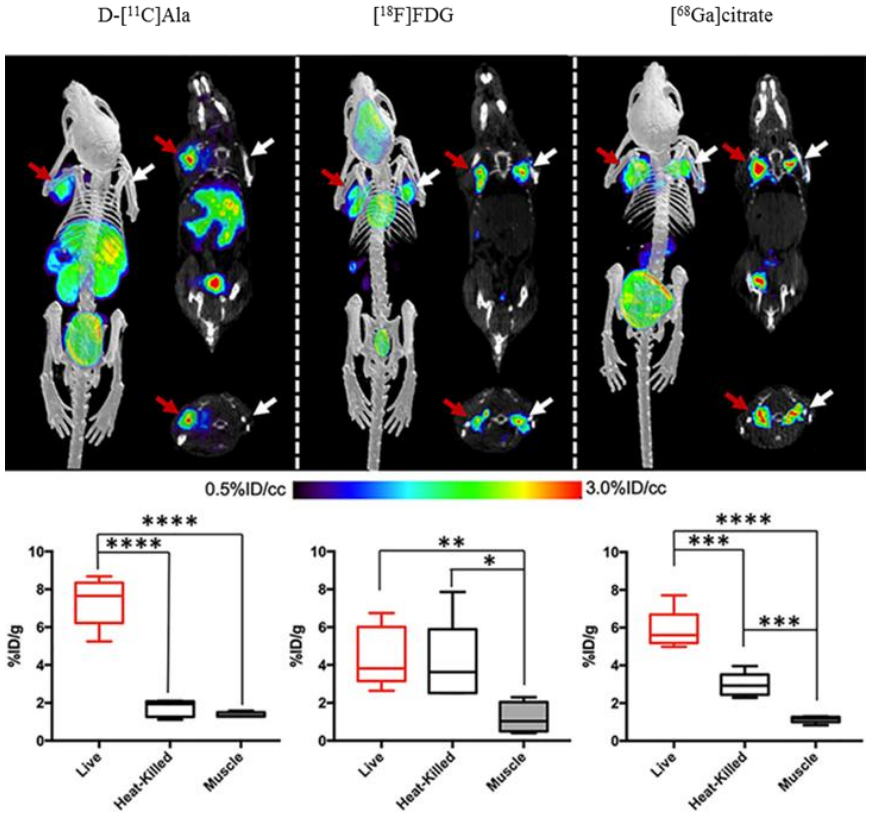

Figure 2-5: PET/CT biodistribution and corresponding *ex vivo* tissue data of D-[^{11}C]Ala, [^{18}F]FDG and [^{68}Ga]citrate in acute infection mice model inoculated with live bacteria (red arrows) and heat-killed bacteria (white arrows). Reprinted with permission from ref [46]. Copyright © 2020 American Chemical Society.

Bacteria can also incorporate D-amino acids with large aromatic substituents, including D-phenylalanine (D-Phe), D-tyrosine (D-Trp), and D-tryptophan (D-Tyr) as substrates for transpeptidation [32, 36]. Similarly [40], Kwak [41] investigated the bacterial uptake of D-[^{14}C]Phe, which showed specific uptake despite its lower rate compared to D-[^{14}C]Met using *E. coli*. However, this study further synthesized (R)-2-amino-3-(4-[^{18}F]-fluorophenyl propanoic acid, an analog of D-Phe by substitution of a proton with [^{18}F], to test the changes in bacterial uptake studies [47]. According to the results, the replacement of ^{14}C with ^{18}F did not affect the uptake of D-Phe and a significant specificity (>14-fold higher than [^{18}F]FDG) occurred in *E. coli* cultures. The study demonstrated the feasibility of D-[^{18}F]Phe in bacterial-specific targeting, which warrants further investigation in mice infection models and PET/CT imaging.

In many gram-positive strains, D-glutamate is converted to D-glutamine (D-Gln) at glutaminase's second position of the peptidoglycan precursor [48]. Kwak [41] reported high bacterial uptake of D-[^{3}H]glutamate, blocked by co-administration of unlabeled glutamate, indicating non-specific uptake. A similar experimental design was used in another study by Renick et al. [49] utilizing D-5-[^{11}C]glutamine (D-5-[^{11}C]Gln) synthesized by a two-step approach by reacting tert-butyl-2-((tert-butoxycarbonyl) amino)-4-iodobutanoate with [^{11}C]-HCN followed by deprotection of the nitrile intermediate (**Figure 2-6**). The *in vitro* investigations of D-5-[^{11}C]Gln showed high uptake in live methicillin-resistant *S. aureus* (MRSA) and *E. coli*, which was inhibited with increasing concentration of unlabeled reference. The PET/CT image guided tracer biodistribution using a dual myositis mouse model showed 1.64-fold higher infection-to-background ratios for both gram-positive and -negative bacteria. Unlike L-5-[^{11}C]Gln, the D-5-[^{11}C]Gln signal also allows for the differentiation of the infection from inflammation (induced heat-killed bacteria) (**Figure 2-7**).

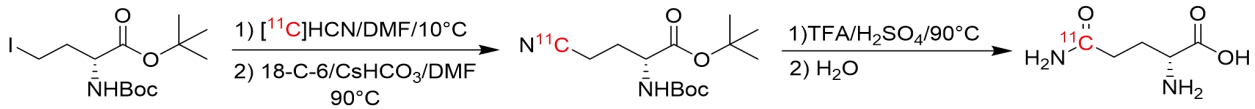

Figure 2- 6: Radiosynthesis of D-5-[^{11}C]glutamine. Reproduced with permission from ref [49]. Copyright 2021 American Chemical Society.

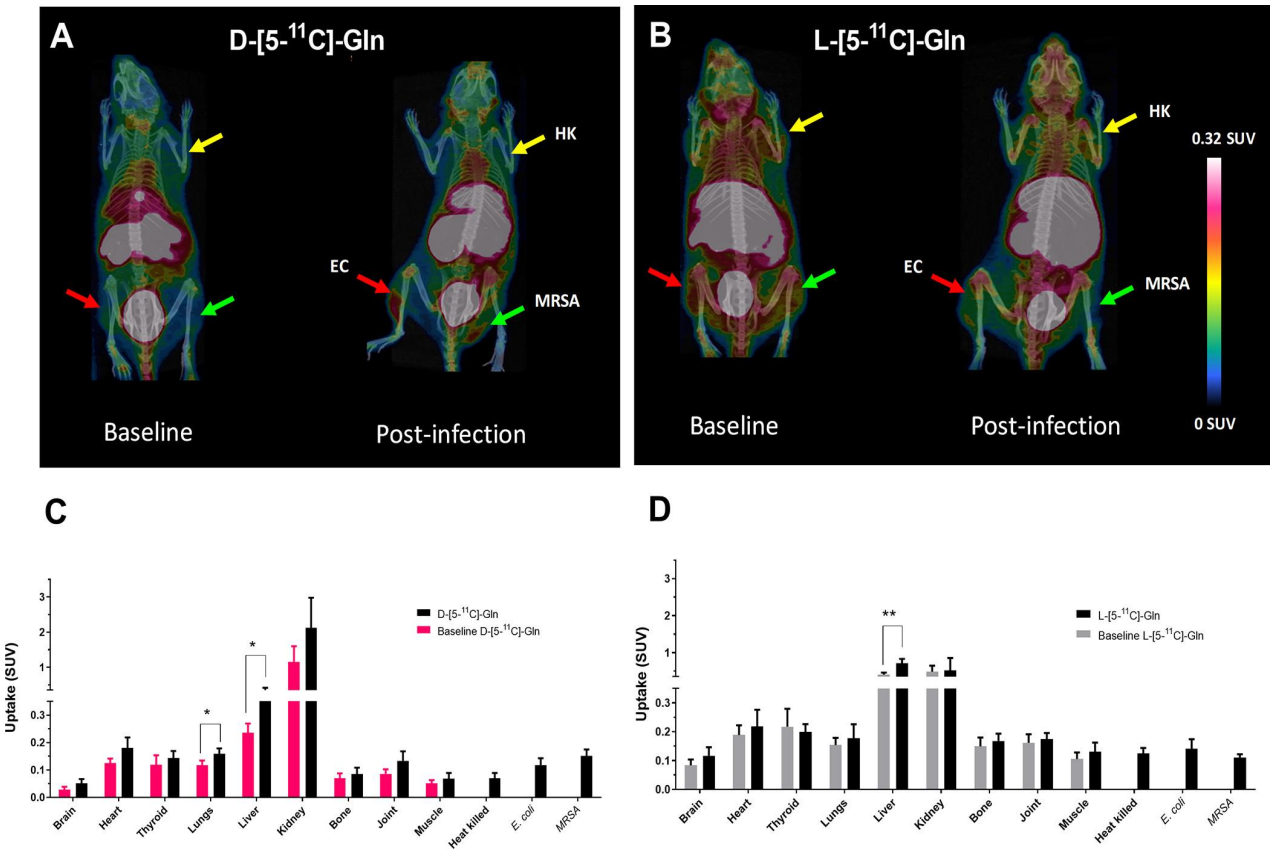

Figure 2- 7: PET/CT scans with corresponding *ex vivo* biodistribution of D-5-[^{11}C]Gln (A and C) vs. L-5-[^{11}C]Gln (B and D) in healthy_baseline and infected mice: inoculated with live methicillin-resistant *S. aureus* (MRSA) (green arrow), *E. coli* (EC) (red arrow) and heat-killed bacteria (HK) (yellow arrow). Reprinted with permission from ref [49]. Copyright 2021 American Chemical Society.

In addition, investigations on PBP enzymatic reactions were conducted using unlabeled lipid II and D-amino acids. PBP hereby recognized the D-enantiomers and not the L-enantiomers, suggesting that the reaction occurs at the amines in the alpha-amino group and not the epsilon-HH_2 moiety with inhibitory effects observed with the addition of β-lactams [32, 36, 50, 51]. Interestingly, previous studies have reported the potential of bacteria cells to make use of L-amino acids as the precursors for cell wall targeting, with uptake observed with L-2, 3-[S-methyl-^{3}H]methionine (L-[^{3}H]Met), L-[^{3}H]alanine (L-[^{3}H]Ala), L-2,3,4-[^{3}H]glutamic acid (L-[^{3}H]Glu), L-2,5-[^{3}H]histidine (L-[^{3}H]His) and L-3-[^{11}C]alanine (L-[^{11}C]Ala) [42, 43, 52]. Contrasting results were obtained in another study with [^{3}H]-L-Met, with no accumulation observed at the infected site, and this discrepancy is hypothesized to be due to the use of

different bacterial strains [40, 43]. This non-stereoselectivity is due to the ability of bacteria to convert L-amino acids to D-amino acids intracellularly using the amino acid racemase pathway for metabolic incorporation into the peptidoglycan. This hypothesis was supported by a previous study that showed a significant accumulation of intracellular L-alanine pools over D-amino acids in cells treated with D-alanine racemase alanine antibiotic (D-cycloserine) [53]. However, experimental studies are required to validate peptidoglycan metabolic incorporation of radiolabeled L-amino acids in bacteria [54-57]. Despite the results, biodistribution studies using mice infection models demonstrated similar target-to-non-target (T/NT) ratios ~1 for both L- and D-amino acids, therefore limiting the sensitivity of PET/CT diagnostics for bacterial infection [49, 52].

D-amino acids are incorporated through the cytoplasmic pathway mediated by Ddl and MurF enzymes [58]. Alternatively, Kuru et al. [59] proposed periplasmic transpeptidase as the main pathway of D-amino acids incorporation in the peptidoglycan with reduced fluorescence intensity observed in β-lactams and D-cycloserine treated bacteria (DCS) including L-, D-TPs mutant strains. Moreover, this study further disputes the cytoplasmic pathway metabolism with persisting fluorescence intensity observed for wild-type and Ddl mutant cells. Based on these findings, the possibility of one- or two-way pathway involvement in bacterial cell incorporation of D-amino acids is substantiated.

Overall, several pre-clinical studies have demonstrated the feasibility of radiolabeled D-amino acids as PET/CT infection imaging agents and prospects for clinical translation. However, one concern noted is the observed active metabolism by the microbiome and other non-infected organs; which might result in data misinterpretation. A limitation would also be the ability of fungi to ultilise D-amino acids in several metabolic activities, including carbon and nitrogen absorption [60, 61]. In particular, D-amino acid-based PET tracers such as D-5-[^{11}C]Gln has been shown to image fungal infection with high specificity [62]. Consequently, it will compromise the relevant tracers to differentiate bacterial from fungal infections in the clinical setting. In addition, the development of ^{18}F-labeled D-amino acids is hampered by poor radiochemical yield and possible defluorination *in vivo* [45, 63]. Despite the mentioned limitations, the reported tolerance of LD-transpeptidase to different modifications at the C-

terminal creates an opportunity to design a library of D-amino acids analogs with more optimized radiosynthesis and a favorable output of primary pharmacology. Moreover, the differentiation of pathogens (bacteria vs. fungi), bacterial species, or phenotypes specific PET imaging might be realized, thus, improving guided therapy and identifying antibiotic-resistant strains [46, 64, 65].

2.3.2 D-Amino Acid dipeptide-based probes

During peptidoglycan biosynthesis, metabolic incorporation of the D-Ala-D-Ala dipeptide at the tripeptide terminal by MurF results in a pentapeptide chain (lipid I), which is ultimately incorporated into the existing peptidoglycan chain. This early-stage pathway has been targeted for cell wall imaging using a fluorescent D-Ala-D-Ala dipeptide analog [59]. The successful incorporation of D-Ala-D-Ala also requires binding compatibility with the MurF enzyme, which has high specificity for the C-terminal residue. This was demonstrated by the previous work with high bacterial uptake of fluorescence-tagged D-amino acid dipeptide modified at the N-terminus compared to C-terminal-modified probes reported [59, 66]. By adopting the same labeling strategy, Parker et al. [67] and co-workers developed a D-amino dipeptide for cell wall targeting by successfully synthesizing D-3-[^{11}C]alanyl-D-alanine (D-[^{11}C]Ala–D-Ala) probe via ^{11}C-alkylation of the N-terminus of D-Ala-D-Ala glycine Schiff precursor followed by deprotection of amine groups (**Figure 2-8**). The *in vitro* screening of D-[^{11}C]Ala–D-Ala showed uptake of 9 Bq/10^6 cfu in *E. coli,* which was near-quantitatively inhibited in heat-killed culture sample. In addition, a partial *in vitro* screen using D-[^{11}C]Ala-D-Ala showed uptake levels ranging 5-35 Bq/10^6 cfu in several other bacteria, which justifies further evaluation *in vivo* imaging by PET/CT.

In another study by Goodell [68], a [^{3}H]A2pm-D-Ala dipeptide was incorporated into the bacterial cell wall at a slow rate. This might explain the lower uptake of D-[^{11}C]Ala–D-Ala in comparison to D-[^{11}C]Ala as reported by a previous study [67]. The study suggested periplasmic degradation of the dipeptide into A2pm and D-Ala as substrates of carboxypeptidase before transportation into the cytoplasm for re-integration into the downstream pathway by the Dld enzyme. This indicate a limit of D-amino acid dipeptide-based probes in cell wall targeting due

to possible reduction in labeling signal, also reported previously for a fluorescent-based tracer with the addition of peptidoglycan-digesting enzyme (lysozyme) [66]. Unfortunately, bacteria have a perpetual built-in resistance to β-lactam-based antibiotics by substituting terminal D-alanine with a variety of D-amino acids, including D-lactate and D-serine [69, 70]. Therefore, to address the mentioned limitation, Flip et al. [71] have reported the synthesis of a variety of ^{11}C-labeled D-amino acid dipeptides substituted with different amino acids at terminal residue, which could indeed preserve the probes from degradation by carboxypeptidases. However, efforts should be made to evaluate these dipeptide derivatives' efficacy in bacterial targeting and determine the value of PET imaging.

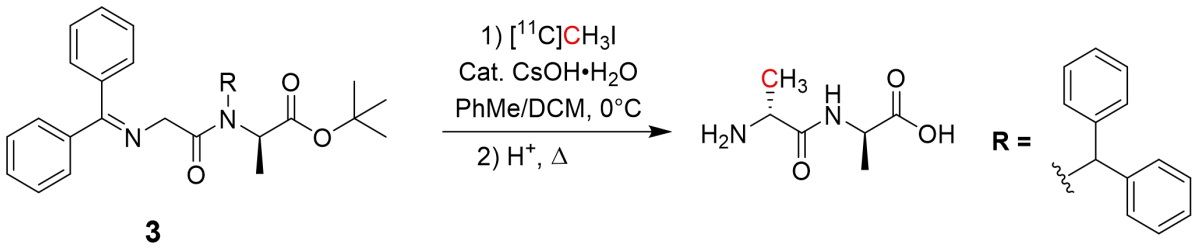

3

Figure 2- 8: Radiosynthesis of D-3-[^{11}C]Ala-D-Ala. Reproduced with permission from ref [46]. Copyright 2020 American Chemical Society.

2.3.3 Park's Nucleotide and Lipid-based probes

The formation of lipid I is the initial membrane-based step of peptidoglycan biosynthesis facilitated by MraY transferase [72, 73]. Previous studies used chemo-enzymatically synthesized UDP-MurNAc-L-[^{14}C]Ala-γ-D-Glu-*meso*-A_2pm/lys-D-Ala-D-Ala (UDP-MurNAc-[^{14}C]pentapeptide) to study the biochemical properties of this enzyme. It demonstrated the MraY selectivity for UDP-MurNAc-pentapeptide analogs during peptidoglycan synthesis with high specificity observed towards nucleotide substrates with alanine as opposed to glycine in position-1 and -4 than in position-5 [74-76]. In particular, UDP-MurNAc-pentapeptides labeled with ^{14}C at L-Ala/ A2pm position in the presence of MraY led to the formation of lipid I [75]. Subsequently, other studies showed that UDP-MurNAc pentapeptide derivatives modified with fluorescein at the meso-diaminopimelic acid (m-DAP) residue were more efficiently incorporated into the cell wall of gram-positive bacteria compared to gram-negative bacteria [77, 78]. This evidence strongly supports the further investigation of ^{14}C-labeled UDP-MurNAc-peptides probes for specific targeting with possible differentiation of infections caused by gram-positive and negative strains, although PET/CT suitable probes using ^{18}F and ^{11}C have not been reported yet.

A further addition of lipid II to the existing murine chain generally occurs in the periplasmic space facilitated by PBP. Born et al. [79] and Bertsche et al. [80] used the *in vitro* murine synthesis assay to study the transglycosylation and transpeptidation reactions which catalysis the cross-linking of glycan and peptide chains, respectively, using an enzymatically produced [^{14}C]GlcNAc-labeled lipid II as PBP substrate. Consequently, the catalytic recognition and turnover of [^{14}C]GlcNAc-labeled lipid II by PBP may be an interesting strategy for bacterial characterization *in vivo*, which has not yet been reported. Of note, Sadamoto et al. [77] attempted this approach in live bacteria using fluorescently labeled 1ipid I/II derivatives; unfortunately, the cells did not take up these probes. The group hypothesized that the lack of uptake might be due to the low affinity of glycosyltransferases (TGase) towards lipid II analogs with shorter lipid chains affecting transglycosylation [81] or due to the high molecular weight (>1,000 g/mol) of these derivatives preventing extracellular membrane permeability. As the intra- and extracellular entrapment of precursor lipids I/II is a key step in peptidoglycan synthesis [16] the latter findings might deter translation into nuclear infection imaging. Park's nucleotides and lipid-derived

335 substrates in bacterial-targeting research are mainly limited due to the complex synthetic
336 processes involved in developing structurally similar compounds. However, newly developed
337 chemical and enzymatic synthesis methods have opened up the opportunity to design precursors
338 with different modifications for the possible incorporation of radioisotopes. Therefore, further
339 exploration in bacterial uptake studies using gram-positive strains is required to assess their role
340 and value for infection imaging [82, 83].

341

2.3.4 Carbohydrate/Glycan core-based probes

Both, N-acetylmuramic acid (MurNAc) and N-acetylglucosamine (GlcNAc), are the first amino sugar substrates of the peptidoglycan biosynthesis, forming the backbone of the polymer chain. Most bacteria are capable of recycling exogenous GlcNAc and MurNAc substrates through phosphorylation by cytoplasmic kinase MurK resulting in GlcNAc-6-phosphate for initiation of peptidoglycan biosynthesis, cell wall macromolecules (lipopolysaccharides, teichoic acids) or catabolic pathway of glycolysis [84-86]. The rapid uptake and integration of [^{3}H]GlcNAc into peptidoglycan were reported in a previous study [68]. A follow-up study by Martínez et al. [87] synthesized an N-acetyl-D-glucosamine analog for bacterial uptake and imaging for the first time (**Figure 2-9**). This study used ^{18}F-labeled 1,3,4,6-tetra-O-acetyl-2-deoxy-2-bromoacetamido-D-glucopyranose followed by hydrolysis to synthesize 2-deoxy-2-[^{18}F]fluoroacetamido-D-glucopyranose ([^{18}F]FAG). The *in vitro* and *in vivo* uptake experiments using *E. coli* showed significant incorporation of [^{18}F]FAG compared to its counterpart [^{18}F]FDG, which made it possible to distinguish bacterial infection from sterile inflammation with a T/NT of 1.68) by PET/CT imaging (**Figure 2-10**).

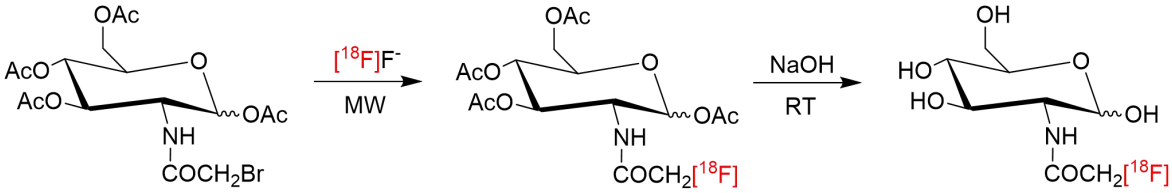

Figure 2-9: Radiosynthesis of 2-deoxy-2-[^{18}F]fluoroacetamido-D-glucopyranose. Reproduced with permission from ref [87]. Copyright 2011 Elsevier Inc.

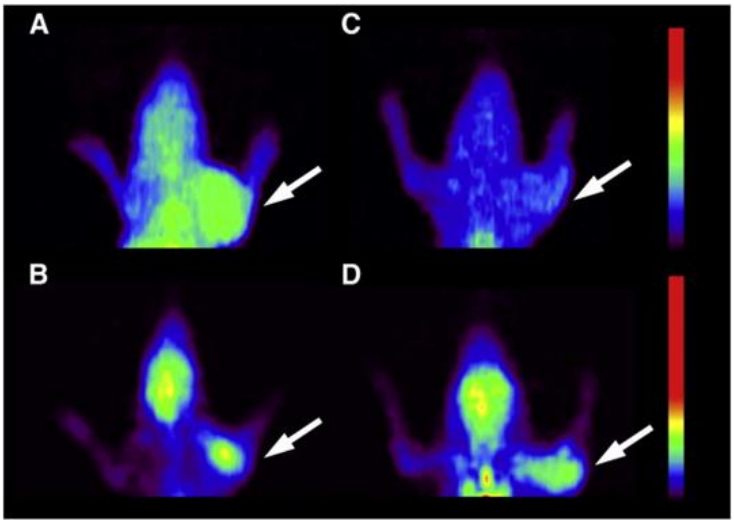

Figure 2- 10: PET localization of [^{18}F]FAG and [^{18}F]FDG in rats bearing bacterial infection or sterile inflammation. The white arrows indicate the accumulation of [^{18}F]FAG (A and C) and [^{18}F]FDG (B and D) at the site of infection (A and B) and inflammation (C and D). Reproduced with permission from ref [87]. Copyright 2011 Elsevier Inc.

A study by Hu et al. [88] revealed that the hydroxyl groups are essential for binding GlcNAc to MurG. Therefore, the ^{18}F-acetyl conjugation strategy did not affect the binding properties of [^{18}F]FAG. This might be due to the acetyl group's inability to participate in the binding interface of MurG as previously reported allowing the synthesis of [^{18}F]FAG containing lipid II for ultimate incorporation into peptidoglycan; however, more work is required to solidify the route of incorporation [89, 90]. Despite the promising results, the probe showed non-specific hepatic and pulmonary uptake. Carroll et al. [91] developed a library of ^{18}F-labeled glucosamine derivatives using different prosthetic groups. However, the probes showed unfavorable pharmacokinetics, including elevated background signals and *in vivo* defluorination. To address these shortcomings, Sadamoto et al. [83] synthesized and demonstrated bacterial uptake of GlcNAc-1-phosphate derivatives modified with a ketone at the N-acetyl position, which presents an attractive alternative to reduce the background noise. Although the hydroxyl groups are required for recognition of [^{18}F]FAG by MurG, the study reported significant association with lactobaccilliar of Alexa-Fluor-488-acetylated glucosamine derivatives due to increased hydrophobicity followed by the intracellular removal of the N-acetyl group for ultimate incorporation into the cell wall [83]. As a result, this supports the investigation of 1,3,4,6-tetra-O-acetyl-2-deoxy-2-[^{18}F]fluoroacetamido-D-glucopyranose as a potential glucosamine derivative for cell wall targeting, which was not previously evaluated [87].

A novel recycling pathway unique to *Pseudomonas putida* involving direct integration of UDP-MurNAc into *de novo* synthesis without requiring UDP-GlcNAc as a substrate has been documented [92]. This was demonstrated by direct bacterial cell wall incorporation of MurNAc derivatives fluorescently labeled at the N acetyl termini using click-chemistry [93]; however, no research has been attempted to develop radioactive MurNAc derivatives for direct *in vivo* diagnostic imaging. Unlike [^{18}F]FAG metabolized by mammalian cells [94]; a MurNAc-based radiolabeled probe will potentially increase the specificity and selectivity of the bacterial foci as it is unique to bacteria. A plausible radiolabeling strategy could be explored with tolerated modifications at the N-acetyl terminus of the MurNAc residue using ^{18}F- or ^{11}C-labeling enabling targeting and imaging of peptidoglycan biosynthesis using PET/CT [93].

2.3.5 Oligopeptide-based probes

One essential pathway of peptidoglycan biosynthesis is the integration of oligopeptides shed from the existing polymer chain into the cytosol to be reused in the formation of *de novo* peptidoglycan polymer chain. To understand this pathway, Goodell [68] reported uptake in *E. coli* for the L-Ala-D-Glu-meso-A2pm tripeptide and the L-Ala-D-Glu-A2pm-D-Ala tetrapeptide labeled at the third position with 3,4,5-[^{3}H]A2pm and demonstrated the enzymatic conversion into UDP-MurNAc-tri- and pentapeptide for ultimate re-integration into the peptidoglycan chain. The study reported degradation of the tetrapeptide at the terminal residue, resulting in tripeptide and D-Ala, suggesting that the tripeptide was responsible for labeling the cell wall.

Olrichs et al. [95] developed an L-alanine-γ-D-glutamine-L-lysine tripeptide fluorescently labeled with N-7-nitro-2,1,3-benzoxadiazol-4-yl (AeK–NBD) at the lysine terminal and demonstrated that peptidoglycan incorporation was not affected by the replacement of the A2pm at position 3 with Lys. The study further showed that recycling depends entirely upon substrate recognition by Mpl with high specificity reported for the tri- or tetrapeptide composed with A2pm/L-Lys at position 3. Furthermore, substrate incorporation was inhibited in Mpl-mutant bacteria [29, 96]. Taking the observations mentioned above into account, L-Ala-D-Glu-meso-A2pm/Lys and L-Ala-D-Glu-A2pm-D-Ala are promising substrates for bacteria-specific targeting and imaging; however; their radiopharmaceutical development and value for PET

imaging of infection is outstanding. Chapter 4 will demonstrate the potential of L-Ala-D-Glu-meso-A2pm/Lys for PET/CT-infection imaging for the first time. In the next Chapter, we present the diagnostic accuracy of highlighted potential peptidoglycan-based radiotracer for clinical translatability and application using qualitative analysis.

Table 2- 1: Mechanism of Action-Based Characteristics of Relevant Radiotracers Including Their *In vitro* and *In vivo* Evaluation

Precursor	**Radiotracer**	**Proposed Mechanism of Action**	**Key Enzymes**	***In vitro* binding to pathogens**	***In vivo* evaluation**	**Bacterial species**	**Comment**	**References**
Amino acids	D-[^{3}H]/[^{11}C]/ [^{18}F]methionine	Extracellular/Intracellular transpeptidation	TPs/Ddl	Uptake/ competition studies Live and/or heat-killed	Murine myositis model D-[^{11}C]Met vs. L-[^{11}C]Met, Lung-infection model [^{18}F]FDG vs. D-[^{3}H]Met, Patients with suspected prosthetic joint infections	Broad spectrum	More sensitive than [^{18}F]FDG and L-[^{11}C]Met. Shows promise for use in clinical settings. Low RCY with [^{18}F]	[1-6]

	D-[^{3}H]/[^{11}C]/[^{18}F]alanine	Extracellular/Intracellular transpeptidation	TPs/Ddl	Competition studies Live and/or heat-killed	Murine myositis model Uptake/biodistribution ([^{18}F]FDG vs. [^{68}Ga]citrate vs. D-[^{11}C]Ala) D-Ala was further tested in vertebral discitis-osteomyelitis model, pneumonia lung infection model, and an anti-microbial therapy model	Broad spectrum	Highest accumulation observed, but low bacterial uptake after ^{18}F-substitution	[3-5, 7]
	D-[^{3}H]glutamate	Extracellular/Intracellular transpeptidation	TPs/Ddl	Uptake/ competition studies	NA	*E. coli*	Non-specific uptake	[3]
	D-[^{11}C]glutamine	Extracellular/Intracellular transpeptidation	TPs/Ddl	Uptake/competition studies Live or heat-	murine myositis model Live vs. heat-killed (D-[^{11}C]Gln vs. L-[^{11}C]Gln vs.	*E. coli* *S. aureus*	Bacterial infection imaging specificity	[8]

				killed	[^{18}F]FDG)			
	D-[^{3}H]/[^{18}F] phenylalanine	Extracellular/ Intracellular transpeptidation	TPs/Ddl	Uptake/ competition studies	NA	*E. coli*	Higher uptake than [^{18}F]FDG	[1, 3]
	D-[^{18}F]azido-alanine	Extracellular/ Intracellular transpeptidation	TPs/Ddl	Metabolic click chemistry assay	NA	*E. coli* *S. aureus*	D-azido-alanine pre-targeting labeling with [^{18}F]sulfo-DBCO	[9]
	L-[^{3}H]alanine	Intracellular racemization	racemases	Uptake/ competition studies	Myositis infection model	*E. coli*	Possible false negative results in practice	[4, 10]
	L-[^{3}H]methionine	Intracellular racemization	racemases	Uptake studies	Lung-infection-model ([^{18}F]FDG vs. L-[^{3}H]Met)	*E. coli*	More sensitive than [^{18}F]FDG	[4, 10]

	L-[^{11}C]glutamine	Intracellular racemization	racemases	Uptake/ competition studies Live vs. heat killed	Murine myositis model Live vs. heat-killed (L-[^{11}C]Gln vs. D-[^{11}C]Gln)	*E. coli* *S. aureus*	Poor imaging contrast and specificity	[8]
	L-[^{3}H]glutamic acid	Intracellular racemization	racemases	Uptake studies	NA	*E. coli*	Highest uptake in log-phase bacteria culture	[10]
	L-[^{3}H]histidine	Intracellular racemization	racemases	Uptake studies	NA	*E. coli*	Highest accumulation in the stationary-phase bacteria culture	[10]
Dipeptides	[^{3}H]-A2pm-D-Ala	Intracellular peptide stem synthesis	Dld	Uptake/ competition studies	NA	*E. coli*	Dipeptide degraded at the terminal before integration into	[11]

							cell wall	
	D-[^{11}C]Ala-D-Ala	Intracellular peptide stem synthesis	MurF	Uptake studies Live vs. heat-killed bacteria	NA	Broad spectrum	Accumulation in a wide variety of gram(+) and (-) strains	[7]
Oligo-peptides	L-Ala-D-Glu-[^{3}H]A2pm	Intracellular peptide stem synthesis	Mpl	Uptake/ competition studies	NA	*E. coli*	Tripeptide stable before integration into cell wall	[11]
	L-Ala-D-Glu-[^{3}H]A2pm-D-Ala	Intracellular peptide stem synthesis	Mpl	Uptake/ competition studies	NA	*E. coli*	Tetrapeptide D-Ala moiety degraded before integration into cell wall	[11]
Park'sNucleotide	UDP-MurNAc-[^{14}C]pentapeptide	Intracellular lipid I synthesis	MraY	Enzymatic studies	NA	*E. coli*	Purified MraY produced Lipid I	[12, 13]

Lipid	[^{14}C]GlcNAc-lipid II	Extracellular transglycosylation / transpeptidation	TGase	Enzymatic studies	NA	*E. coli*	PBP1A is a key enzyme in peptidoglycan synthesis	[14]
Glycan core	[^{3}H]acetylglucosamine	Intracellular transglycosylation	MurG	Uptake studies	NA	*E. coli*	Rapid bacterial uptake	[11]
	[^{18}F]fluoroacetamido-D-glucopyranose	Intracellular transglycosylation	MurG	Uptake/ competition studies	Murine myositis model Infection vs. sterile inflammation ([^{18}F]FAG vs. [^{18}F]FDG)	*E. coli*	Clearly visualized infections, not inflammations	[15]

Abbreviations: RCY = Radiochemical yield; E. coli = Escherichia coli gram (-); S. aureus = Staphylococcus aureus gram (+); NA= Not applicable

ABBREVIATIONS

A2pm	2,6-diaminopimelic acid
Ala	Alanine
AmpD	N-acetylmuramyl-L-alanine amidase
C55-P	Undecaprenyl phosphate
CT	Computed tomography
DAP	2,6-Diaminopimelic Aacid
Ddl	D-alanine- D-alanine ligase
DOTA	1,4,7,10-tetraazacyclododecane-1,4,7,10-tetraacetic acid
E. coli	*Escherichia coli*
EC	Electron capture
FAG	Fluoroacetamido-D-glucopyranose
FDG	Fluorodeoxyglucose
GlcNAc	N-Acetylglucosamine
Glu	Glutamate
Gln	Glutamine
GTases	Glycosyltransferases
Gram (+)	Gram-positive
Gram (-)	Gram-negative
His	Histidine
HMPAO	Hexamethylproplyleneamine oxime

HPLC	High-pressure liquid chromatography
LAFOV	Large axial field of view
LdcA	LD-Carboxypeptidase
Lys	Lysine
Met	Methionine
MIP	Maximum intensity projection
MpaA	Murein peptide amidase
Mpl	Murein peptide ligase
MRI	Magnetic resonance Imaging
MurA	UDP-N-Acetylglucosamine enolpyruvyl transferase
MurB	UDP-N-Acetylenolpyruvoyl glucosamine reductase
MurC	UDP-N-Acetylmuramoyl-L-alanine ligase
MurD	UDP-N-Acetylmuramoyl-L-alanine-D-glutamate ligase
MurE	UDP-N-Acetylmuramoyl-Lalanyl-D-glutamate-2,6-diaminopimelate ligase
MurF	UDP-N-Acetylmuramoyl-tripeptide-D-alanyl-D-alanine ligase
MurG	N-Acetylglucosaminyl transferase
MraY	Phospho-N-acetylmuramoyl-pentapeptide-transferase
MurNAc	N-Acetylmuramic acid
NMR	Nuclear magnetic resonance
NOTA	1,4,7-triazacyclononane-1,4,7-triacetic acid

PBP	Penicillin-binding protein
PCR	Polymerase chain reaction
PET	Positron emission tomography
Phe	Phenylalanine
PJI	Prosthetic joint infections
PAGE	Polyacrylamide gel electrophoresis
PP	Pyrophosphoryl
RCY	Radiochemical yield
S. aureus	Staphylococcus aureus
SPECT	Single-photon emission computed tomography
TPs	Transpeptidases
Trp	Tyrosine
Tyr	Tryptophan
UBI	Ubiquicidin
UDP	Uridine diphosphate
US	Ultrasound
Val	Valine

2.4 REFERENCES

1. Dörr T, Moynihan PJ, Mayer C. Editorial: Bacterial Cell Wall Structure and Dynamics. Frontiers in Microbiology. 2019;10.

2. Coico R. Gram Staining. Current Protocols in Microbiology. 2006;00(1):A.3C.1-A.3C.2.

3. Green DW. The bacterial cell wall as a source of antibacterial targets. Expert Opinion on Therapeutic Targets. 2002;6(1):1-20.

4. Bugg TDH, Braddick D, Dowson CG, Roper DI. Bacterial cell wall assembly: still an attractive antibacterial target. Trends in Biotechnology. 2011;29(4):167-73.

5. Auer GK, Weibel DB. Bacterial cell mechanics. Biochemistry. 2017;56(29):3710-24.

6. Silhavy TJ, Kahne D, Walker S. The bacterial cell envelope. Cold Spring Harb Perspect Biol. 2010;2(5):a000414-a.

7. Epand RM, Walker C, Epand RF, Magarvey NA. Molecular mechanisms of membrane targeting antibiotics. Biochimica et Biophysica Acta Biomembranes. 2016;1858(5):980-7.

8. Meroueh SO, Bencze KZ, Hesek D, Lee M, Fisher JF, Stemmler TL, Mobashery S. Three-dimensional structure of the bacterial cell wall peptidoglycan. Proc Natl Acad Sci U S A. 2006;103(12):4404-9.

9. Cabeen MT, Jacobs-Wagner C. Bacterial cell shape. Nature Reviews Microbiology. 2005;3(8):601-10.

10. Ordonez AA, Weinstein EA, Bambarger LE, Saini V, Chang YS, DeMarco VP, Klunk MH, Urbanowski ME, Moulton KL, Murawski AM. A systematic approach for developing bacteria-specific imaging tracers. Journal of Nuclear Medicine. 2017;58(1):144-50.

11. Smith CA. Structure, Function and Dynamics in the mur Family of Bacterial Cell Wall Ligases. Journal of Molecular Biology. 2006;362(4):640-55.

12. Sauvage E, Kerff F, Terrak M, Ayala JA, Charlier P. The penicillin-binding proteins: structure and role in peptidoglycan biosynthesis. FEMS Microbiology Reviews. 2008;32(2):234-58.

13. Barreteau H, Kovač A, Boniface A, Sova M, Gobec S, Blanot D. Cytoplasmic steps of peptidoglycan biosynthesis. FEMS microbiology reviews. 2008;32(2):168-207.

14. Chung BC, Zhao J, Gillespie RA, Kwon DY, Guan Z, Hong J, Zhou P, Lee SY. Crystal structure of MraY, an essential membrane enzyme for bacterial cell wall synthesis. Science. 2013;341(6149):1012-6.

15. Liu Y, 刘 垚, Rodrigues JPGLM, Bonvin AMJJ, Zaal EA, Berkers CR, Heger M, Gawarecka K, Swiezewska E, Breukink E, Egmond MR. New Insight into the Catalytic Mechanism of Bacterial MraY from Enzyme Kinetics and Docking Studies. Journal of Biological Chemistry. 2016;291(29):15057-68.

16. Van Dam V, Sijbrandi R, Kol M, Swiezewska E, De Kruijff B, Breukink E. Transmembrane transport of peptidoglycan precursors across model and bacterial membranes. Molecular Microbiology. 2007;64(4):1105-14.

17. Sham L-T, Butler EK, Lebar MD, Kahne D, Bernhardt TG, Ruiz N. MurJ is the flippase of lipid-linked precursors for peptidoglycan biogenesis. Science. 2014;345(6193):220-2.

18. Mohammadi T, van Dam V, Sijbrandi R, Vernet T, Zapun A, Bouhss A, Diepeveen-de Bruin M, Nguyen-Distèche M, de Kruijff B, Breukink E. Identification of FtsW as a transporter of lipid-linked cell wall precursors across the membrane. The EMBO Journal. 2011;30(8):1425-32.

19. Heijenoort Jv. Formation of the glycan chains in the synthesis of bacterial peptidoglycan. Glycobiology. 2001;11(3):25R-36R.

20. Buynak JD. Cutting and Stitching: The Cross-Linking of Peptidoglycan in the Assembly of the Bacterial Cell Wall. ACS Chemical Biology. 2007;2(9):602-5.

21. Vollmer W, Joris B, Charlier P, Foster S. Bacterial peptidoglycan (murein) hydrolases. FEMS Microbiology Reviews. 2008;32(2):259-86.

22. Vermassen A, Leroy S, Talon R, Provot C, Popowska M, Desvaux M. Cell wall hydrolases in bacteria: insight on the diversity of cell wall amidases, glycosidases and peptidases toward peptidoglycan. Frontiers in Microbiology. 2019;10:331.

23. Cheng Q, Park JT. Substrate specificity of the AmpG permease required for recycling of cell wall anhydro-muropeptides. J Bacteriol. 2002;184(23):6434-6.

24. Zhang Y, Bao Q, Gagnon LA, Huletsky A, Oliver A, Jin S, Langaee T. ampG Gene of Pseudomonas aeruginosa and Its Role in β-Lactamase Expression. Antimicrobial Agents and Chemotherapy. 2010;54(11):4772-9.

25. Lee M, Zhang W, Hesek D, Noll BC, Boggess B, Mobashery S. Bacterial AmpD at the crossroads of peptidoglycan recycling and manifestation of antibiotic resistance. Journal of the American Chemical Society. 2009;131(25):8742-3.

26. Carrasco-López C, Rojas-Altuve A, Zhang W, Hesek D, Lee M, Barbe S, André I, Ferrer P, Silva-Martin N, Castro GR, Martínez-Ripoll M, Mobashery S, Hermoso JA. Crystal structures of bacterial peptidoglycan amidase AmpD and an unprecedented activation mechanism. Journal of Biological Chemistry. 2011;286(36):31714-22.

27. Vermassen A, Leroy S, Talon R, Provot C, Popowska M, Desvaux M. Cell Wall Hydrolases in Bacteria: Insight on the Diversity of Cell Wall Amidases, Glycosidases and Peptidases Toward Peptidoglycan. Frontiers in Microbiology. 2019;10.

28. Hoyland CN, Aldridge C, Cleverley RM, Duchêne MC, Minasov G, Onopriyenko O, Sidiq K, Stogios PJ, Anderson WF, Daniel RA, Savchenko A, Vollmer W, Lewis RJ. Structure of the LdcB LD-carboxypeptidase reveals the molecular basis of peptidoglycan recognition. Structure. 2014;22(7):949-60.

29. Mengin-Lecreulx D, van Heijenoort J, Park JT. Identification of the mpl gene encoding UDP-N-acetylmuramate: L-alanyl-gamma-D-glutamyl-meso-diaminopimelate ligase in Escherichia coli and its role in recycling of cell wall peptidoglycan. J Bacteriol. 1996;178(18):5347-52.

30. Das D, Hervé M, Feuerhelm J, Farr CL, Chiu H-J, Elsliger M-A, Knuth MW, Klock HE, Miller MD, Godzik A, Lesley SA, Deacon AM, Mengin-Lecreulx D, Wilson IA. Structure and Function of the First Full-Length Murein Peptide Ligase (Mpl) Cell Wall Recycling Protein. PLOS ONE. 2011;6(3):e17624.

31. Maqbool A, Hervé M, Mengin-Lecreulx D, Wilkinson Anthony J, Thomas Gavin H. MpaA is a murein-tripeptide-specific zinc carboxypeptidase that functions as part of a catabolic pathway for peptidoglycan-derived peptides in γ-proteobacteria. Biochemical Journal. 2012;448(3):329-41.

32. Lupoli TJ, Tsukamoto H, Doud EH, Wang T-SA, Walker S, Kahne D. Transpeptidase-Mediated Incorporation of d-Amino Acids into Bacterial Peptidoglycan. Journal of the American Chemical Society. 2011;133(28):10748-51.

33. Lin H, Yang C, Wang W. Imitate to illuminate: labeling of bacterial peptidoglycan with fluorescent and bio-orthogonal stem peptide-mimicking probes. RSC Chemical Biology. 2022;3(10):1198-208.

34. Lam H, Oh DC, Cava F, Takacs CN, Clardy J, de Pedro MA, Waldor MK. D-amino acids govern stationary phase cell wall remodeling in bacteria. Science. 2009;325(5947):1552-5.

35. Caldwell M, Hughes M, Wei F, Ngo C, Pascua R, Pugazhendhi AS, Coathup MJ. Promising applications of D-amino acids in periprosthetic joint infection. Bone Research. 2023;11(1):14.

36. Caparrós M, Pisabarro AG, Pedro MAd. Effect of D-amino acids on structure and synthesis of peptidoglycan in Escherichia coli. J Bacteriol. 1992;174(17):5549-59.

37. Caparrós M, Torrecuadrada JLM, de Pedro MA. Effect of D-amino acids on Escherichia coli strains with impaired penicillin-binding proteins. Research in Microbiology. 1991;142(2):345-50.

38. Cava F, de Pedro MA, Lam H, Davis BM, Waldor MK. Distinct pathways for modification of the bacterial cell wall by non-canonical D-amino acids. The EMBO Journal. 2011;30(16):3442-53.

39. Lam H, Oh D-C, Cava F, Takacs CN, Clardy J, de Pedro MA, Waldor MK. D-Amino Acids Govern Stationary Phase Cell Wall Remodeling in Bacteria. Science. 2009;325(5947):1552-5.

40. Neumann KD, Villanueva-Meyer JE, Mutch CA, Flavell RR, Blecha JE, Kwak T, Sriram R, VanBrocklin HF, Rosenberg OS, Ohliger MA, Wilson DM. Imaging Active Infection in vivo Using D-Amino Acid Derived PET Radiotracers. Scientific Reports. 2017;7(1):7903.

41. Kwak TS. Evaluation of D-Amino Acids as Probes for Molecular Imaging of Bacterial Infections [Msc Thesis]: University of California, San Francisco; 2015.

42. Stewart MN, Parker MFL, Jivan S, Luu JM, Huynh TL, Schulte B, Seo Y, Blecha JE, Villanueva-Meyer JE, Flavell RR, VanBrocklin HF, Ohliger MA, Rosenberg O, Wilson DM. High Enantiomeric Excess In-Loop Synthesis of d-[methyl-11C]Methionine for Use as a Diagnostic Positron Emission Tomography Radiotracer in Bacterial Infection. ACS Infect Dis. 2020;6(1):43-9.

43. Muranaka Y, Mizutani A, Kobayashi M, Nakamoto K, Matsue M, Nishi K, Yamazaki K, Nishii R, Shikano N, Okamoto S, Kawai K. Comparison of L- and D-Amino Acids for Bacterial Imaging in Lung Infection Mouse Model. International Journal of Molecular Sciences. 2022;23(5):2467.

44. Polvoy I, Seo Y, Parker M, Stewart M, Siddiqua K, Manacsa HS, Ravanfar V, Blecha J, Hope TA, Vanbrocklin H, Flavell RR, Barry J, Hansen E, Villanueva-Meyer JE, Engel J, Rosenberg OS, Wilson DM, Ohliger MA. Imaging joint infections using D-methyl-11C-methionine PET/MRI: initial experience in humans. Eur J Nucl Med Mol Imaging. 2022;49(11):3761-71.

45. Sorlin A, Parker M, Wilson D. P-032 - Radiosynthesis of 18F labelled D-amino acid tracers and their use for bacteria imaging. Nuclear Medicine and Biology. 2022;108-109:S68.

46. Parker MFL, Luu JM, Schulte B, Huynh TL, Stewart MN, Sriram R, Yu MA, Jivan S, Turnbaugh PJ, Flavell RR, Rosenberg OS, Ohliger MA, Wilson DM. Sensing Living Bacteria in Vivo Using d-Alanine-Derived 11C Radiotracers. ACS Cent Sci. 2020;6(2):155-65.

47. Ermert J, Coenen HH. Methods for 11C- and 18F-labelling of amino acids and derivatives for positron emission tomography imaging. Journal of Labelled Compounds and Radiopharmaceuticals. 2013;56(3-4):225-36.

48. Morlot C, Straume D, Peters K, Hegnar OA, Simon N, Villard A-M, Contreras-Martel C, Leisico F, Breukink E, Gravier-Pelletier C, Le Corre L, Vollmer W, Pietrancosta N, Håvarstein LS, Zapun A. Structure of the essential peptidoglycan amidotransferase MurT/GatD complex from Streptococcus pneumoniae. Nature Communications. 2018;9(1):3180.

49. Renick PJ, Mulgaonkar A, Co CM, Wu C-Y, Zhou N, Velazquez A, Pennington J, Sherwood A, Dong H, Castellino L, Öz OK, Tang L, Sun X. Imaging of Actively Proliferating Bacterial Infections by Targeting the Bacterial Metabolic Footprint with d-[5-11C]-Glutamine. ACS Infect Dis. 2021;7(2):347-61.

50. Münch D, Engels I, Müller A, Reder-Christ K, Falkenstein-Paul H, Bierbaum G, Grein F, Bendas G, Sahl HG, Schneider T. Structural variations of the cell wall precursor lipid II and their influence on binding and activity of the lipoglycopeptide antibiotic oritavancin. Antimicrob Agents Chemother. 2015;59(2):772-81.

51. Schwartz B, Markwalder JA, Wang Y. Lipid II: Total Synthesis of the Bacterial Cell Wall Precursor and Utilization as a Substrate for Glycosyltransfer and Transpeptidation by Penicillin Binding Protein (PBP) 1b of Eschericia coli. Journal of the American Chemical Society. 2001;123(47):11638-43.

52. Muranaka Y, Matsue M, Mizutani A, Kobayashi M, Sato K, Kondo A, Nishiyama Y, Ohata S, Nishi K, Yamazaki K, Nishii R, Shikano N, Okamoto S, Kawai K. Evaluation of L-

Alanine Metabolism in Bacteria and Whole-Body Distribution with Bacterial Infection Model Mice. International Journal of Molecular Sciences. 2023;24(5):4775.

53. Rowan-Nash AD, Korry BJ, Mylonakis E, Belenky P. Cross-Domain and Viral Interactions in the Microbiome. Microbiology and Molecular Biology Reviews. 2019;83(1):e00044-18.

54. Radkov AD, Moe LA. Bacterial synthesis of d-amino acids. Applied Microbiology and Biotechnology. 2014;98(12):5363-74.

55. Tanner ME. Understanding Nature's Strategies for Enzyme-Catalyzed Racemization and Epimerization. Accounts of Chemical Research. 2002;35(4):237-46.

56. Cava F, Lam H, de Pedro MA, Waldor MK. Emerging knowledge of regulatory roles of d-amino acids in bacteria. Cellular and Molecular Life Sciences. 2011;68(5):817-31.

57. Espaillat A, Carrasco-López C, Bernardo-García N, Rojas-Altuve A, Klett J, Morreale A, Hermoso JA, Cava F. Binding of non-canonical peptidoglycan controls Vibrio cholerae broad spectrum racemase activity. Comput Struct Biotechnol J. 2021;19:1119-26.

58. Wu H, Xue E, Zhi N, Song Q, Tian K, Caiyin Q, Yuan L, Qiao J. d-Methionine and d-Phenylalanine Improve Lactococcus lactis F44 Acid Resistance and Nisin Yield by Governing Cell Wall Remodeling. Appl Environ Microbiol. 2020;86(9).

59. Kuru E, Radkov A, Meng X, Egan A, Alvarez L, Dowson A, Booher G, Breukink E, Roper DI, Cava F, Vollmer W, Brun Y, VanNieuwenhze MS. Mechanisms of Incorporation for D-Amino Acid Probes That Target Peptidoglycan Biosynthesis. ACS Chemical Biology. 2019;14(12):2745-56.

60. Ene IV, Brunke S, Brown AJ, Hube B. Metabolism in fungal pathogenesis. Cold Spring Harb Perspect Med. 2014;4(12):a019695.

61. Garbe E, Vylkova S. Role of Amino Acid Metabolism in the Virulence of Human Pathogenic Fungi. Current Clinical Microbiology Reports. 2019;6(3):108-19.

62. Co CM, Mulgaonkar A, Zhou N, Harris S, Öz OK, Tang L, Sun X. PET Imaging of Active Invasive Fungal Infections with d-[5-11C]-Glutamine. ACS Infectious Diseases. 2022;8(8):1663-73.

63. Wang L, Zha Z, Qu W, Qiao H, Lieberman BP, Plössl K, Kung HF. Synthesis and evaluation of 18F labeled alanine derivatives as potential tumor imaging agents. Nuclear Medicine and Biology. 2012;39(7):933-43.

64. Pidgeon SE, Fura JM, Leon W, Birabaharan M, Vezenov D, Pires MM. Metabolic Profiling of Bacteria by Unnatural C-terminated D-Amino Acids. Angew Chem Int Ed Engl. 2015;54(21):6158-62.

65. Mota F, Jain SK. Flagging Bacteria with Radiolabeled d-Amino Acids. ACS Central Science. 2020;6(2):97-9.

66. Liechti GW, Kuru E, Hall E, Kalinda A, Brun YV, VanNieuwenhze M, Maurelli AT. A new metabolic cell-wall labelling method reveals peptidoglycan in Chlamydia trachomatis. Nature. 2014;506(7489):507-10.

67. Parker MFL, Luu JM, Schulte B, Huynh TL, Stewart MN, Sriram R, Yu MA, Jivan S, Turnbaugh PJ, Flavell RR, Rosenberg OS, Ohliger MA, Wilson DM. Sensing Living Bacteria in Vivo Using d-Alanine-Derived 11C Radiotracers. ACS Central Science. 2020;6(2):155-65.

68. Goodell EW. Recycling of murein by Escherichia coli. J Bacteriol. 1985;163(1):305-10.

69. T. Tsuruoka AT, A. Miyata, T. Takei, s. Snouye and M. Matsuhashi. Second lytic target of β-lactam compounds that have a terminal d-amino acid residue. European Journal of Biochemistry. 1985;151(2):209-16.

70. Browne S, Bhatia S, Sarkar N, Kaushik M. Antibiotic-resistant bacteria and antibiotic-resistant genes in agriculture: a rising alarm for future. In: Singh P, Sillanpää M, editors. Degradation of Antibiotics and Antibiotic-Resistant Bacteria from Various Sources. India: Academic Press; 2023. p. 247-74.

71. Filp U, Pekošak A, Poot AJ, Windhorst AD. Stereocontrolled [11C]Alkylation of N-Terminal Glycine Schiff Bases To Obtain Dipeptides. European Journal of Organic Chemistry. 2017;2017(37):5592-6.

72. Al-Dabbagh B, Henry X, Ghachi ME, Auger G, Blanot D, Parquet C, Mengin-Lecreulx D, Bouhss A. Active site mapping of MraY, a member of the polyprenyl-phosphate N-acetylhexosamine 1-phosphate transferase superfamily, catalyzing the first membrane step of peptidoglycan biosynthesis. Biochemistry. 2008;47(34):8919-28.

73. Huang L-Y, Huang S-H, Chang Y-C, Cheng W-C, Cheng T-JR, Wong C-H. Enzymatic Synthesis of Lipid II and Analogues. Angewandte Chemie International Edition. 2014;53(31):8060-5.

74. Al-Dabbagh B, Olatunji S, Crouvoisier M, El Ghachi M, Blanot D, Mengin-Lecreulx D, Bouhss A. Catalytic mechanism of MraY and WecA, two paralogues of the polyprenyl-phosphate N-acetylhexosamine 1-phosphate transferase superfamily. Biochimie. 2016;127:249-57.

75. Bouhss A, Crouvoisier M, Blanot D, Mengin-Lecreulx D. Purification and characterization of the bacterial MraY translocase catalyzing the first membrane step of peptidoglycan biosynthesis. J Biol Chem. 2004;279(29):29974-80.

76. Hammes WP, Neuhaus FC. On the Specificity of Phospho-N-acetylmuramyl-pentapeptide Translocase: THE PEPTIDE SUBUNIT OF URIDINE DIPHOSPHATE-N-ACETYLMURAMYL-PENTAPEPTIDE. Journal of Biological Chemistry. 1974;249(10):3140-50.

77. Sadamoto R, Niikura K, Sears PS, Liu H, Wong C-H, Suksomcheep A, Tomita F, Monde K, Nishimura S-I. Cell-Wall Engineering of Living Bacteria. Journal of the American Chemical Society. 2002;124(31):9018-9.

78. Sadamoto R, Niikura K, Ueda T, Monde K, Fukuhara N, Nishimura S-I. Control of Bacteria Adhesion by Cell-Wall Engineering. Journal of the American Chemical Society. 2004;126(12):3755-61.

79. Born P, Breukink E, Vollmer W. In Vitro Synthesis of Cross-linked Murein and Its Attachment to Sacculi by PBP1A from Escherichia coli. Journal of Biological Chemistry. 2006;281(37):26985-93.

80. Bertsche U, Breukink E, Kast T, Vollmer W. In Vitro Murein (Peptidoglycan) Synthesis by Dimers of the Bifunctional Transglycosylase-Transpeptidase PBP1B from Escherichia coli. Journal of Biological Chemistry. 2005;280(45):38096-101.

81. Ye X-Y, Lo M-C, Brunner L, Walker D, Kahne D, Walker S. Better Substrates for Bacterial Transglycosylases. Journal of the American Chemical Society. 2001;123(13):3155-6.

82. van Heijenoort J. Lipid intermediates in the biosynthesis of bacterial peptidoglycan. Microbiol Mol Biol Rev. 2007;71(4):620-35.

83. Sadamoto R, Matsubayashi T, Shimizu M, Ueda T, Koshida S, Koda T, Nishimura S-I. Bacterial Surface Engineering Utilizing Glucosamine Phosphate Derivatives as Cell Wall Precursor Surrogates. Chemistry – A European Journal. 2008;14(33):10192-5.

84. Uehara T, Park JT. The N-acetyl-D-Glucosamine Kinase of Escherichia coli and Its Role in Murein Recycling. J Bacteriol. 2004;186(21):7273-9.

85. Reith J, Berking A, Mayer C. Characterization of an N-acetylmuramic acid/N-acetylglucosamine kinase of Clostridium acetobutylicum. J Bacteriol. 2011;193(19):5386-92.

86. Reith J, Mayer C. Peptidoglycan turnover and recycling in Gram-positive bacteria. Applied Microbiology and Biotechnology. 2011;92(1):1-11.

87. Martínez ME, Kiyono Y, Noriki S, Inai K, Mandap KS, Kobayashi M, Mori T, Tokunaga Y, Tiwari VN, Okazawa H, Fujibayashi Y, Ido T. New radiosynthesis of 2-deoxy-2-[18F]fluoroacetamido-d-glucopyranose and its evaluation as a bacterial infections imaging agent. Nuclear Medicine and Biology. 2011;38(6):807-17.

88. Hu Y, Chen L, Ha S, Gross B, Falcone B, Walker D, Mokhtarzadeh M, Walker S. Crystal structure of the MurG: UDP-GlcNAc complex reveals common structural principles of a superfamily of glycosyltransferases. Proceedings of the National Academy of Sciences. 2003;100(3):845-9.

89. Xu Y, Hernández-Rocamora VM, Lorent JH, Cox R, Wang X, Bao X, Stel M, Vos G, van den Bos RM, Pieters RJ, Gray J, Vollmer W, Breukink E. Metabolic labeling of the bacterial peptidoglycan by functionalized glucosamine. iScience. 2022;25(8):104753.

90. Helm JS, Hu Y, Chen L, Gross B, Walker S. Identification of Active-Site Inhibitors of MurG Using a Generalizable, High-Throughput Glycosyltransferase Screen. Journal of the American Chemical Society. 2003;125(37):11168-9.

91. Carroll L, Witney TH, Aboagye EO. Design and synthesis of novel 18F-radiolabelled glucosamine derivatives for cancer imaging. MedChemComm. 2013;4(4):653-6.

92. Gisin J, Schneider A, Nägele B, Borisova M, Mayer C. A cell wall recycling shortcut that bypasses peptidoglycan de novo biosynthesis. Nature Chemical Biology. 2013;9(8):491-3.

93. Liang H, DeMeester KE, Hou C-W, Parent MA, Caplan JL, Grimes CL. Metabolic labelling of the carbohydrate core in bacterial peptidoglycan and its applications. Nature communications. 2017;8(1):15015.

94. Fujiwara T, Kubota K, Sato T, Matsuzawa T, Tada M, Iwata R, Itoh M, Hatazawa J, Sato K, Fukuda H, Ido T. N-[18F]fluoroacetyl-D-glucosamine: a potential agent for cancer diagnosis. J Nucl Med. 1990;31(10):1654-8.

95. Olrichs NK, Aarsman MEG, Verheul J, Arnusch CJ, Martin NI, Hervé M, Vollmer W, de Kruijff B, Breukink E, den Blaauwen T. A novel in vivo cell-wall labeling approach sheds new light on peptidoglycan synthesis in Escherichia coli. ChemBioChem. 2011;12(7):1124-33.

96. Hervé M, Boniface A, Gobec S, Blanot D, Mengin-Lecreulx D. Biochemical characterization and physiological properties of Escherichia coli UDP-N-acetylmuramate:L-alanyl-gamma-D-glutamyl-meso-diaminopimelate ligase. J Bacteriol. 2007;189(11):3987-95.

CHAPTER 3EVALUATING THE POTENTIAL PEPTIDOGLYCAN RADIOTRACERS FOR CLINICAL INFECTION IMAGING TRANSLATION: A SYSTEMATIC ANALYSIS

Palesa. C. Koatale[a, b], Amanda Mdlophane[a, b], Mike .M. Sathekge [a,b], Thomas Ebenhan[a, b, c *]

a. Department of Nuclear Medicine, University of Pretoria, 0001 Pretoria, South Africa

b. Nuclear Medicine Research Infrastructure (NuMeRI) NPC, 0001 Pretoria, South Africa

c. DSI/NWU Pre-clinical Drug Development Platform, North-west University, 2520 Potchefstroom, South Africa

Corresponding author

*) Authors to whom correspondence should be addressed.
Thomas.Ebenhan@up.co.za

Manuscript in preparation for submission

ABSTRACT

Peptidoglycan PET imaging has been proposed as a diagnostic tool for the specific detection and localization of bacterial infections with the potential to identify the causative pathogen. Numerous radiotracers targeting the peptidoglycan biosynthesis pathway have been established and tested in the preclinical phase, however, clinical data is still outstanding. A meta-analysis was conducted to assess the diagnostic accuracy, and clinical impact of peptidoglycan-based radiotracers for bacterial infection imaging using PET. A total of six studies met the eligibility criteria and were assessed for quality in terms of study designs and applicability using the Quality Assessment of Diagnostic Accuracy Studies (QUADAS) tool. Most of the radiotracers reported showed potential to discriminate infection from inflammation, however, the high background signal observed with some radiotracers might jeopardize diagnostics accuracy and ultimate translation into routine clinical use.

Keywords: Peptidoglycan- bacteria-radiotracers- PET imaging-preclinical-clinical- QUADAS

3.1 INTRODUCTION

Clinical diagnosis of bacterial infections using nuclear medicine modalities such as positron emission tomography (PET) and single-photon emission computed tomography (SPECT) remains a challenge [1, 2]. This is mainly due to a lack of bacteria-specific radiotracers, as a result, there is a great demand for innovative imaging radiotracers capable of specifically targeting bacterial-associated infections [3, 4]. Peptidoglycan, found on bacterial cell walls, has emerged as a promising target for molecular imaging, with a focus on the detection and characterisation of bacterial infections, due to its unique biochemical structure and essential function in bacterial physiology [5, 6]. Several preclinical studies utilising peptidoglycan-targeted imaging radiotracers have been evaluated in various animal models of mainly gram-negative and -positive bacterial-induced infections [7].

These studies have demonstrated the ability of peptidoglycan imaging to accurately localise and quantify bacterial burdens in different tissues and organs, providing valuable insights into disease pathogenesis and treatment outcomes. In addition, a clinical trial evaluating a peptidoglycan-based radiotracer in human participants has shown encouraging results, validating the feasibility and safety of this approach in the clinical setting [8]. This highlights the significant progress made in development of peptidoglycan-targeted imaging tracers for nuclear medicine applications. However, as it currently stands, none of the peptidoglycan-based radiotracers have been approved for clinical use.

This investigation is aimed to perform a semi-meta-analysis to evaluate the diagnostic accuracy, and clinical impact of currently available peptidoglycan-based radiotracers for imaging of bacterial infections, using the QUADAS (Quality Assessment of Diagnostic Accuracy Studies) tool.

3.2 MATERIALS AND METHODS

3.2.1 Inclusion and Exclusion Criteria

The original published research articles that assessed the performance of peptidoglycan-based radiotracers for bacterial infection imaging, were included. The research studies with radiotracers that were not specific to bacteria, had no imaging evaluation reported and focused only on *in vitro* studies,or technical data were excluded (**Figure 1**).

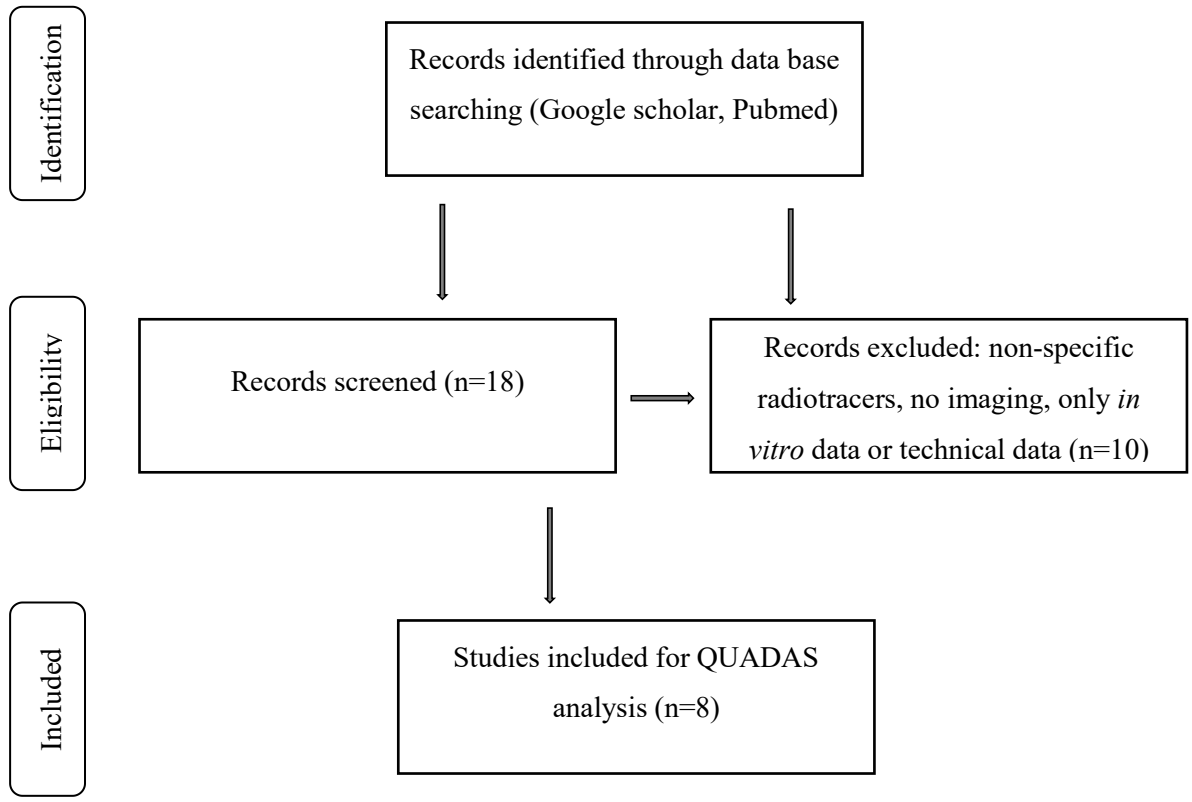

Figure 3- 1: Exclusion and inclusion criteria for studies included in the systematic analysis.

3.2.2 Quality Assessment

The analysis of the radiotracers for potential clinical translation was carried out using QUADAS as guidance to address any potential bias and variation [9]. The standardised questionnaire and assessment approach described by Auletta et al. [10] was implemented by evaluating the following variables for risk assessment of any potential bias (**Annexure A-B**):

(1) Animal selection bias (animal origin, animal model);

(2) Infection model bias (bacterium origin, bacterium number);

(3) Experimental design variation (infection model and radiopharmaceutical purity);

(4) Reference standard bias (inappropriate reference standard, incorporation bias);

(5) Reference standard variation (definition of control model);

(6) Flow and timing bias (infection progression bias, radiopharmaceutical administration time, imaging time bias, uninterpretable test results, and sample size).

3.3 RESULTS

Based on the database valuation, 6 research articles that investigated peptidoglycan-based radiotracers for infection imaging using PET/CT, as summarised in **Table 1**, were included for analysis (**Table 2**) to assess the diagnostic potential in the clinical setting.

3.3.1 Carbon-11 labeled radiopharmaceuticals

Radionuclide Carbon-11 (^{11}C; C-11) has been widely explored for PET/CT-based infection imaging due to its attractive chemical properties. C-11 has a short half-life of 20.4 min and can be directly complexed to target molecules with less isotopic dilution required for quality control [11, 12]. The advances in radiolabelling strategies using C-11 have been well demonstrated for amino acids [12]. D- and L-amino acids are the main building blocks of the peptidoglycan's peptide structure. A few studies have evaluated D-amino acids for PET/CT imaging of gram-negative and -positive-induced infections using C-11.

In a study by Neumann et al. [13] that screened several D-amino acid radiotracers in a panel of gram-negative and -positive bacteria, D-[^{11}C]Met showed promising results for infection imaging. The *in vivo* uptake of D-[^{11}C]Met in live and heat-killed *Escherichia coli* (*E. coli)* and *Staphylococcus aureus* (*S. aureus)* in a dual-murine myositis model was compared to L-[^{11}C]Met as a reference standard. Although rapid and high specific accumulation (>2-fold higher) was reported at the site of infection in comparison with the inflammation site, the visibility of D-[^{11}C]Met at the site of inflammation and high-background signal, might limit the applicability of the tracer in clinical translation. However, the unspecified number of bacteria that were inoculated, and the choice of the reference standard might have been the source of bias in the study. Polvoy et al. [8] reported the first-in-Human administration of D-[^{11}C]Met in patients with suspected prosthetic joint infection, thereby, comparing the tracer signal to the contralateral non-infected joints. Similar to the animal studies by Neumann et al. [13], D-[^{11}C]Met demonstrated high non-specific uptake in major organs (liver, lungs, heart, and kidneys). Although the study reported 1.5 times higher tracer accumulation in infected (suspected) prosthetic joints infection than contralateral joints, the selection of patients, the unspecified source of infection, the number of patients and the exclusion of reference standards might have introduced a high risk of bias. The authors concluded that the data obtained could not highlight the diagnostic power of D-[^{11}C]Met for joint infections, however, further studies are required to validate the promising results. We believe that a carefully selected patient population with confirmed infection sites will provide the desired results to support a decision on the role and value of D-[^{11}C]Met as an infection PET-imaging agent.

Renick et al. [14] investigated the diagnostic potential of D-[^{11}C]Gln dual-infection murine myositis model of *E. coli* and methicillin-resistant *Staphylococcus aureus* (MRSA) *versus* heat-killed bacterial strains following promising results obtained from *in vitro* uptake studies. The authors reported high imaging contrast in muscle tissue infected with either live *E. coli* (1.79 ± 0.29) or MRSA (2.30 ± 0.59) in comparison to tissue exposed to heat-killed bacteria. Furthermore, the study reported non-specific uptake with L-[^{11}C]Gln (control) in a similar infection model. Subsequently, the study compared the head-to-head performance of D-[^{11}C]Gln against [^{18}F]FDG in a sterile model with turpentine oil-induced tissue inflammation. Although the group reported high specificity of D-[^{11}C]Gln over [^{18}F]FDG at the site of inflammation, a non-dual model of infection and inflammation was used, respectively, the type of animal model

used and the study design can be seen as bias risks. The type of animal model and the study design can be seen as bias risks. Furthermore, the high background signal seen with both D-[^{11}C]Gln and [^{18}F]FDG might have introduced biases in the interpretation of the data. Therefore, in agreement with the authors, reducing the limitations of the study design is needed to obtain more robust results to justify D-[^{11}C]Gln for clinical investigations.

Parker et al. [15] evaluated the specificity of D-[^{11}C]Ala in different animal infection models representative of different conditions. Using a dual-infection murine myositis model of *E. coli* and *S. aureus*, D-[^{11}C]Ala was able to outperform [^{18}F]FDG and [^{68}Ga]citrate differentiating infection from inflammation. The QUADAS analysis revealed no sources of biases for this study.

The same study further evaluated the performance D-[^{11}C]Ala-PET imaging for the tissue response assessment following antibiotic treatment using a dual-infection model of antibiotic-sensitive and antibiotic-resistant *E. coli*. Interestingly, the data showed that D-[^{11}C]Ala efficiently monitored treatment response, which is a key challenge in clinical practice. However, we analysed that the unspecified number of animals used, and the short imaging time (3 hrs) post-treatment might have introduced the source of bias and thereby questioned the clinical bedside value of the results. Additionally, the study also evaluated D-[^{11}C]Ala for the diagnostic potential of discitis-osteomyelitis induced by inoculation of a bioluminescent *S. aureus* strain (5×10^6 cfu) within the third intervertebral base of the tail. The study reported a 3.3-fold increase of D-[^{11}C]Ala accumulation at the infection site compared to the normal background tissue. However, as much as we understand the proof-of-concept character of the presented results, the tail vein administration of the radiotracer which was in the direct vicinity of the infectious foci might be a risk for a biased outcome (for this particular preclinical setting). We expect that the D-[^{11}C]Ala tissue/background ratio may be higher than reported, which would recommend D-[^{11}C]Ala-PET for localization of discitis.

Finally, the study investigated the specificity of D-[^{11}C]Ala-PET/CT towards detection of *Pseudomonas aeruginosa (P. aeruginosa)* -induced pneumonia. Although the study demonstrated a significant (1.8-fold) accumulation of D-[^{11}C]Ala in the infected lung lobes relative to healthy lungs, the non-specific background signal observed in the healthy lungs might have introduced a high risk of bias. In agreement with the authors, the high-background signal observed with D-[^{11}C]Ala might limit the applicability in lung-related infection detection.

3.3.2 Fluorine-18 (^{18}F) labeled radiopharmaceuticals

Fluorine-18 (^{18}F, F-18) is the most used radioisotope for PET/CT imaging procedures due to its half-life of 109 min and its ability to conjugate with a wide variety of molecules including proteins, peptides and oligopeptides [16]. The F-18 radiosynthesis has been reported in a few studies using peptidoglycan backbone molecules including N-acetylglucosamine (GlcNAc) and N-acetylmuramic acid (MurNAc) for specific targeting of bacterial infections.

Martínez et al. [17] investigated [^{18}F]FAG, a radioactive N-acetylglucosamine derivative, both *in vitro* and *in vivo* for PET/CT imaging of bacterial infections. Following positive findings in *vitro*, further evaluation included E. *coli* murine myositis model of infection (against sterile tissue inflammation). The QUADAS analysis on [^{18}F]FAG highlights the level of tracer specificity and selectivity for infection (also compared to [^{18}F]FDG-PET). This study's results could be even firmer if the dual model of infection and inflammation was utilized; the different scan protocol between the infection- versus inflammation cohort might have introduced biases. The realistic level of accuracy and specificity may be even higher than reported making [^{18}F]FAG an attractive infection imaging candidate.

Lee et al. [18], evaluated N-acetylmuramic acid (MurNAc) derivatives, (S)-[^{18}F]FMA and (R)-[^{18}F]FMA, for specific targeting of bacterial infections. After screening the radiotracers in a panel of gram-negative and -positive bacterial strains, the diagnostic potential of the radiotracers was further investigated using *S. aureus*, *E. coli*, or *Staphylococcus epidermidis* (*S. epidermidis)*-induced murine myositis models. The authors demonstrated that (S)-[^{18}F]FMA and (R)-[^{18}F]FMA have high specificity for infection over inflammation, with a partial selectivity for gram-positive and -negative bacteria, respectively. The study design further explored the limit of detection (sensitivity) for (R)-[^{18}F]FMA at 10^5 cfu, which is below the bacterial burden in the acute phase ($\geq 10^7$ cfu) [19]. The QUADA analysis found no sources of risk or bias and we can thereby suggest clinical exploration to ascertain the preclinical findings. Following strict inclusion and exclusion criteria for the enrolment of patients and the capability of (R)-[^{18}F]FMA-PET/CT to even differentiate gram-positive from -negative bacteria species *in vivo* (or not) can be addressed within the clinical setting.

In 2024, Sirlon et al. [20], synthesised ^{18}F-trifluoromethylated D-alanine, [^{18}F]3,3,3-trifluoro-d-alanine (D-[^{18}F]-CF_3-Ala) for bacterial infection imaging. The study screened the bacterial uptake of the radiotracer in a panel of gram-negative and positive bacteria with highest uptake mostly recorded for gram-negative species. The *in vivo* evaluation of [^{18}F]-CF_3-Ala in *E. coli* induced murine myositis model showed 2.4-fold higher selectivity for infection compared to heat-killed infection.

This was followed by a study by Li et al. [21] which reported the peptidoglycan targeting of potential of ^{18}F-monofluorinated D-alanine. The group synthesised D-[^{18}F]Fluoroalanine (D-[^{18}F]FAla) and deuterium- analogue_D-[^{18}F]Fluoroalanine-d_3 (D-[^{18}F]FAla-d_3) for analysis in *E. coli* and *S. aureus*. Similar to [^{18}F]-CF_3-Ala, D-[18F]FAla and D-[^{18}F]FAla-d_3 showed high selective uptake for gram-negative compared to gram-positive bacterial. This observation may be attributed to differences in cell wall structural properties and/or metabolic pathways of gram-negative vs positive bacteria. The in *vivo* PET/CT performance of [^{18}F]FAla and D-[^{18}F]FAla-d_3 was analysed using *S. aureus* infection model and the results demonstrated significant radiotracer uptake at the site of infection in comparison to heat-killed inflammation (Infection/Inflammation ratio= [^{18}F]FAla _1.92 ± 0.42 vs D-[^{18}F]FAla-d3_ 1.77 ± 0.32). The QUADA analysis of both studies found no sources of risk or bias, however, head-to-head comparison of D-[^{18}F]FAla,[^{18}F]-CF_3-Ala and D-[^{18}F]FAla under same conditions is recommended to further evaluate performance and qualify for clinical evaluation.

Table 3- 1: Summary of experimental design and outcomes of studies included in the systematic analysis.

First author reference	Tracer	Pathogen	%RCP	Stability	Model	Amount (cfu) and Infection site	Scan Time
Neumann, KD [13]	D-[^{11}C]Met	*E. coli* *S. aureus*	92.6 % ± 2. 4 %	-	CBA/J mice	NA, shoulder muscle	-
Polyvoy, I [8]	D-[^{11}C]Met	-	>95 %	-	Patients suspected with PJI	-	Sequential up to 81 min post-injection
Renick, PJ [14]	D-[^{11}C]Gln	*E. coli* MRSA	>90 %	-	CD-1 IGS mice	NA, hind limb muscles (MRSA to the right and E. coli to the left)	12 hr post-inoculation
Parker, MF [15]	D-[^{11}C]Ala	*E. coli* *S. aureus*	>95 % in all cases	-	CBA/J mice	10^6, shoulder muscle	10 hr post-inoculation
		P. aeruginosa	>95 %		CBA/J mice	10^6, intratracheally	6 hr post-

			in all cases				infection
		bioluminescent *S. aureus*	>95 % in all cases		Sprague/Dawley rats	10^6, intervertebral base of tail	14 days post-infection
		ampicillin-sensitive and resistant *E. coli*	>95 % in all cases		CBA/J mice	10^6, shoulder muscule	5 hr post-infection 3 hr post-treatment
Martínez, ME [17]	[^{18}F]FAG	*E. coli*	>98 %	-	Sprague-Dawley rats	10^7, right front leg muscle	2 days post-inoculation
Lee, SH [18]	(S)-[^{18}F]FMA	*E. coli* *S. aureus* *S. epidermidis*	>99 %	>95% in saline & serum up to 90 min	CBA/J mice	10^6 cfu, left shoulder muscle	10 hr post-inoculation
	(R)-[^{18}F]FMA	*E. coli* *S. aureus* *S. epidermidis*	>99 %	>95% in saline & serum up to 90 min	CBA/J mice	10^6 cfu, left shoulder muscle	10 hr post-inoculation

Sorlin, MA[20]	D-[^{18}F]-CF_3-Ala	*E. coli*	> 99 %	>95% in saline & serum up to 120 min	CBA/J mice	~ 2 × 10^7 left deltoid muscle	12h post-inoculation
Li, K[21]	D-[^{18}F]FAla	*S. aureus*	>99 %	>98% in saline up to 3 h	Sprague–Dawley rats	~10^8 cfu right triceps	2–3 days post-inoculation
	D-[^{18}F]FAla-d_3	*S. aureus*	>99 %	>98% in saline up to 3 h	Sprague–Dawley rats	~10^8 cfu right triceps	2–3 days post-inoculation

Abbreviations: RCP = radiochemical purity; NA: Not applicable; E. *coli* = *Escherichia coli*_gram-positive, *P. aeruginosa=Pseudomonas aeruginosa*_gram-negative*; S. aureus* = *Staphylococcus aureus*_gram-positive; Methicillin-resistant *S. aureus* (MRSA); *S. epidermidis=Staphylococcus epidermidis*_gram-positive; T/NT= Target-to-non-Target

Table 3-1: Summary of experimental design and outcomes of studies included in the systematic analysis. (Continue)

First author reference	Tracer	Control Experiment	Metabolic Route	Max T/NT Ratio	Reference	Author's comments
Neumann, KD [13]	D-[^{11}C]Met	heat-killed bacteria	Kidneys, liver	-	Compared with [^{11}C] L-Met	Attractive radiotracer for infection imaging in clinical practice.
Polyvoy, I [8]	D-[^{11}C]Met	Healthy patients	Kidneys, liver	-	-	Data cannot establish diagnostic utility application
Renick, PJ [14]	D-[^{11}C]Gln	heat-killed bacteria, Turpentine oil	urine and faeces	E. coli: 1.79 ± 0.29 MRSA: 2.30 ± 0.59	Compared with L-[^{11}C]Gln and [^{18}F]FDG	Systematic approach needs to be implemented
Parker, MF [15]	D-[^{11}C]Ala	heat-killed bacteria	lungs, pancreas, kidneys and liver	-	Compared with[^{18}F]FDG, [^{68}Ga]citrate	Data justifies for clinical translation

		-	lungs, pancreas, kidneys and liver	-	-	Easy detection in high background areas
		-	-	-	-	Suitable for sterile areas eg spine and joint infections
		Post-treatment with ampicillin	lungs, pancreas, kidneys and liver	-	-	Evaluate antibiotic response
Martínez, ME [17]	[^{18}F]FAG	Turpentine oil (Scan 24hr post-induction)	Kidneys, liver	-	Compared with [^{18}F]FDG	Ability to discriminate infection from inflammation
Lee, SH [18]	(S)-[^{18}F]FMA	heat-killed bacteria	kidneys	*S. aureus: 7.47 ± 0.87* *E. coli: 3.55 ± 0.84* *S. epidermidis: 1.65 ± 0.02* *(Live vs heat killed)*	-	Partial selectivity for Gram-positive bacteria
	(R)-	heat-killed	kidneys	*S. aureus:* 6.67 ± 2.73;	10^4 vs 10^5 vs 10^6	Partial selectivity

	[^{18}F]FMA	bacteria		*E. coli*: 2.02 ± 0.63 *S. epidermidis*: 3.82 ± 0.49 (Live vs heat killed)	cfus *S. aureus*	for Gram-negative bacteria
Sorlin, MA[20]	D-[^{18}F]-CF_3-Ala	heat-killed bacteria	kidneys	-	-	Robust incorporation into peptidoglycan
Li, K[21]	D-[^{18}F]FAla	heat-killed bacteria	Kidneys Bone	1.92 ± 0.42 (infected vs heat-killed) 2.01 ± 0.32 (infected vs healthy muscle)	-	Ability to differentiate infection from inflammation
	D-[^{18}F]FAla-d_3	heat-killed bacteria	Kidneys Bone	1.77 ± 0.32 (infected vs heat-killed) 2.08 ± 0.43 (infected vs healthy muscle)	-	Ability to differentiate infection from inflammation

Abbreviations: RCP = radiochemical purity; NA: Not applicable; E. *coli* = *Escherichia coli*_gram-positive, *P. aeruginosa*=*Pseudomonas aeruginosa*_gram-negative*; S. aureus* = *Staphylococcus aureus*_gram-positive; Methicillin-resistant *S. aureus* (MRSA); *S. epidermidis*=*Staphylococcus epidermidis*_gram-positive; T/NT= Target-to-non-Target

Table 3- 2: Summary of QUADAS analysis.

	Study details		Risk Bias				Applicability Concerns		
Fist Author	**Animal model/patient population**	**Radiotracer**	**Animal/patient selection**	**Index text**	**Reference standard**	**Experim. Flow /Timing**	**Animal/patient Selection**	**Index Text**	**Reference Standard**
			Carbon-11 Radiopharmaceuticals						
Neumann, KD [13]	Murine (myositis)	D-[^{11}C]Met							
Polvoy, I [8]	Human PJI (suspected)	D-[^{11}C]Met							
Renick, PJ [14]	Murine (myositis)	D-[^{11}C]Gln							
Parker, MF [22]	Murine (myositis)	D-[^{11}C]Ala							
	Murine (AM therapy)								
	Vertebral discitis-								

	osteomyelitis			
	Pneumonia via lung injection)			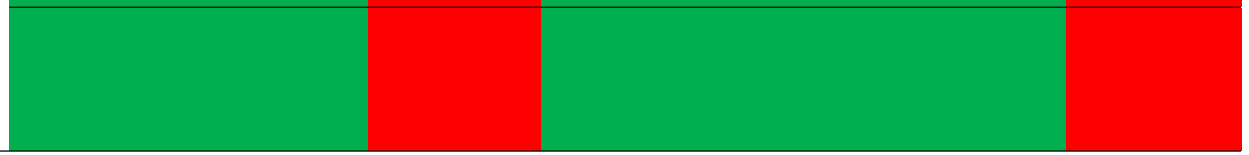

Flourine-18 Radiopharmaceuticals

Martínez, ME [17]	Murine model	myositis	[^{18}F]FAG	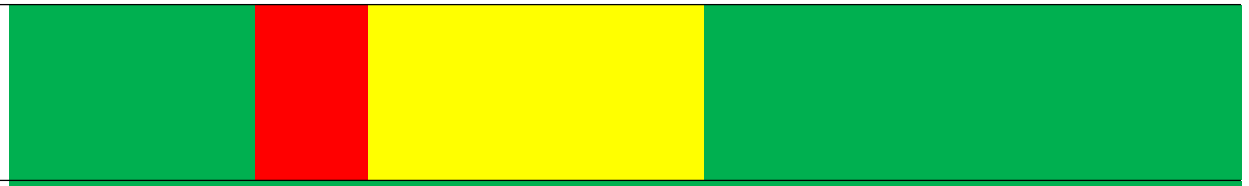
Lee, SH [18]	Murine model	myositis	[^{18}F]FMA	
Sorlin, MA [20]	Murine model	myositis	D-[^{18}F]-CF_3-Ala	
Li, K[21]	Murine model	myositis	D-[^{18}F]FAla	

Abbreviations: AM= Antimicrobial; PJI= prosthetic joint infection (suspected on patient enrolment); Box colours=Studies with low (green), high (red) or unclear (yellow) risk of bias or applicability concerns

3.4 DISCUSSION AND CONCLUSION

The structural heterogeneity and complexity continue to make peptidoglycan a unique target of interest for drug development and for developing bacteria-specific radiotracers; offering an opportunity to differentiate gram-negative from gram-positive strains, which is currently lacking in infection imaging. A recent review article has highlighted promising results on the development status of peptidoglycan-targeting radiotracers for bacterial infection imaging [7]. Herewith, QUADAS analysis was performed for assessing peptidoglycan-targeting radiotracers that are in the preclinical development phase, questioning tracer applicability and performance for possible clinical translation.

Recently, there has been increased interest in the research of D-amino acids and amino sugars as peptidoglycan precursors for bacterial-specific infection imaging using ^{11}C- and ^{18}F-radioisotopes, respectively. Among the D-amino acids, ^{18}F labelled D-Ala radiotracers demonstrated promising results with high specificity for infection imaging and low background signal compared to D-[^{11}C]Ala and D-[^{11}C]Met. This demonstrates the influence of structural manipulation on biodistribution of D-amino acids. The QUADAS analysis also revealed that most sources of bias in these studies were related to the choice of the infection model and reference standard. To date, only D-[^{11}C]Met was cautiously evaluated in the clinical setting; its QUADAS analysis was inconclusive, due to a high risk of bias introduced by the selection of the patient population, the study design flow and the choice of reference standard [8].

In studies that evaluated amino sugars, [^{18}F]FMA received excellent status quo from QUADAS assuring it the diagnostic potential to discriminate infection from inflammation with minimal background signal [18, 23]. However, further validation (preferably during first-in-human explorations) can ensure success during clinical translation. Moreover, the capability of the radiotracer to identify the source of infection (gram-negative versus gram-positive) is still not clear; therefore, recommending more robust clinical study parameters seems plausible for this scenario.

The QUADAS analysis of peptidoglycan-targeting radiotracers revealed several issues in the preclinical study designs, which often introduced a high risk of biasness in data interpretation. Better guidelines and study scope harmonization are required for utilizing animal infection models in a standardized way, thereby applying correct reference standards and producing robust readouts from the site of injection and numbers of bacterial inoculum.

Furthermore, despite the preclinical success for ^{18}F labeled D-amino acids or amino sugars, further evaluation in chronic infection mostly seen in clinical setting and potential in treatment response assessment is required for better judgement for clinical translation and performance. In conclusion, infection imaging has narrow performance criteria and the high background signal observed with other radiotracers could hamper diagnostic accuracy and ultimately limit the implementation to routine clinical use. Carefully guided research developing more specific and selective peptidoglycan-targeting radiotracers is therefore desired.

In the next Chapter, we present for the first time L-Ala-D-Glu-Lys tripeptide radiotracer for peptidoglycan targeting in bacterial infection imaging using ^{68}Ga-PET/CT.

3.5 AUTHOR CONTRIBUTIONS AND DECLARATION OF INTEREST.

PC Koatale and T Ebenhan conceived the idea and PC Koatale drafted the first edition of the manuscript. T Ebenhan and M Mdlophane revised the manuscript for soundness, impact and significance. All co-authours reviewed the final manuscript for input and granted permission for submission. All authors declare no conflict of interest.

3.6 ACKNOWLEDGEMENTS

None.

ABBREVIATIONS

AM	Antimicrobial therapy
cfu	Colony forming unit
CT	Computed tomography
E. coli	*Escherichia coli*
MA	N-acetylmuramic acid
MRSA	Methicillin-resistant Staphylococcus aureus
Na	Not available
P. aeruginosa	*Pseudomonas aeruginosa*
PET	Positron emission tomography tomography
PJI	Prosthetic joint infection
QC	Quality control
RCP	Radiochemical purity
QUADAS	Quality Assessment of Diagnostic Accuracy Studies
SPECT	Single-photon emission computed tomography
S. aureus	*Staphylococcus aureus*
S. epidermidis	*Staphylococcus epidermidis*
T/NT	Target/Non-target ration

ANNEXURE A: QUADAS QUESTIONNAIRE FOR PRECLINICAL STUDIES [10].

Domain	Animals Selection	Index Test	Reference Standard	Study Flow and Timing
Signalling question (yes, no or unclear)	Is the animal's origin from a certified laboratory or company?	Is the origin of the bacterial cells certified?	Is the used reference standard appropriate for the study?	Is the imaging time appropriate for the study?
		Is it a standardized infection model?		
		Can the radiopharmaceutical synthesis be a source of bias? (QCs)		Can the differences in interval time between bacteria inoculation and radiopharmaceutical administration be a source of bias?
		Were further *in vitro*, *in vivo*, and *ex-vivo* tests performed to support the main results?		
Risk of bias (high, low or unclear)	Could the selection of animals have introduced bias?	Could the methodology of experiments have introduced bias?	Could the reference standard or its interpretation have introduced bias?	Could the study flow have introduced bias?
Concerns about applicability (high, low, or unclear)	Are there concerns that the included animals do not match the review question?	Are there concerns that the index test or its interpretation differs from the review question?	Are there concerns that the target condition as defined by the reference standard does not match the review question?	-

Abbreviations: QC= Quality control

ANNEXURE B: QUADAS QUESTIONNAIRE FOR HUMAN STUDIES [10].

Domain	Patient Selection	Index Test	Reference Standard	Study flow and Timings
Signalling question (yes, no or unclear)	Was a consecutive or random sample of patients enrolled?		Is the reference standard likely to correctly classify the target condition?	Was there an appropriate interval between index tests and reference standards?
	Did the study avoid inappropriate exclusions?	Were the index test results interpreted without knowledge of the results of the reference standard?	Were the reference standard results interpreted without knowledge of the results of the index test?	Did all patients receive a reference standard?
				Did all patients receive the same reference standard?
Risk of bias (high, low or unclear)	Could the selection of patients have introduced bias?	Could the conduct or interpretation of the index test have introduced bias?	Could the reference standard or its interpretation have introduced bias?	Could the study flow have introduced bias?
Concerns about applicability (high, low, or unclear)	Are there concerns that the included patients do not match the review question?	Are there concerns that the index test or its interpretation differs from the review question?	Are there concerns that the target condition as defined by the reference standard does not match the review question?	-

3.7 REFERENCES

1. Polvoy I, Flavell RR, Rosenberg OS, Ohliger MA, Wilson DM. Nuclear Imaging of Bacterial Infection: The State of the Art and Future Directions. Journal of Nuclear Medicine. 2020;61(12):1708-16.

2. Palestro CJ. A Brief History of Nuclear Medicine Imaging of Infection. The Journal of Infectious Diseases. 2023;228(Supplement_4):S237-S40.

3. Ordonez AA, Jain SK. Pathogen-Specific Bacterial Imaging in Nuclear Medicine. Semin Nucl Med. 2018;48(2):182-94.

4. Kleynhans J, Sathekge MM, Ebenhan T. Preclinical Research Highlighting Contemporary Targeting Mechanisms of Radiolabelled Compounds for PET Based Infection Imaging. Semin Nucl Med. 2023.

5. Radkov AD, Hsu Y-P, Booher G, VanNieuwenhze MS. Imaging bacterial cell wall biosynthesis. Annu Rev Biochem. 2018;87:991-1014.

6. Lin H, Yang C, Wang W. Imitate to illuminate: labeling of bacterial peptidoglycan with fluorescent and bio-orthogonal stem peptide-mimicking probes. RSC Chemical Biology. 2022;3(10):1198-208.

7. Koatale PC, Welling MM, Ndlovu H, Kgatle M, Mdanda S, Mdlophane A, Okem A, Takyi-Williams J, Sathekge MM, Ebenhan T. Insights into Peptidoglycan-Targeting Radiotracers for Imaging Bacterial Infections: Updates, Challenges, and Future Perspectives. ACS Infect Dis. 2024.

8. Polvoy I, Seo Y, Parker M, Stewart M, Siddiqua K, Manacsa HS, Ravanfar V, Blecha J, Hope TA, Vanbrocklin H, Flavell RR, Barry J, Hansen E, Villanueva-Meyer JE, Engel J, Rosenberg OS, Wilson DM, Ohliger MA. Imaging joint infections using D-methyl-(11)C-methionine PET/MRI: initial experience in humans. Eur J Nucl Med Mol Imaging. 2022;49(11):3761-71.

9. Whiting PF, Rutjes AW, Westwood ME, Mallett S, Deeks JJ, Reitsma JB, Leeflang MM, Sterne JA, Bossuyt PM. QUADAS-2: a revised tool for the quality assessment of diagnostic accuracy studies. Annals of Internal Medicine. 2011;155(8):529-36.

10. Auletta S, Varani M, Horvat R, Galli F, Signore A, Hess S. PET radiopharmaceuticals for specific bacteria imaging: a systematic review. Journal of Clinical Medicine. 2019;8(2):197.

11. Nerella SG, Singh P, Tulja S. Carbon-11 patents (2012–2022): synthetic methodologies and novel radiotracers for PET imaging. Expert Opinion on Therapeutic Patents. 2022;32(7):817-31.

12. Pekošak A, Filp U, Poot AJ, Windhorst AD. From Carbon-11-Labeled Amino Acids to Peptides in Positron Emission Tomography: the Synthesis and Clinical Application. Molecular Imaging and Biology. 2018;20(4):510-32.

13. Neumann KD, Villanueva-Meyer JE, Mutch CA, Flavell RR, Blecha JE, Kwak T, Sriram R, VanBrocklin HF, Rosenberg OS, Ohliger MA, Wilson DM. Imaging Active Infection in vivo Using D-Amino Acid Derived PET Radiotracers. Scientific Reports. 2017;7(1):7903.

14. Renick PJ, Mulgaonkar A, Co CM, Wu C-Y, Zhou N, Velazquez A, Pennington J, Sherwood A, Dong H, Castellino L, Öz OK, Tang L, Sun X. Imaging of Actively Proliferating Bacterial Infections by Targeting the Bacterial Metabolic Footprint with d-[5-11C]-Glutamine. ACS Infect Dis. 2021;7(2):347-61.

15. Parker MFL, Luu JM, Schulte B, Huynh TL, Stewart MN, Sriram R, Yu MA, Jivan S, Turnbaugh PJ, Flavell RR, Rosenberg OS, Ohliger MA, Wilson DM. Sensing Living Bacteria in Vivo Using d-Alanine-Derived 11C Radiotracers. ACS Cent Sci. 2020;6(2):155-65.

16. Le Bars D. Fluorine-18 and medical imaging: Radiopharmaceuticals for positron emission tomography. Journal of Fluorine Chemistry. 2006;127(11):1488-93.

17. Martínez ME, Kiyono Y, Noriki S, Inai K, Mandap KS, Kobayashi M, Mori T, Tokunaga Y, Tiwari VN, Okazawa H, Fujibayashi Y, Ido T. New radiosynthesis of 2-deoxy-2-[18F]fluoroacetamido-d-glucopyranose and its evaluation as a bacterial infections imaging agent. Nuclear Medicine and Biology. 2011;38(6):807-17.

18. Lee SH, Kim JM, López-Álvarez M, Wang C, Sorlin AM, Bobba KN, Pichardo-González PA, Blecha J, Seo Y, Flavell RR, Engel J, Ohliger MA, Wilson DM. Imaging the Bacterial Cell Wall Using N-Acetyl Muramic Acid-Derived Positron Emission Tomography Radiotracers. ACS Sensors. 2023;8(12):4554-65.

19. Ordonez AA, Sellmyer MA, Gowrishankar G, Ruiz-Bedoya CA, Tucker EW, Palestro CJ, Hammoud DA, Jain SK. Molecular imaging of bacterial infections: Overcoming the barriers to clinical translation. Sci Transl Med. 2019;11(508).

20. Sorlin AM, López-Álvarez M, Biboy J, Gray J, Rabbitt SJ, Rahim JU, Lee SH, Bobba KN, Blecha J, Parker MFL, Flavell RR, Engel J, Ohliger M, Vollmer W, Wilson DM. Peptidoglycan-Targeted [18F]3,3,3-Trifluoro-d-alanine Tracer for Imaging Bacterial Infection. JACS Au. 2024;4(3):1039-47.

21. Li K, Tolentino Collado J, Marden JA, Pollard AC, Guo S, Tonge PJ, Qu W. Biological Evaluation of d-[18F]Fluoroalanine and d-[18F]Fluoroalanine-d3 as Positron Emission Tomography Imaging Tracers for Bacterial Infection. Journal of Medicinal Chemistry. 2024;67(16):13975-84.

22. Parker MF, Luu JM, Schulte B, Huynh TL, Stewart MN, Sriram R, Yu MA, Jivan S, Turnbaugh PJ, Flavell RR. Sensing living bacteria in vivo using d-alanine-derived 11C radiotracers. ACS central science. 2020;6(2):155-65.

23. Carrasco-López C, Rojas-Altuve A, Zhang W, Hesek D, Lee M, Barbe S, André I, Ferrer P, Silva-Martin N, Castro GR, Martínez-Ripoll M, Mobashery S, Hermoso JA. Crystal structures of bacterial peptidoglycan amidase AmpD and an unprecedented activation mechanism. Journal of Biological Chemistry. 2011;286(36):31714-22.

CHAPTER 4EVALUATION OF [68GA]GA-DOTA-AEK AS A POTENTIAL IMAGING TOOL FOR PET IMAGING OF CELL WALL SYNTHESIS IN BACTERIAL INFECTIONS

Palesa C. Koatale[1, 2], Mick M. Welling[3], Sipho Mdanda[1, 2], Amanda Mdlophane[1, 2], John Takyi-Williams [4], Chrisna Durandt [5,6], Iman van den Bout[7], Frederik Cleeren[8], Mike M. Sathekge[1,2] and Thomas Ebenhan[1,2] *

1. Department of Nuclear Medicine, University of Pretoria, Pretoria 0001, South Africa

2. Nuclear Medicine Research Infrastructure (NuMeRI), Steve Biko Academic Hospital, Pretoria 0001, South Africa

3. Department of Radiology, Interventional Molecular Imaging Laboratory, Leiden University Medical Center, 2333 ZA Leiden, The Netherlands

4. Therapeutics Systems Research Laboratories (TSRL), Inc., Ann Arbor, MI 48109, USA

5. Department of Medical Immunology, Institute for Cellular and Molecular Medicine, University of Pretoria, Pretoria 0001, South Africa

6. South African Medical Research Council Extramural Unit for Stem Cell Research and Therapy, University of Pretoria, Pretoria 0001, South Africa

7. Department of Physiology, University of Pretoria, Pretoria 0001, South Africa

8. Department of Pharmacy and Pharmacological Sciences, Radiopharmaceutical Research, KU Leuven, 3000 Leuven, Belgium

***Corresponding author**: thomas.ebenhan@up.ac.za

Pharmaceuticals **2024**, 17(9), 1150

ABSTRACT

The ability of bacteria to recycle exogenous amino acid-based peptides and amino sugars for peptidoglycan biosynthesis was extensively investigated using optical imaging. In particular, fluorescent AeK–NBD was effectively utilized to study the peptidoglycan recycling pathway in gram-negative bacteria. Based on these promising results, we were inspired to develop the radioactive AeK conjugate [^{68}Ga]Ga-DOTA-AeK for the *in vivo* localization of bacterial infection using PET/CT. An easy-to-implement radiolabeling procedure for DOTA-AeK with [^{68}Ga]$GaCl_3$ followed by solid-phase purification was successfully established to obtain [^{68}Ga]Ga-DOTA-AeK with a radiochemical purity of ≥95 %. [^{68}Ga]Ga-DOTA-AeK showed good stability over time with less protein binding under physiological conditions. The bacterial incorporation of [^{68}Ga]Ga-DOTA-AeK and its fluorescent Aek-NBD analog were investigated in live and heat-killed *Escherichia coli* (*E. coli*) and *Staphylococcus aureus* (*S .aureus*). Unfortunately, no conclusive *in vitro* intracellular uptake of [^{68}Ga]Ga-DOTA-AeK was observed for *E. coli* or *S. aureus* live and heat-killed bacterial strains ($p > 0.05$). In contrast, AeK-NBD showed significantly higher intracellular incorporation in live bacteria compared to the heat-killed control ($p < 0.05$). Preliminary biodistribution studies of [^{68}Ga]Ga-DOTA-AeK in a dual-model of chronic infection and inflammation revealed limited localization at the infection site with non-specific accumulation in response to inflammatory markers. Finally, our study demonstrates proof that the intracellular incorporation of AeK is necessary for successful bacteria-specific imaging using PET/CT. Therefore, Ga-68 was not a suitable radioisotope for tracing the bacterial uptake of AeK tripeptide, as it required chelation with a bulky metal chelator such as DOTA, which may have limited its active membrane transportation. An alternative for optimization is to explore diverse chemical structures of AeK that would allow for radiolabeling with ^{18}F or ^{11}C.

Keywords: PET tracer; cell wall; synthesis; purification; quality control; bacterial infection; PET imaging

4.1 INTRODUCTION

Bacterial infections remain a significant health concern, in part due to the growing incidence of antibacterial resistance. Accurate diagnosis of bacterial infections is crucial to avoid unnecessary antibiotic use, and implementing effective antibiotic stewardship requires rapid diagnostic tests [1]. However, the traditional approach to diagnosing infections requires sampling bodily fluids or performing an invasive biopsy followed by microbiological culturing or molecular typing, which often requires several days to weeks to obtain results [2, 3]. To address these limitations, morphological imaging techniques, including ultrasound, computed tomography (CT), and magnetic resonance imaging (MRI), have been used for real-time, non-invasive diagnosis. However, early infections and infections with dormant bacteria often remain undetectable [4]. As a result, a dual-nuclear imaging modality such as positron emission tomography/ computed tomography (PET/CT) is considered a good alternative due to its ability to non-invasively assess anatomical and physiological abnormalities, especially in the early stages of infection or for deeply seated infections, where sampling is challenging.

PET/CT can be used efficiently in monitoring treatment response and relapse [5, 6]. For infection detection and imaging, current nuclear medicine techniques rely on direct or indirect targeting of infected sites using [^{67}Ga]Ga-Citrate ([^{99m}Tc]Tc/[^{111}In]-labeled leucocytes) or via active glucose metabolism using 2-deoxy-2[^{18}F]fluoro-D-glucose ([^{18}F]-FDG). Unfortunately, these radiotracers fail to discriminate infection from inflammation and often suffer from poor resolution [7-9]. Thus, the current clinical radiotracers have limited diagnostic power in differentiating infections from other inflammatory processes. Unlike eukaryotic cells, bacteria possess a complex and unique biological cell machinery that offers multiple opportunities for pathogen-specific targeting. Therefore, improvements in the diagnostic strategy require the development of tailored radiotracers depending on bacteria-specific features that allow for rapid and specific localization of infectious foci that may be selective for the type of bacteria involved in an infection [10, 11]. With this shift in focus, several potential candidates targeting bacterial biochemical processes have emerged, including antibiotics ([^{99m}Tc]Tc-/[^{18}F]F-Ciprofloxacin), antimicrobial peptides ([^{99m}Tc]Tc/[^{68}Ga]Ga-UBI$_{29–41}$), metabolites ([^{18}F]F-D-sorbitol), antibodies ([^{89}Zr]Zr-human monoclonal antibody 1D9), bacteriophages ([^{99m}Tc]Tc-M13 phages) and oligomers (e.g., [^{99m}Tc]Tc-MORF oligomer) [12, 13].

Of particular interest is the bacterial cell wall, which is of use in classifying bacteria (gram-negative versus gram-positive) based on the complexity and heterogeneity of the peptidoglycan (PG) building blocks [14]. Evident in all bacteria, PG forms an integral net-like structure of the cell wall, composed of alternating N-acetylglucosamine and N-acetylmuramic acid amino sugars cross-linked by oligopeptides. PG biosynthesis and remodeling involve a well-understood, dynamically regulated mechanism [15]. During cell proliferation, the PG polymer is enzymatically digested into L-Ala-γ-D-Glu-meso-A2pm (or L-Lys)-D-Ala tetrapeptide and L-Ala-γ-D-Glu-meso-A2pm (or L-Lys) tripeptides, and then enters the PG recycling pathway via oligopeptide permease (Opp) membrane protein transporters found in both *Escherichia coli* (*E. coli*) and *Staphylococcus aureus* (*S. aureus*) [16]. Once in the intracellular space, the amino acids chains (tri- and tetrapeptides) are covalently linked to amino sugars by murein peptide ligase (Mpl), resulting in the formation of uridine diphosphate-N-acetylmuramic acid (UDP-MurNAc)-tripeptide/tetrapeptides, a process which is integral for the reintegration of the peptides into the bacterial cell wall. These muropeptides are further processed and incorporated into a newly formed PG layer during cell proliferation (**Figure 4-1**) [15, 17, 18].

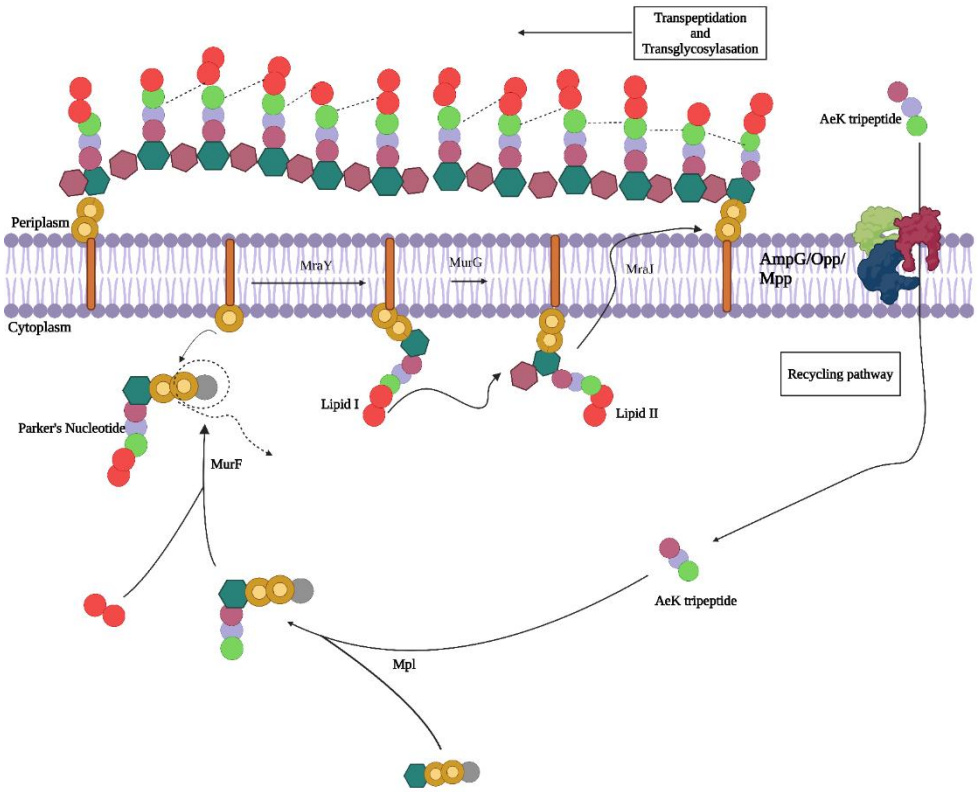

Figure 4-1: Proposed peptidoglycan recycling targeting pathway of AeK tripetide. Adapted with permission from ref [19] ,published 2024 under a Creative Commons Attribution 4.0 International License**.** Created with BioRender.com.

We recently studied PG targeting molecules and reviewed their potential as future agents for PET imaging of infection [19]. Various studies have demonstrated the ability of bacteria to utilize synthetic D-amino acids and tripeptides for the reconstruction of the PG, and that extends to their fluorescence and radioactive analogs [20-23]. For example, in a study by Goodell [24], the radiolabeled tripeptide L-Ala-γ-D-Glu-[^{3}H]A2pm was effectively utilized by *E. coli* in the PG recycling pathway without tracer degradation. Interestingly, similar results were reported in another study using the fluorescent tripeptide L-Ala-γ-D-Glu-L-Lys-N-7-nitro-2,1,3-benzoxadiazol-4-yl (AeK–NBD; **Figure 4-2a**), in which the conjugation of diaminopimelic acid to the epsilon amino group of lysine did not compromise the bacterial uptake [25].

(a) **(b)**

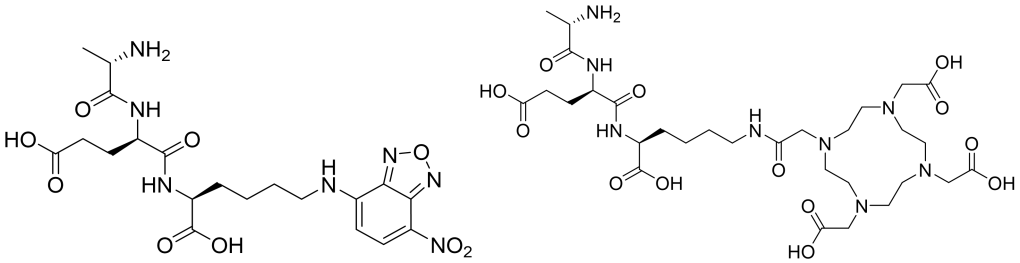

Figure 4- 2: Chemical structure of **a)** AeK–NBD and **b)** AeK–DOTA

In recent years, we have seen an evolvement in the synergistic approach to using translate fluorescent probes for targeting the bacterial cell wall, primarily limited to *in vitro* into infection imaging radiotracers for the advancement of target-specific diagnostic tools, which is a critical need in the medical field [14]. In the current study, we intended to replace the fluorescent entity NBD with the bifunctional chelator 4,7,10 tetraaza-cyclododecane-N,N′,N″,N‴-tetraacetic acid (DOTA), thereby forming L-Ala-γ-D-Glu-L-Lys-DOTA (AeK–DOTA, **Figure 4-2b**) to allow for radiolabeling with the radioisotope Gallium-68 (^{68}Ga) for prospective bacterial imaging using PET/CT. A ^{68}Ga-labeling method for AeK-DOTA was developed, followed by a tailored purification procedure for [^{68}Ga]Ga-DOTA-AeK to enable initial radiopharmacological and physicochemical characterization (lipophilicity, protein binding, and plasma stability). Subsequently, a preliminary animal study was performed using [^{68}Ga]Ga-DOTA-AeK-PET/CT for pharmacokinetics and biodistribution investigations to study its suitability for PET imaging

4.2 MATERIALS AND METHODS

Information on materials, biochemicals and selected equipment is referred to in Appendix A.

4.2.1 Testing radio-analytical methods for [^{68}Ga]Ga-DOTA-AeK quality control

General equipment setting and processes (e.g., known stationary- and mobile-phase materials) for instant thin-layer chromatography (ITLC), high-performance liquid chromatography (HPLC) and liquid chromatography–mass spectrometry (LC/MS) were adopted from a previously published paper [26].

The purified DOTA-AeK was characterized via HPLC and LC/MS. The purity of DOTA-AeK was determined via a Waters Acquity LC/MS system equipped with a Waters XBridge BEH C18 column (3.5 µm, 100 mm × 3 mm, 130 Å) at a flow rate of 5 mL/min using a gradient of acetonitrile with 0.1 % formic acid (5–95 % over 10 min) and H_2O with 0.1 % formic acid. The HPLC method was first tested for its capability to accurately identify [^{68}Ga]Ga-DOTA-AeK and separate it from various other radiolabeled by-products. An Agilent 1290 Infinity II HPLC apparatus equipped with an Agilent Infinity Lab Poroshell 120 EC-C18 (3.0 × 150 mm, 2.7 µm) column and a diode array UV detector (set at 220 nm) alongside a Gabi γ-HPLC flow detector (Elysia-raytest, Straubenhardt, Germany) were used for analysis. The method setup included a 20 min-long A/B gradient mobile phase protocol (0.5 mL/min flow rate; A: H_2O, 0.1 % TFA, B: acetonitrile, 0.1% TFA) with the elution set as follows: 0–1 min: 97 % A; 1–10 min: decrease 97 % A to 72 % A; 10–15 min 72 % A; 15–20 min: 97 % A.

The ITLC method was first tested for its selectivity to determine the radiolabeling efficiency and radiochemical purity (RCP) in crude or purified [^{68}Ga]Ga-DOTA-AeK product samples. Retention factors (R*f*) were determined to calculate the method resolution (R*s*). Peak identification was performed via baseline-gated “area-under-the-curve” analysis.

4.2.2 Development of a radiosynthesis method for [^{68}Ga]Ga-DOTA-AeK

Optimal conditions for radiolabeling were first determined. For this purpose, a strategy described by Mokaleng et al. [27] was adopted to facilitate the general radiolabeling principle for DOTA-AeK by investigating parameters such as the influence of pH, compound concentration and incubation time on the labeling efficiency. First, the [^{68}Ga]$GaCl_3$ was eluted with 0.6 M HCI via generator eluate fractionation, and sodium acetate trihydrate solution (2.5M; pH 8.5) was used as the buffering agent. To investigate the effect of pH and the concentration parameters on the labeling yield, 2-fold serial dilutions of 25 µL of DOTA-AeK (0–137 µM) were prepared from stock solutions of DOTA-AeK (50 µg, 68.2 nmol) followed by the addition of 200 µL of buffered [^{68}Ga]$GaCI_3$ (pH 4.0 and 3.0). The total reaction mixtures (225 µL, pH 4.0 and 3.0) constituting different peptide concentrations (5–303 µM) were heated at 95 °C for 15 min using a heat block. Thereafter, the effect of incubation time (5–20 min) on the complexation of DOTA-AeK and [^{68}Ga]$GaCI_3$ was reported. Samples of the reaction solution were tested for labeling efficiency and radiochemical purity by performing radio-ITLC and radio-HPLC analysis.

4.2.3 Optimization of a purification technique for [68Ga]Ga-DOTA-AeK

A step-by-step radiochemical purification procedure for [^{68}Ga]Ga-DOTA-AeK was developed using different solid phase extraction (SPE) cartridges: (a) SepPak C18, (b) SepPak C-8 Plus (light), (c) Oasis hydrophilic-lipophilic balance (HLB) (Waters Corporation, Milford, MA, USA) and (d) Strata X (Phenomenex, Torrance, CA, USA). The essential parameters, including the cartridge binding efficiency, rinse, type of elution solution, and product recovery, were investigated. In brief, the cartridges were pre-conditioned using EtOH, followed by H_2O. The [^{68}Ga]Ga-DOTA-AeK reaction solution was loaded onto the cartridges and rinsed with aqueous-based solutions. The recovery of [^{68}Ga]Ga-DOTA-AeK from the cartridge adsorbent was performed using organic solutions. The radioactivity was measured at each step by measuring the loaded cartridges, wash steps, and elution fractions in the dose calibrator. The cartridge loading, rinse/wash, and recovery efficiency was determined as the percentage of radioactivity used out of the total starting radioactivity. Thereafter, the overall purification performance was assessed based on the recovery efficiency (factoring in the loading and elution efficiency) and RCP of the purified product using radio-HPLC.

4.2.4 Radiochemical and thermodynamical stability

The stability of [^{68}Ga]Ga-DOTA-AeK using samples of the post-purification formulation was investigated for up to 120 min at room temperature by comparing the benchtop condition (pH 4.0) and neutralized product formulation adjusted to pH 7.0 (2M NaOH) using radio-HPLC, determining the %RCP for each time point.

4.2.5 Log P determination

The compound hydrophobicity was determined using the octanol–water partition coefficient "shake flask method" described by Lambidis et al. [28]. In brief, 100 µL of purified [^{68}Ga]Ga-DOTA-AeK was added to 400 µL of ultrapure water. The aqueous solution was added to an equal volume of 1-octanol (Sigma-Aldrich, Germany), and the mixture was mechanically shaken for approximately 3 min at room temperature. The sample was centrifuged at 16211 g for 5 min using a Digicen 21 R centrifuge (Orto Alresa, Madrid, Spain). The aqueous and organic phases of the sample were separated, and samples from each phase were analyzed using a dose calibrator. The logarithmic partition coefficient, LogP, was calculated using the following equation:

$$\text{LogP} = \text{Log}\,[(\text{counts in octanol}/\text{counts in water})] \quad (1)$$

4.2.6 Proteolytic stability and serum protein binding of [^{68}Ga]Ga-DOTA-AeK

The plasma protein binding filter assay described by Müller et al. [29] was adopted. Before the experiment, Amicon® Ultra-0.5 centrifugal 10 kDa MWCO filter units (Merck, Darmstadt, Germany) were pre-washed with 200 µL of phosphate-buffered saline (PBS) for 20 min at 18611 g using the Microfuge 16 centrifuge (Beckman Coulter Life Sciences, Brea, CA , USA). Subsequently, 800 µL of plasma was spiked with 200 µL of purified [^{68}Ga]Ga-DOTA-AeK, vortexed for 3 s, and incubated for 120 min at 37 °C. For radioanalysis, a 100 µL plasma sample was taken at different time intervals (30, 60, and 120 min), diluted (1:1) with PBS, aliquoted into filter units, and centrifuged at 14,800 rpm for 20 min. A similar procedure was carried out in PBS (140 mM NaCl, 10 mM phosphate buffer, and 3 mM KCl, pH 7.4) as a control. After centrifugation, each filter unit was washed by adding 100 µL of PBS (140 mM NaCl, 10 mM phosphate buffer, and 3 mM KCl, at pH 7.4, and centrifuged as described above. The counts of

the filtrate fraction (representing unbound compound) and on the filter (protein-bound compound) were measured using a Capintec Captus 4000E well counter (Florham Park, NJ, USA). The percentage of the protein-bound radiotracer was calculated using the following equation:

$$\% \text{ Protein bound} = [\text{counts in filter} \div \text{total counts (filtrate fraction+ filter)}] \times 100 \quad (2)$$

In addition, the filtrated fraction was analyzed via radio-HPLC to evaluate the radiotracer stability in plasma and PBS by determining the %RCP.

4.2.7 Bacterial cell uptake of [^{68}Ga]Ga-DOTA-AeK

Overnight bacterial cell cultures of *E. coli* or *S. aureus* were grown in Tryptic Soy Broth (TSB) medium at 37 °C. The 6.0 McFarland standard was prepared using DEN-18 McFarland Densitometer (Biosan, Riga, Latvia). For control studies, the same amount of bacterial culture was heat-killed via 30 min incubation at 90 °C. The culture viability was confirmed using agar plating with overnight incubation. All tests were initiated by adding 4.1 ± 1.23 MBq of [^{68}Ga]Ga-DOTA-AeK product solution (4.86 ± 1.45 GBq/µmol) to 1.0 mL of the bacterial suspension (1.8×10^8 cells/mL), and mixtures were maintained while shaking at 37 °C. At specific time intervals (10, 60, and 120 min), samples of the suspension were centrifuged at 16,211 *g* for 10 min (Digicen 21R, United Scientific, Goodwood, South Africa), and the supernatant was transferred into a plastic tube. The pellet was washed with 3 mL of PBS (140 mM sodium chloride, 10 mM phosphate buffer, and 3 mM potassium chloride, pH 7.4) and centrifuged at 16,211 *g* for 10 min. For measurement, all volumes of supernatant were pooled into one single liquid fraction. The radioactivity in the supernatant and pellet fraction were measured using an automatic gamma counter (Hidex AMG, LabLogic, Turku, Finland). The percentile of [^{68}Ga]Ga-DOTA-AeK cell uptake was calculated as follows:

$$\text{Uptake (\%)} = [\text{counts in cell pellet} \div \text{total counts (cell pellet + supernatants)}] \times 100 \quad (3)$$

4.2.8 Bacterial cell uptake and incorporation of AeK-NBD

4.2.8.1 Flow-cytometry

Bacterial cell cultures (either live or heat-killed) of *E. coli* or *S. aureus* (1.0 McFarland standard) were prepared as described above. For bacterial staining, 2.0 µL (100 mM in DMSO) of fluorescent AeK-NBD was added to 198 µL of bacterial culture (7.7 x 10^7 cells/mL), and cells were counterstained with 2.0 µL (10 µM in DMSO) of membrane-permeable DNA Vybrant DyeCycle (VDC) Ruby dye (Thermo Fisher Scientific, Waltham, MA, USA). All cultures were incubated at 37 °C, and samples were taken at different intervals (10, 30, and 60 min) to perform flow cytometric analysis (Cytoflex, Beckman Coulter Life Sciences, Brea, CA, USA). AeK-NBD was excited with a 488 nm laser, and the emitted fluorescence was collected using a 540/30 nm band pass filter, as carried out previously [25]. The VDC Ruby dye was excited with a 638 nm laser, and the emitted fluorescence was collected using a 712/25 nm band pass filter. No noticeable spillover was observed when VDC Ruby 'only' and AeK-NBD 'only' controls were used as controls for possible fluorescence spillover. Thus, no compensation was applied when using both dyes. The NBD-AeK median fluorescence intensity (MFI) of VDC Ruby-positive bacteria was reported. Post-acquisition data analysis was performed using Kaluza Analysis Software (version 2.2; Beckman Coulter, Miami, Brea, CA, USA).

4.2.8.2 Confocal microscopy

Sample preparation of *E. coli* and *S. aureus* suspensions for confocal fluorescence microscopy imaging involved immediate staining with AeK-NBD and membrane-permeable DNA VDC Ruby dye for 10 min, as described in the previous section. Cells were subsequently fixed in 10 % formalin for 15 min, followed by centrifugation at 76,471 *g* for 3 min using a Microfuge 16 centrifuge (Beckman Coulter Life Sciences, Brea, CA USA), and the cell pellet was washed in PBS. The bacterial suspension was centrifuged, and the cells were deposited in Molwiol/DABCO mounting fluid on a microscope slide and overlaid with a No 1 thickness coverslip. Images were collected on a Zeiss LSM800 confocal microscope (Oberkochen, Germany) using a 63×1.4 NA oil objective with 2.5× scan zoom and 4× averaging. Furthermore, 488 and 561 excitation wavelengths were used at 0.30 % and 1.87 % power and 852 V and 845 V, respectively, along with 0.82 and 0.69 AU pinholes.

4.2.9 Exploratory [^{68}Ga]Ga-DOTA-AeK-PET/CT imaging

4.2.9.1 Animals

All animal handling and experimental procedures were conducted by a licensed veterinary professional and performed with approval (see Institutional Review Board Statement).
Six-to-eight-week-old mixed-gender BALB/c mice (20.0 ± 2.1 g) were utilized. Animals were pre-grouped (two mice/cage) into individually ventilated cages (IVC, Tecniplast, Buguggiate, Italy) and kept under standard housing conditions (22 ± 2˚C, 55 ± 10 % humidity, 15 ± 5 Pa, and 12 hrs light/dark cycles) with food and water being provided ad libitum. Each experimental group consisted of 5 animals.

4.2.9.2 Establishment of the murine infection and inflammation animal model

A thigh muscle mouse model of infection and inflammation was developed for imaging purposes by adopting procedures from a previous study with some modifications [27]. In brief, animals were inoculated intramuscularly (right hind leg) with 1.5×10^7 colony forming units (cfu)/mL of *S. aureus* or *E. coli* suspended in 100 µL of culture media. To induce sterile inflammation, the same mice received 100 µL of a turpentine oil solution intramuscularly into the left hind leg. Infection was allowed to develop for 3–5 days, which is typical for a model of chronic infections, and a health check, including monitoring of the infection and inflammation sites, was conducted. At 3 and 5 days after the inoculations, all animals underwent whole-body [^{68}Ga]Ga-DOTA-AeK microPET/CT imaging, and after euthanasia, a complete *ex vivo* organ tissue biodistribution radioactive assay was performed.

4.2.9.3 Animal imaging procedure

A total volume of 100 µL of [^{68}Ga]Ga-DOTA-AeK (7.4 ± 2.0 MBq, 4.86 ± 1.45 GBq/µmol 5 % EtOH/PBS, pH 7.0) was administered as an intravenous bolus via the tail vein. At the same time, the animals were kept anesthetized, (4 % isoflurane in oxygen for induction and 1.5–2.5 % for maintenance). Non-invasive, whole-body microPET/CT imaging was performed using a Mediso nanoScan® PET/CT scanner (Budapest, Hungary). A previously described, image acquisition was performed [30]. The PET/CT imaging procedure consisted of static whole-body scans per animal commencing at 60 min post-injection. The imaging protocol included the X-ray topogram (30 sec) to ascertain the correct animal placement followed by CT image acquisition (4–5 min) and 20 min long PET image acquisition. Image reconstruction and analysis were performed as previously described [30].

4.2.9.4 *Ex vivo* biodistribution studies and histopathology

After PET/CT imaging, the mice were euthanized via cervical dislocation while still under anesthesia. The different organs (spleen, pancreas, stomach, intestine, kidneys, liver, heart, lung, muscle, and femur) were collected into pre-weighed tubes. The radioactivity of each sample was determined using an automatic gamma counter (Hidex AMG, Turku, Finland). Results were expressed as a percentage of injected dose per gram organ (%ID/g). Subsequently, both muscles on the left and right thighs were fixed in 4 % paraformaldehyde and submitted to the University of Pretoria, Department of Paraclinical Science, for hematoxylin and eosin (H&E) and Gram staining. Infection and inflammation tissue analysis was performed by a qualified pathologist.

4.2.10 Statistical analysis

Unless stated otherwise, the results were analyzed using Microsoft Excel 365 Software (Redmond, WA, USA) and GraphPad Prism 9.5.1 Software (San Diego, CA, USA). Results from experimental repetitions are expressed as mean ± standard deviation (SD). Means were compared using the unpaired two-tailed Student *t*-test, and differences in values were considered statistically significant when $p < 0.05$.

4.3 RESULTS AND DISCUSSION

4.3.1 Development of ^{68}Ga-radiolabeling method for DOTA-AeK

Aside from various peptides with longer amino acid sequences, we previously developed kit-based radiosynthesis for the pentapeptide NOTA-cyclo-Arg-Gly-Asp-d-Tyr-Lys (NOTA-RGD) [31]; this confirmed the safe use of sodium acetate as a buffering agent, which was subsequently used in this study. Furthermore, original results concerning the radiosynthesis of DOTA-AeK (732.79 g/mol, **Figures A1 and A2A**) with Ga-68 are reported below.

Firstly, to ensure accurate analysis of radiosynthesis, the validity of radioanalytical methods for [^{68}Ga]Ga-DOTA-AeK quality control were tested. Both HPLC and ITLC methods were assessed for their ability to identify [^{68}Ga]Ga-DOTA-AeK and were found to accurately measure the compound. Thus, both methods can be used as radioanalytical quality control measurements for crude and purified [^{68}Ga]Ga-DOTA-AeK samples. The required labeling efficiency and product purity was confirmed via radio-HPLC (Figure A2B) and the ITLC method (**Figure A3A,B** and **Table A1**).

4.3.1.1 Effects of radiolabeling conditions on Ga-68-complexation of DOTA-AeK

DOTA was selected as a chelator, along with a 95 °C incubation temperature and sodium acetate as the buffering agent (pH capacity range 3.7–5.6), with eluate fractionation as the preferred generator elution technique based on previous experience and similar outcomes from the radiolabeling of different research peptides [32-34].
Therefore, crucial changes to vector concentration, eluate acidity, and incubation time were investigated to determine the optimal radiolabeling parameters. These parameters were set at ≥95 % RCP.

4.3.1.2 Ga-68-eluate acidity and vector concentration (DOTA-AeK)

A serial radiolabeling strategy was carried out to investigate the influence of pH (3 and 4) and vector concentration on the complexation of [^{68}Ga]$GaCl_3$ and DOTA-AeK. **Figure 4-3a,b** show that radiolabeling efficiency is directly proportional to the vector concentration. In addition, the

data demonstrate the critical role the pH plays in coordinating the chemistry of [^{68}Ga]$GaCl_3$ with DOTA. At pH 3, a radiolabeling efficiency of at least ≥85.9 ± 2.3 % was observed at the highest peptide concentration of 303 µM. In contrast, the labeling efficiency was significantly improved at pH 4, with the highest RCY of ≥95 % obtained from a 76 µM peptide concentration. This difference in efficiency may have been a result of carboxylic acid group protonation and the formation of hydrolyzed $^{68}Ga^{3+}$ colloidal species $[^{68}Ga(H_2O)_6]^{3+}$ observed at pH ≤ 3.5, resulting in lower RCY. At pH 4, the carboxylic acid group were partially deprotonated, forming an ionic bond with $^{68}Ga^{3+}$ and optimum RCY at a low peptide concentration [35-38].

(a)

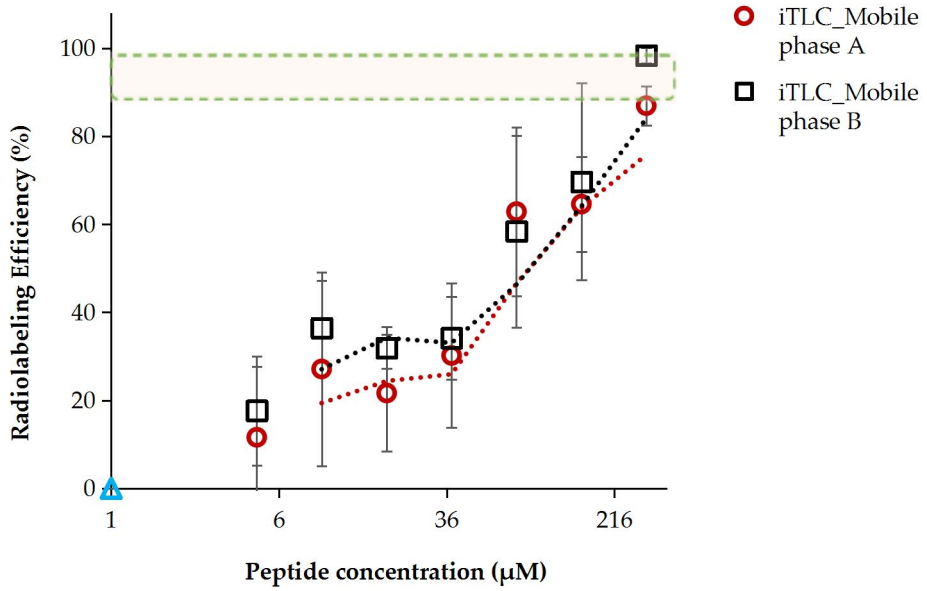

(b)

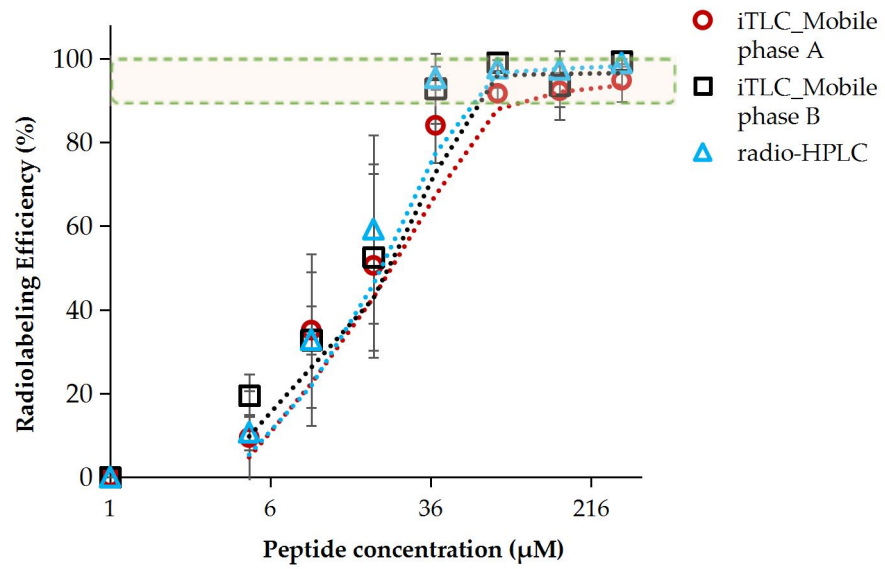

Figure 4-3 : The influence of peptide concentration and pH on radiolabelling efficiency performed at (**a**) pH 3 and (**b**) pH 4 (95°C, 15 min). The results are expressed as mean ± SD (n=3) with fitted lines indicated. Green-shaded area indicates the desired level of radiolabelling efficiency.

4.3.1.3 Optimization of incubation parameters

To investigate the effect of incubation time on the labeling efficiency, 76 µM [^{68}Ga]Ga-DOTA-AeK was prepared via incubation for different durations (5–20 min). Our findings show an optimum radiolabeling efficiency of ≥95 % between 10 and 20 min at 95 °C for [^{68}Ga]Ga-DOTA-AeK (**Figure 4-4**, green areal). This is mainly due to the fairly slow reaction kinetics of DOTA (the dotted light blue line was added for kinetics that were estimated early-on), requiring a higher heating temperature (60–100 °C) for extended reaction times (range 10–60 min) for radiometal complexation to occur [39, 40].

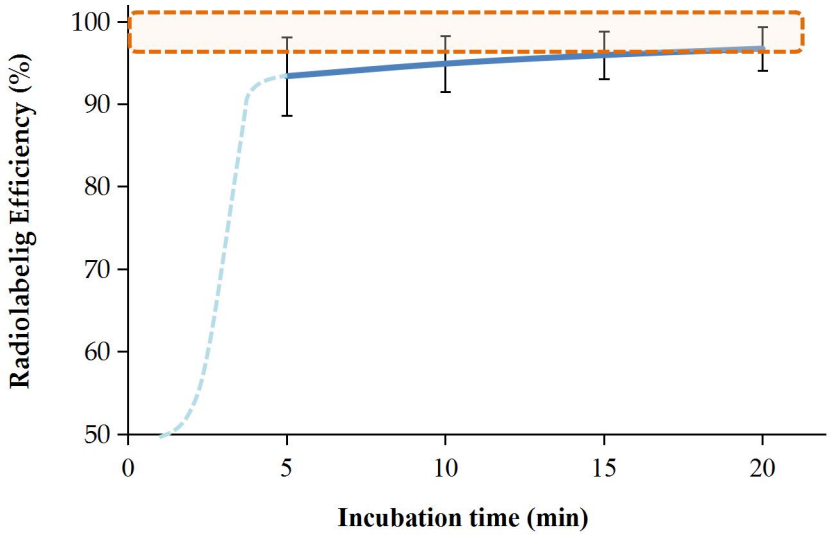

Figure 4-4: The effect of incubation time on the complexation of [^{68}Ga]$GaCl_3$ with DOTA-AeK (76 µM; pH 4; 95°C) up to 20 min using radio-HPLC. The results are represented as mean ± SD (n=3). The green-shaded area shows the required radiolabeling efficiency >95 %.

To maintain optimum labeling efficiency and %RCP, the following parameters were adopted for all routine radiolabeling during [^{68}Ga]Ga-DOTA-AeK characterization and its preclinical assessment: 76 µM DOTA-AeK mixed with Ga-68 eluate buffered with sodium acetate to an acidity of pH 4.0 followed by 15 min incubation at 95 °C.

4.3.2 Development of a purification method of [^{68}Ga]Ga-DOTA-AeK

Solid-phase extraction (SPE) is often suggested for improving the radiochemical purity (RCP) of a radiotracer via the removal of impurities, such as uncomplexed-^{68}Ga, colloidal-^{68}Ga, traces of Germanium-68 (^{68}Ge) and co-eluted metals [41, 42]. Here, we tested the product purification procedure for radiolabeled [^{68}Ga]Ga-DOTA-AeK using the different strategies tested, which are listed in **Table A2**.

Firstly, the cartridge retention of [^{68}Ga]Ga-DOTA-AeK by different cartridges was investigated (**Table A2**). The C18 cartridge showed a maximum retention capacity of 84.9 ± 10.6 % of the total amount of radiotracer radioactivity applied, while the lowest retention capacities were observed with the HBL and Stata X cartridges. Since C18 showed the highest [^{68}Ga]Ga-DOTA-AeK retention, it was chosen for further optimization. It was hypothesized that the retention capacity of C18 cartridges could be negatively affected by sample overload, with 15.2 ± 10.6 % of the radiotracer detected in the flow-through when using radio-HPLC (**Table A2**); therefore, two C18 cartridges were combined (290 mg sorbent mass) for purification to test this theory. Based on our results, the 290 mg sorbent C18 cartridge improved the retention capacity, allowing it to reach ≥98 % (**Table A2**). Based on these observations, we conclude that the combined cartridge capacity significantly improved the retention capacity. This finding agrees with that of a study by Alhankawi et al. [43], which reported the improved retention capacity of hydrophilic peptides using C18-C18 loaded with a larger mass of absorbent.

The second optimization procedure concerned the critical effects of wash/rinse solution and volume. and compared the consistencies of purification performance for recovery efficiency and radiotracer purity (**Table 4-1**). Although it was possible to retain [^{68}Ga]Ga-DOTA-AeK on a non-polar C18 absorbent, removing impurities using 1 mL of an aqueous solution resulted in cartridge retention loss with 85.8 ± 6.9 % activity reported post-wash. This was mainly due to the hydrophilic properties of [^{68}Ga]Ga-DOTA-AeK. Therefore, reducing the washing solution volume (0.4 mL) minimized the radiotracer loss to a reported 94.9 ± 6.2 % retained radioactivity (**Table 4-1).**

Finally, efficient recovery of [^{68}Ga]Ga-DOTA-AeK from the cartridge was evaluated using different ethanol concentrations (**Table A2**). Due to the hydrophilic properties of [^{68}Ga]Ga-

DOTA-AeK, 5 % *v*/*v* ethanol solution was sufficient to recover the compound, resulting in a high RCP of ≥9 5% and an excellent recovery of 83.5 ± 7.6 %.

Based on these results, purification using the 290 mg C18 cartridge, 0.4 mL 1× PBS wash solution, and 5 % *v*/*v* EtOH (in PBS pH 7.4) for elution was adopted as a standard SPE purification method for [^{68}Ga]Ga-DOTA-AeK.

Table 4- 1: Influence of reducing washing agent volume during purification performance of SepPak C18 light (in tandem alignment connected back-to-back).

Treatment (Wash & Rinse)	Activity Retention (%LA)	Activity Retention (%LA) Post-Wash	Recovery Efficiency (%RA)	RCP (%)
1 mL PBS (n = 9)	99.7 ± 0.2	85.8 ± 6.9	60.7 ± 12.7	100
0.4 mL PBS (n = 6)	99.8 ± 0.1	94.9 ± 6.2	83.5 ± 7.6	100

SepPak C18 tandem setting was pre-conditioned with 10 mL EtOH and 10 mL H_2O. Product activity was recovered from the cartridge by slow elution with 1 mL 5 % v/v EtOH (aqua) solution. Before purification, the RCP was determined by HPLC analysis of a crude reaction solution of≥95 %. (%LA) = percentage of the total loaded radioactivity from the starting radioactivity with %LA measured (MBq) on the cartridges after the loading step pre- and post-wash. (%RA) = percentage of the total recovered radioactivity from the starting radioactivity with RA measured (MBq) after the activity elution (recovery) step.

4.3.3 Log P determination for [68Ga]Ga-DOTA-AeK

The determination of the radiotracer's hydrophobicity is a critical part of development as it critically affects the biodistribution of the radiotracer [44]. The hydrophobicity of [^{68}Ga]Ga-DOTA-AeK was investigated using the octanol/water partition procedure. Based on the results, 92.3 ± 0.04 % of the tracer was recovered within the aqueous phase with a calculated partition coefficient (LogP) of −1.08 ± 0.00 (n = 3). The results indicate that [^{68}Ga]Ga-DOTA-AeK shows a high level of hydrophilicity.

4.3.4 Serum protein binding of [^{68}Ga]Ga-DOTA-AeK and proteolytic stability

The plasma protein binding properties of [^{68}Ga]Ga-DOTA-AeK were investigated using rapid protein ultrafiltration and separation at different time points. Based on the results (**Figure 4-5**), [^{68}Ga]Ga-DOTA-AeK demonstrated low protein binding properties with an approximately 10.18 ± 6.9 % protein-bound fraction, recorded up to 120 min with no significant difference observed between 30 and 120 min. This observation is mainly attributed to the hydrophilic nature of the radiotracer, as previous studies have demonstrated a positive correlation between hydrophobicity and plasma protein binding [43, 45].

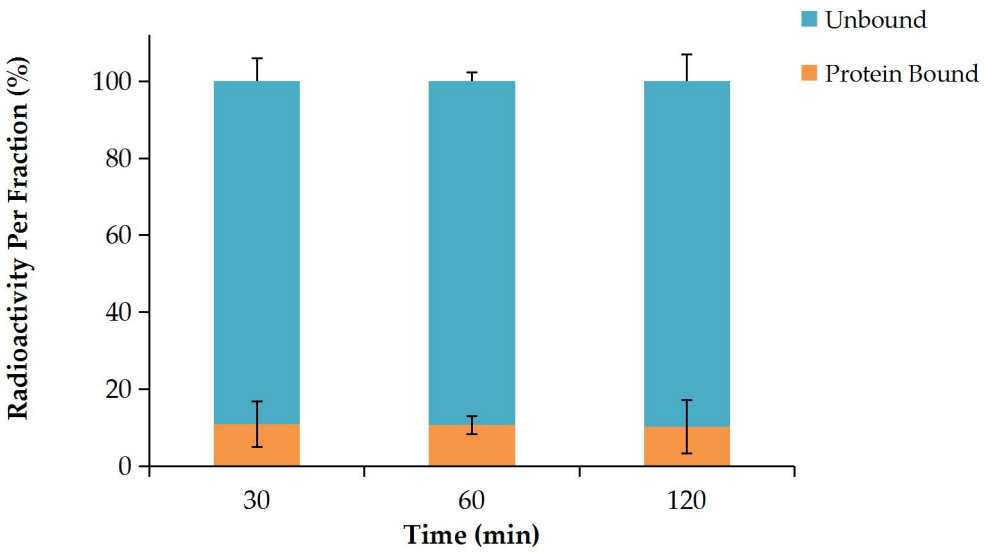

452

453 **Figure 4- 5**: Plasma protein binding of [^{68}Ga]Ga-DOTA-AeK (37°C; over 120 min). The results
454 are represented as mean ± SD (n=3).

455

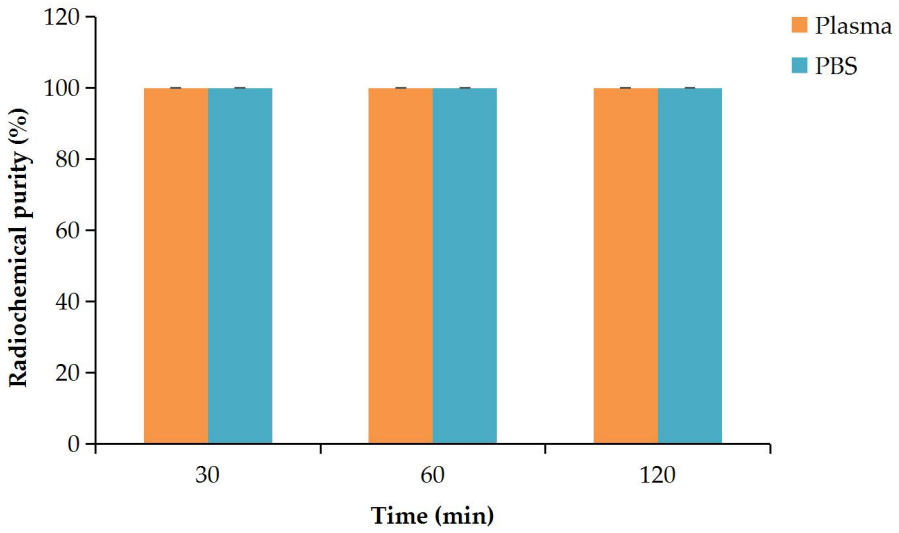

456

457 **Figure 4- 6**: Plasma and PBS stability of [^{68}Ga]Ga-DOTA-AeK at 37°C. The results are
458 represented as mean ± SD (n=3).

459

460 After centrifugal filtration, the unbound radioactivity found in the liquid fraction in the collection
461 tubes was further tested for plasma and PBS stability and analyzed via radio-HPLC. [^{68}Ga]Ga-
462 DOTA-AeK showed no degradation in plasma and PBS (control) over an extended incubation
463 time, thereby maintaining the desired RCP of ≥95 % (**Figure 4-6**).

4.3.5 Formulation stability

The stability of [^{68}Ga]Ga-DOTA-AeK was tested in different product formulations (pH 4.0 and 7.0) post-purification at room temperature. As displayed in **Figure 4-7**, the post-purification eluate (pH 4.0) and neutralized formulation (pH 7.0) remained stable up to 120 min with an RCP of 100 ± 0 % and 98.8 ± 2.0 %, respectively,. In neutral and slightly basic conditions, deprotonation of donor atoms (e.g., nitrogen) might occur, potentially increasing the metal-binding capacity. However, if the solution becomes too basic, the metal ion may hydrolyze, forming metal hydroxides, which reduces the stability and purity of the radiotracer, with a non-specific distribution likely to be seen in the liver, spleen, and bone [46, 47]. Based on the results, we achieved a <10 % *v*/*v* EtOH formulation with the RCP of ≥95 % required for preclinical investigations.

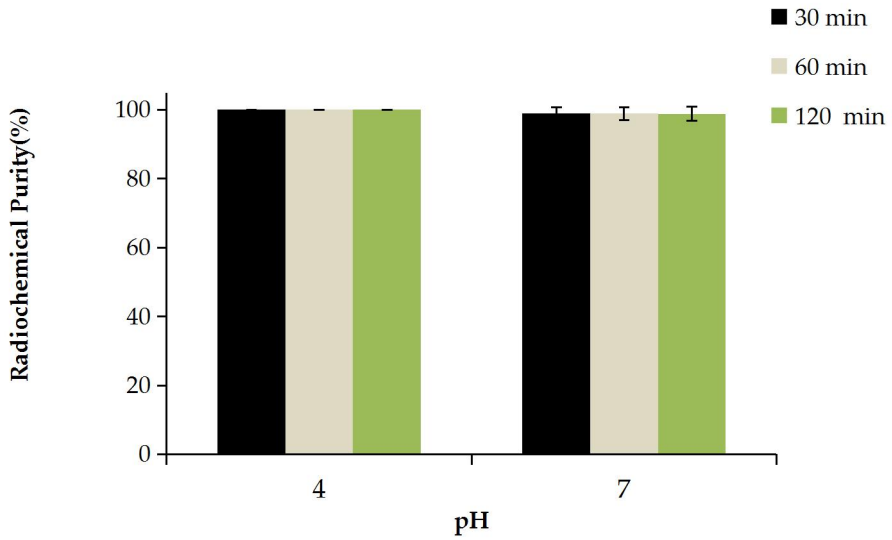

Figure 4-7: Stability of purified [^{68}Ga]Ga-DOTA-AeK formulation (pH 4.0 and 7.0; room temperature; up to 120 min) analysed by radio-HPLC (re-occurrence of free Ga-68 species). The results are represented as mean ± SD (n=3).

4.3.6 Bacterial cell uptake of [^{68}Ga]Ga-DOTA-AeK

To test if bacteria were able utilize [^{68}Ga]Ga-DOTA-AeK, *in vitro* studies were performed by incubating live and heat-killed bacterial cultures of *E. coli* and *S. aureus* with the tracer for different time periods. No significant increase in radioactivity above the heat-killed bacterial cells was measured at any time point up to 120 min with ~98 % of the radiotracer detected in the medium (**Figure 8a,b**). Similar to our results, a lack of bacterial uptake and internalization was previously reported for ^{3}H-labeled disaccharide-(L-Ala-D-Glu-meso-A2pm) tripeptide (800 g/mol), an analogue of AeK, while the same study demonstrated successful *in vitro* integration of L-Ala-γ-D-Glu-[^{3}H]A2pm into the PG layer of *E. coli* [24]. Thus, *in vitro* results of our study suggest the unsuccessful integration of [^{68}Ga]Ga-DOTA-AeK.

(a)

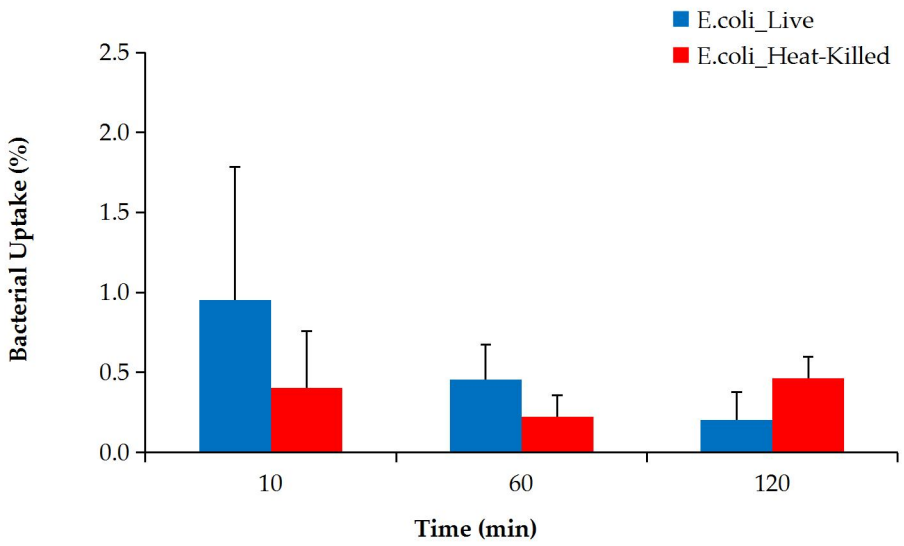

(b)

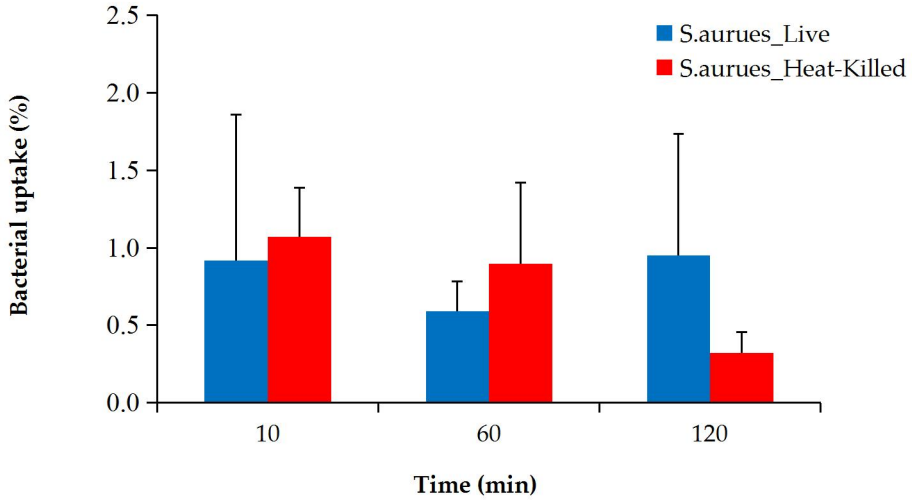

Figure 4- 8: Cellular uptake of [^{68}Ga]Ga-DOTA-AeK in live and heat-killed bacterial cultures of (**a**) *E. coli* and (**b**) *S. aureus* incubated at 37°C for up to 120 min (n=3). Unpaired Student's t-tests were performed for comparison. $p<0.05$ values were considered statistically significant. All measured were not significant.

Based on these findings, it was hypothesized that the conjugation of DOTA to the AeK tripeptide interfered with the targeting properties of [^{68}Ga]Ga-DOTA-AeK. To justify this interpretation, the *in vitro* incorporation of the initially studied fluorescent analogue of AeK (AeK-NBD) was measured in live and heat-killed *E. coli* and *S. aureus* cells using flow cytometry and confocal imaging. The flow cytometry analysis demonstrated (**Figure 4-9a,b**) high fluorescence intensity in both live *E. coli* and *S. aureus* cells, which was significantly decreased in heat-killed cell cultures ($p < 0.05$). Furthermore, as demonstrated in our experiments and a previous study [25], the bacterial incorporation of AeK-NBD was observed at 10 min, indicating that uptake occurred immediately after adding the tracer to the bacterial cultures (**Figure 4-9a,b**). This observation was supported by confocal imaging (**Figure A4**).

(a)

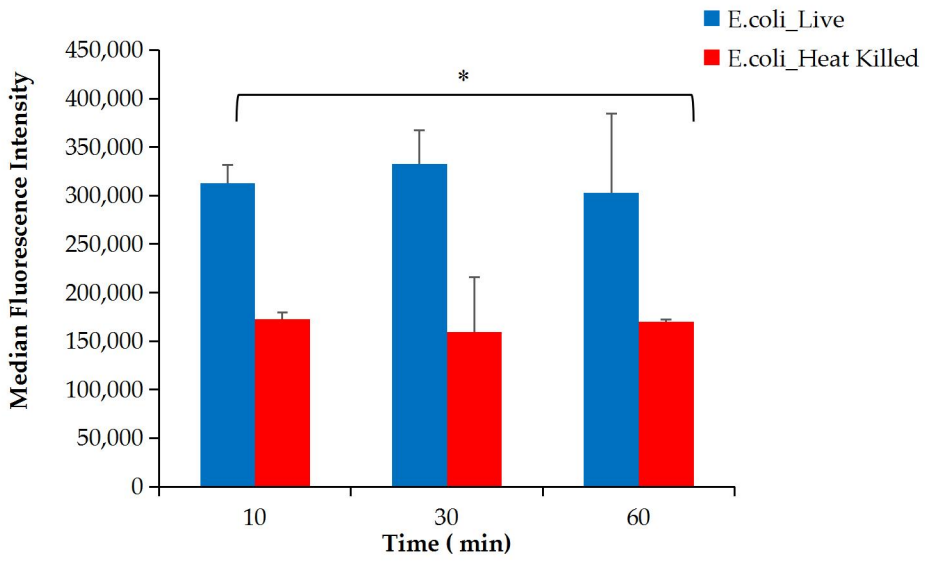

(b)

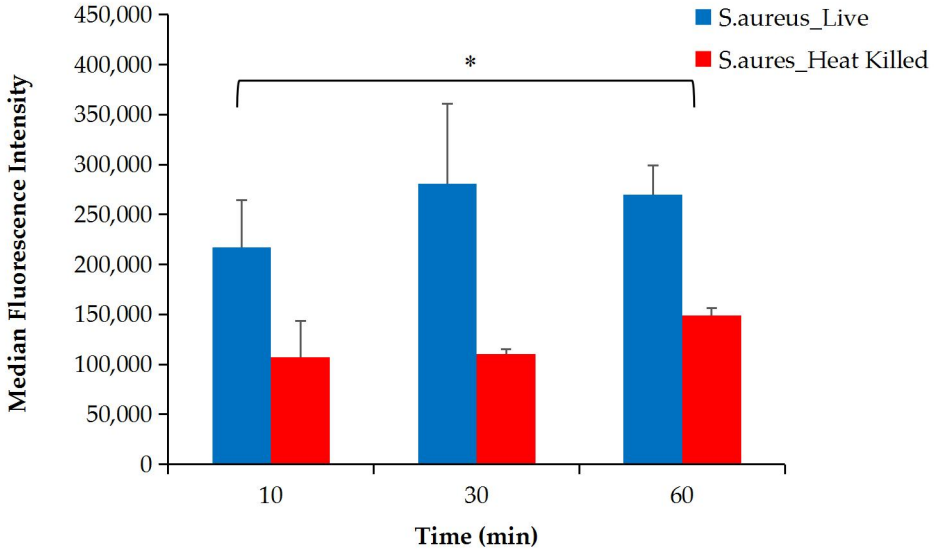

Figure 4-9: Flow cytometry analysis of live and heat-killed (**a**) *E. coli* and (**b**) *S. aureus* cell cultures incubated with AeK-NBD for up to 60 min (counterstained with Vybrant DyeCycle). Results are represented as mean and SD (n=2 for each parameter). Unpaired Student's t-tests were performed for comparison, with *p* values <0.05 (*) considered statistically significant.

Therefore, it is plausible from previous studies that PG-targeting tripeptides containing either diaminopimelic acid (A2pm) or lysine can be taken up by bacteria, which was evident with [^{3}H]L-Ala-γ-D-Glu-meso-A2pm and AeK-NBD [24, 25]. Interestingly, contrary to previous findings in the literature, we demonstrated bacterial uptake of AeK-NBD not only in *E. coli* but also in *S.aureus* cultures, which was not tested for accuracy and specificity. However, our data suggest that although DOTA-AeK (732.79 g/mol) and AeK-NBD (509.48 g/mol) have the same targeting entity (AeK), the imaging vector can interfere with the metabolic integration of AeK into the PG macrostructure. There is some evidence supporting the assumption of a molecular weight cut off, with a ≤600 g/mol requirement for active membrane transportation, as seen with other PG targeting molecules [48]. We may therefore attribute the lack of bacterial uptake seen with [^{68}Ga]Ga-DOTA-AeK to its unfitting molecular size preventing active transportation or influx across the cellular membrane, and crucially hindering the intracellular enzymatic metabolism necessary for incorporating [^{68}Ga]Ga-DOTA-AeK into the PG.

4.3.7 Exploratory biodistribution of [^{68}Ga]Ga-DOTA-AeK

4.3.7.1 PET/CT imaging and *ex vivo* biodistribution

Despite the lack of bacterial incorporation of [^{68}Ga]Ga-DOTA-AeK in this study, the intracellular uptake observed earlier with AeK-NBD encouraged us to further characterize AeK in an *in vivo* setting, including PET imaging of infected animals. Therefore, preliminary *in vivo* biodistribution studies of [^{68}Ga]Ga-DOTA-AeK were performed to understand the pharmacokinetics of AeK using *E. coli*- or *S. aureus*-bearing mice also suffering from sterile muscular inflammation. Results from qualitative PET/CT image analysis and *ex vivo* tissue counting suggest that [^{68}Ga]Ga-DOTA-AeK showed no significant uptake in the infectious foci (tested at Day 3 and Day 5 post-inoculation of either *E. coli* or *S. aureus*). In contrast, the radiotracer was more pronounced in the sterile inflammation site in both cohorts (**Figure 4-10a,b**).

However, the results should be interpreted with caution due to limitations in the experimental model, since active infections could not be confirmed (**Figure A5A–D**) and the imaging protocol was carried out later than at the standard 24 hrs post-inoculation. A critical reason is that after 3 or 5 days, most of the bacteria in the infected tissue were phagocytosed by host macrophages or otherwise had been encapsulated or included in a biofilm, therefore possibly being inaccessible for the radiotracer [49].

(**a**)

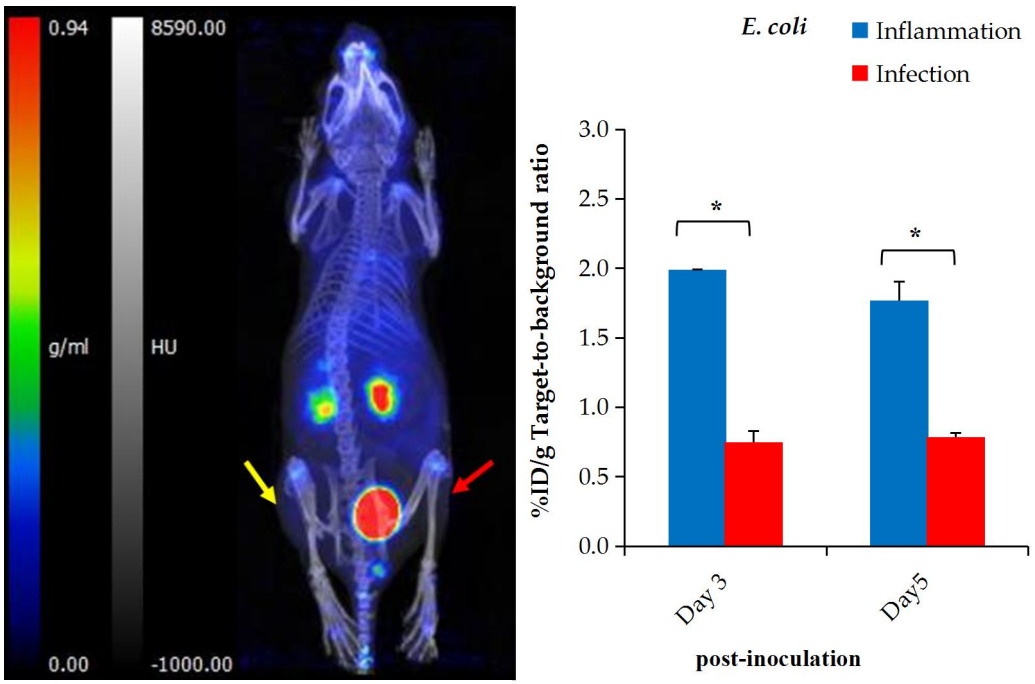

(b)

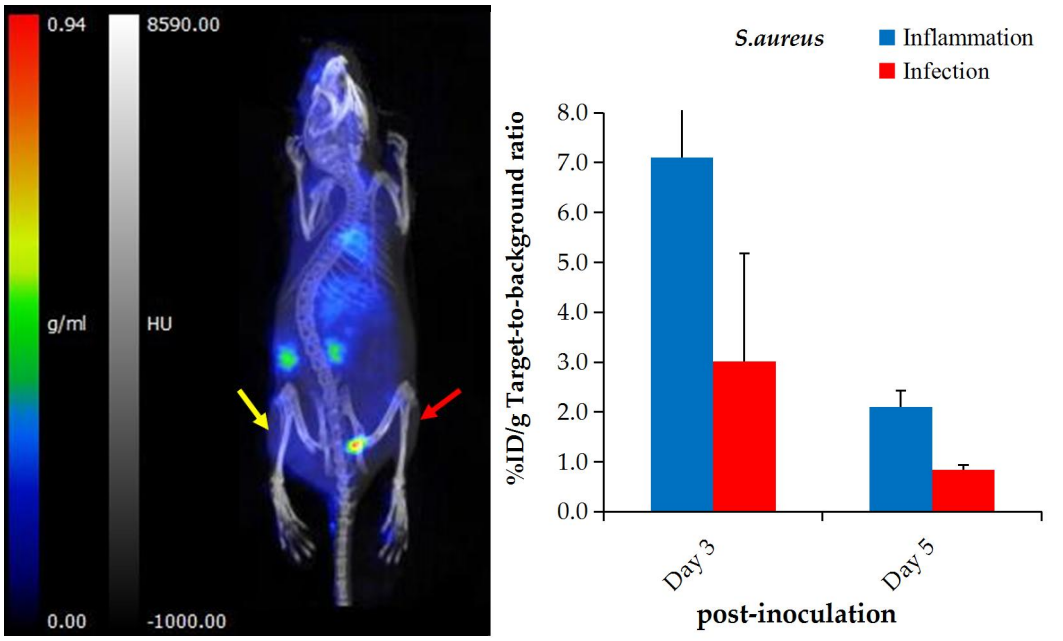

Figure 4-10: Representative PET/CT images and corresponding *ex vivo* biodistribution of [^{68}Ga]Ga-DOTA-AeK after 60 min of intravenous injection in (**a**) *E. coli* and (**b**) *S .aureus* model of infection (*red arrow*) and inflammation (*yellow arrow*) at 3 and 5 days post-inoculation. Unpaired Student's t-tests were performed for comparison, with *p* values <0.05 (*) considered statistically significant.

The *ex vivo* biodistribution data correlated with the findings from PET/CT imaging **Figure4-10a-b**. Unlike other PG targeting radiotracers [9, 50-52], [^{68}Ga]Ga-DOTA-AeK showed minimum signal in background organs Interestingly, significant increased uptake was observed in the heart, liver, lungs of the *S .aureus* group at Day 5 post-inoculation and this is more likely due to physiology changes induced from the initial infection and/or inflammation (**Table A3**).Despite traces of the radiotracer detected in the liver, hepatobiliary excretion was excluded with rapid clearance mainly by renal excretion. This can be explained by the hydrophilic properties of [^{68}Ga]Ga-DOTA-AeK under physiological conditions. In addition, the *in vivo* stability of [^{68}Ga]Ga-DOTA-AeK was confirmed as indicated, with very limited uptake of radioactivity in the bone (≤2 %D/g) (**Table A3**).

4.4 CONCLUSION

An initial preclinical investigation of the tripeptide AeK to determine its potential role as a prospective PET imaging agent for the visualization of bacterial infections by the targeting PG salvage pathway was presented. We provided new insights for NBD-AeK analog internalization by Gram-negative bacteria (*E. coli*) and a Gram-positive (*S. aureus*) strain. Motivated by the results, a ^{68}Ga radiosynthesis protocol was developed for the DOTA-AeK analog, featuring optimal labeling parameters and a tailored purification procedure that further allowed for initial radiochemical characterization and early bio-pharmacological preclinical investigations. Promising radiochemical and proteolytic compound stability result motivated us to conduct non-invasive small animal PET imaging.

The achieved results from both *in vitro* and *in vivo* bacteria uptake studies are sufficient for us to conclude that the overall low uptake rate and cellular turnover, attributed to the large molecular weight, compromise the ability of [^{68}Ga]Ga-DOTA-AeK to be qualified as a sensitive and infection-specific radiopharmaceutical. Of interest is that minimal accumulation of [^{68}Ga]Ga-DOTA-AeK in response to inflammation was observed; however, whether this might impact the specificity of AeK as a potential radiotracer in infection imaging remains unclear.

While the results of this study prove that AeK is a PG biosynthesis-targeting molecule (even when conjugated to NBD), intracellular or membrane incorporation of [^{68}Ga]Ga-DOTA-AeK will be a prerequisite for thriving dedicated bacteria-specific imaging. Plausibly, ^{68}Ga-DOTA functionalization of AeK (i.e., a necessary replacement of the NBD entity) made the resulting molecule lose valuable functionality for the PG recycling pathway by hindering active membrane transportation. Addressing such a shortcoming, the approach for future studies will focus on preserving the targeting moiety of AeK tripeptide with minimal structural alterations, which can be achieved using alternative direct radiolabeling strategies without the need for radioisotope chelation (e.g., ^{11}C and ^{18}F, or $^{131/124}$I). This will include exploration into the diverse chemical structures of AeK tripeptide and subsequent structure–activity relationship investigations for the optimization and improvement of biodistribution and specificity.

4.5 AUTHOR CONTRIBUTIONS:

Conceptualization, P.C.K. and T.E.; methodology, P.C.K. and T.E.; investigation, P.C.K.; resources, C.D., I.v.d.B. and F.C.; data curation, P.C.K.; data validation, P.C.K., T.E., M.M.W., S.M., A.M., J.T-W., C.D., I.v.d.B., F.C.; writing—original draft preparation, P.C.K.; writing—review and editing, P.C.K., T.E., M.M.W., S.M., A.M., J.T.-W., C.D., I.v.d.B., F.C. and M.M.S.; supervision, T.E., A.M. and M.M.S. All co-authors granted permission for submission. All authors have read and agreed to the published version of the manuscript.

4.6 FUNDING

This work was supported by the National Research Foundation DSI-NRF Innovation Doctoral Scholarship (Reference No.: MND190517436945) and the Oppenheimer Memorial Trust Award (OMT Ref. 2023-1567).

4.7 INSTITUTIONAL REVIEW BOARD STATEMENT

All procedures were conducted according to the ARRIVE guidelines as prescribed by the European Communities Council Directive (86/609 EEC) and approved by the University of Pretoria Animal Ethics Committee Ethics approval number: 435/2020.

4.8 INFORMED CONSENT STATEMENT

Not applicable.

4.9 DATA AVAILABILITY STATEMENT

Data are contained within the article and **Appendix A**.

4.10 ACKNOWLEDGEMENTS

The authors would like to thank Thato Sello from Radiochemistry, Necsa, for providing guidance on purification development, Prof Duncan Cromarty from the Department of Pharmacology, UP, for providing consumables and equipment, Prof Marleen Kock from Medical Microbiology, UP, for providing bacterial strains and equipment, Janke Kleynhans for assisting us with mass spectrometry, The Paraclinical Science Faculty of Veterinary Science, section of

pathology, UP, for providing histopathology analysis, and the staff from NuMeri who assisted with the animal studies and analysis of the images.

4.11 AUTHOR DECLARATIONS

Author John Takyi-Williams was employed by the company Therapeutics Systems Research Laboratories (TSRL), Inc during the manuscript preparation. The remaining authors declare that the research was conducted in the absence of any commercial or financial relationships that could be construed as a potential conflict of interest.

ABBREVIATIONS

AeK	L-Ala-γ-D-Glu-L-Lys
CFU	Colony forming units
CT	Computed tomography
DOTA	4,7,10 tetraaza-cyclododecane-N,N′,N″,N‴-tetraacetic acid
E. coli	*Escherichia coli*
HLB	Hydrophilic–lipophilic balance
HPLC	High-performance liquid chromatography
%ID/g	Percentage of injected dose per gram organ
ITLC	Instant thin-layer chromatography
IVC	Individually ventilated cages
MFI	Median fluorescence intensity
MRI	Magnetic resonance imaging
NBD	N-7-nitro-2,1,3-benzoxadiazol-4-yl
Opp	Oligopeptide permease
PBS	Phosphate-buffered saline
PET	Positron emission tomography
PG	Peptidoglycan
R*f*	Retention factors
R*s*	Resolution
RCP	Radiochemical purity
S. aureus	*Staphylococcus aureus*
SD	Standard deviation
SPE	Solid-phase extraction
TSB	Tryptic soy broth

UDP-MurNAc	Uridine diphosphate -N-acetylmuramic acid
VDC	Vybrant DyeCycle

APPENDIX A: SUPPLEMENTARY DATA

4.1 APPENDIX A.1. MATERIAL

4.1.1 General Information

All chemicals and solvents were purchased from Merck (Darmstadt, Germany), Thermo Fisher Scientific (Waltham, MA, USA), Sigma-Aldrich (St. Louis, MO USA), and Anatech Analytical Technology (Gauteng, South Africa). The AeK-NBD (509.48 g/mol) and DOTA-AeK (732.79 g/mol) peptides were purchased from GLBiochem (Shanghai, China). All the reagents used were prepared using ultra-purified water produced in-house by a Simplicity 185 Millipore system (Merck, Darmstadt, Germany). ^{68}Ga-activity was produced by a SnO_2 matrix-based ^{68}Ge/^{68}Ga generator (iThemba Labs, Cape Town, South Africa) and eluted in 0.6 M hydrochloric acid (HCI). The eluted radioactivity was routinely measured using a Capintec CRC-25R dose calibrator (Florham Park, NJ, USA); eluate acidity was determined using MQuant pH indicator strips (Merck, Darmstadt, Germany). The purity of DOTA-AEK was determined via a Waters Acquity LC/MS system equipped with a Waters XBridge BEH C18 column (3.5 µm, 100 mm × 3 mm, 130 Å) at a flow rate of 5 mL/min using a gradient of Acetonitrile 0.1 % formic acid (5–95 % over 10 min) and Water 0.1 % formic acid. Instant thin layer chromatography (ITLC) using TLC-Silical gel (TLC-SG)-impregnated paper (Agilent Technologies, Santa Clara, CA, USA) as the stationary phase was conducted for the analysis of [68Ga]Ga-DOTA-AeK using a Veenstra VCS-201 multi-channel chromatogram (Veenstra Instruments, Friesland, The Netherlands). The bacterial strains *Escherichia coli* (*E. coli*, ATCC 29213) and *Staphylococcus aureus* (*S. aureus*, ATCC 29213) were provided by the Department of Medical Microbiology, University of Pretoria, South Africa.

4.2 APPENDIX A.2. RESULTS

4.2.1 Appendix A.2.1. Testing radioanalytical methods for [^{68}Ga]Ga-DOTA-AeK quality control

4.2.1.1 HPLC and LC/MS

The chemical purity of DOTA-AeK was determined via C18-reverse-phase HPLC. LC/MS analysis of DOTA-AEK confirmed that the compound was pure and demonstrated the correct mass (calculated 732.79 g/mol) with the presence of the following peaks: 733.4 ($[M+H]^{+}$), 734.4 ($[M+H]^{2+}$), 755.40 ($[M+H+Na]^{+}$), 756.35 ($[M+H+Na]^{2+}$), 367.39 ($½[M+H]^{1+}$), and 368.13 ($½[M+H]^{2}$) (**Figure A1**). The chromatogram showed a dominant peak at a retention time of 5.2 min, which was not detected in the run with pure water (**Figure A2A**)

The radio-HPLC analysis of [^{68}Ga]Ga-DOTA-AeK is shown in **Figure A2B,** indicating a retention time of 5.9 min. This peak is clearly separated from the retentions of ^{68}Ga species eluting at ≤1.5 min. The assay provided an appropriate resolution, >1.5 (i.e., baseline peak separation), to analyze the radiochemical purity and was able to observe plausible radiolabeled by-products.

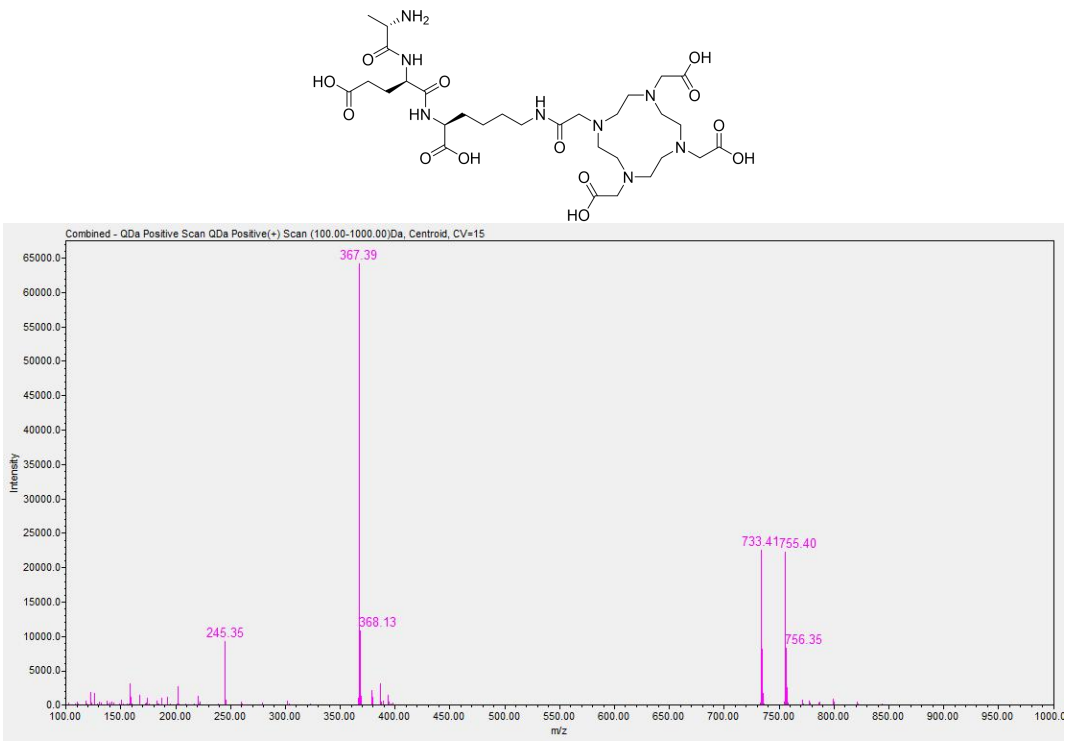

Figure A1: LC/MS spectrum of DOTA-AeK showing m/z ratios of 733.4 ($[M+H]+$), 734.4 ($[M+H]^{2}+$) ,755.40($[M+H+Na]^{+}$), 756.35 ($[M+H+Na]^{2+}$)· 367.39 ($½[M+H]^{1+}$), 368.13 ($½[M+H]^{2}$).

A.

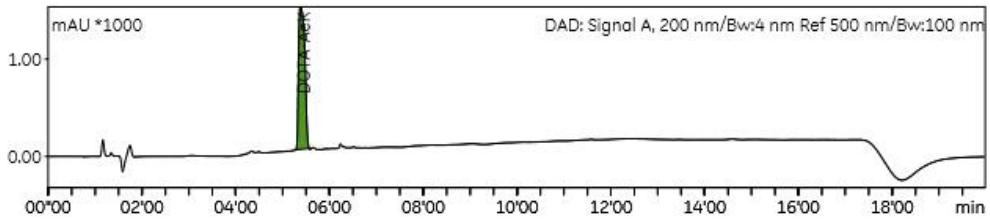

B.

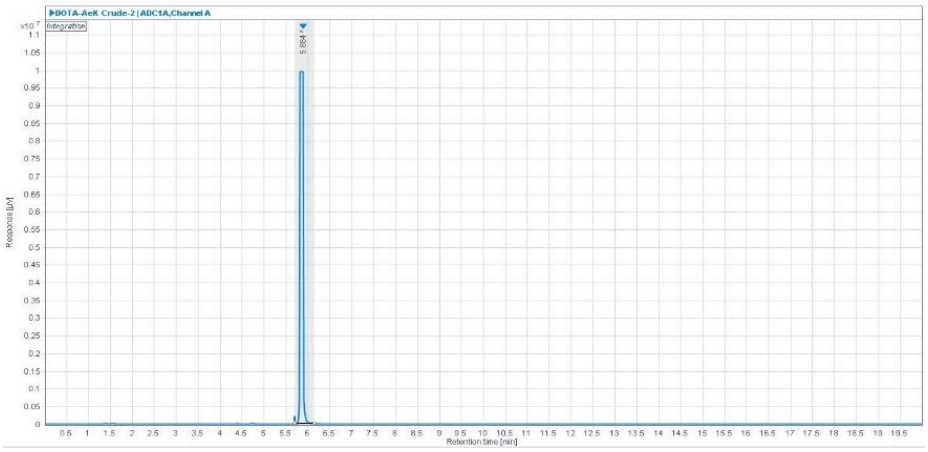

Figure A2: Representative analytical HPLC chromatogram of (**A**) DOTA-AeK with a retention time of 5.2 min and (**B**) crude *[^{68}Ga]Ga-DOTA-AeK with retention time 5.9 min.

4.2.2 ITLC

Radio-ITLC methods A and B were tested to study the fit-for-purpose aspect of the method and determine the %RCP and %RCY (**Figures A3A,B**). Both samples demonstrate the confirmed [^{68}Ga]Ga-DOTA-AeK product acquired during radio-HPLC analysis. Results for R*f* and R*s* calculations are displayed in **Table A1**.

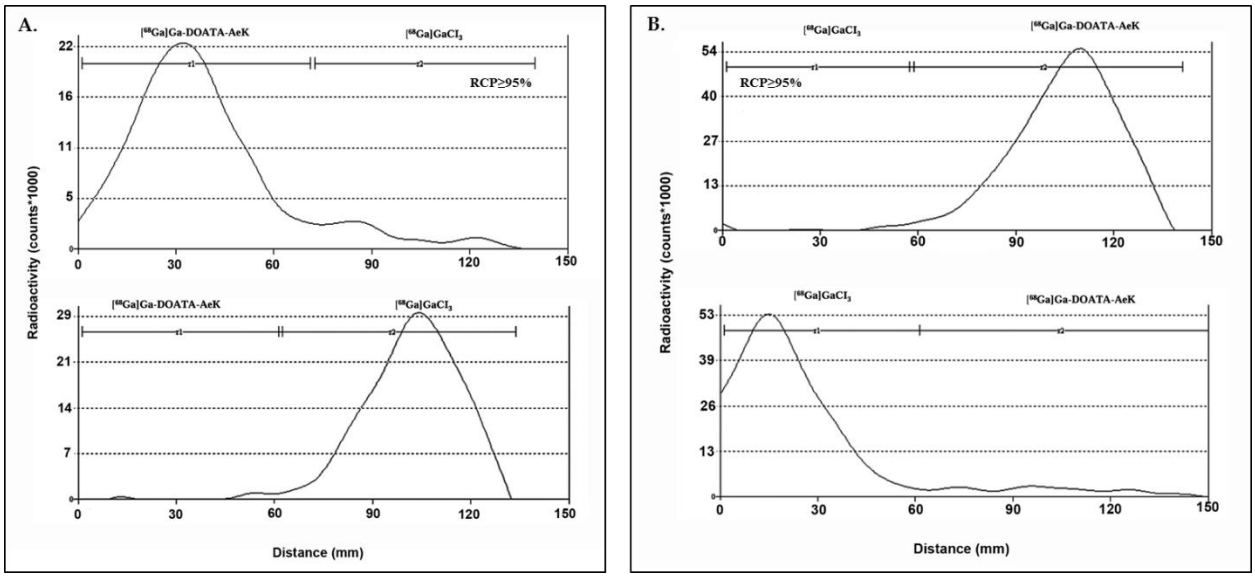

Figure A3: ITLC chromatogram of [^{68}Ga]Ga-DOTA-AeK (*top*) and [^{68}Ga]$GaCl_3$ (pH 4) (*bottom*) using (**A**) mobile phase A: 0.1M citric acid (pH 5.0) and (**B**) mobile phase B: 1 M Ammonium Acetate: Methanol (1:1).

Table A1: ITLC retention factors and method resolution for [^{68}Ga]Ga-DOTA-AeK

	Mobile Phase A		**Mobile Phase B**	
	[^{68}Ga]Ga-DOTA-AeK	**[^{68}Ga]$GaCl_3$ (Ionic + Colloidal)**	**[^{68}Ga]Ga-DOTA-AeK**	**[^{68}Ga]$GaCl_3$ (Ionic + Colloidal)**
Rf	0.2	0.7	0.7	0.1
Rs	1.6		1.1	

Mobile phase A: 0. 1M citric acid (pH 5.0); mobile phase B: 1 M ammonium acetate: methanol (1:1). Rf: retention factors; Rs: resolution

4.2.3 Appendix A.2.2. Development of a purification method of [^{68}Ga]Ga-DOTA-AeK

Table A2: Summary of results comparing different purification strategies

Cartridge-Absorbent	Conditioning (volume/agent)	Activity Retention (%$_{LA}$)	Wash and Rinse (volume/agent)	Activity Retention (%$_{LA}$) Post-wash	Activity Elution (volume/agent)	Recovery Efficiency (%$_{RA}$)	%RCP
(A) C-18 145 mg	4 mL EtOH + 2 mL H_2O	72.8	1 mL H_2O	-	1 mL 50 % *v/v* EtOH *	37.3	39.9
	4 mL EtOH + 2 mL H_2O	92.6	1 mL Saline	60	1 mL 50 % *v/v* EtOH**	46.2	11.8
	4 mL EtOH + 2 mL H_2O	89.2	1 mL PBS	55.7	1 mL 50 % *v/v* EtOH *	41.6	11.9
(B) C-8 145 mg	3 mL EtOH + 3 mL H_2O	83.8	1 mL Saline	32.5	1 mL 100 % *v/v* EtOH	19.4	12.6
(C) HBL 200mg	1 mL EtOH + 1 mL H_2O	42.4	1 mL H_2O	-	1 mL 100 % *v/v* EtOH	5.5	11.2
(D) Strata X 100 mg	4 mL EtOH + 2 mL H_2O	63.6	1 mL H_2O	7.5	1 mL 100 % *v/v* EtOH	6.1	19.7
(A–A) C-18 290 mg	10 mL EtOH + 10 mL H_2O	98.4	1 mL 50 % EtOH *	35.2	1 mL50 % *v/v* EtOH *	29.1	15.3
	10 mL EtOH + 10 mL H_2O (n = 9)	99.7 ± 0.2	1 mL PBS	85.8 ± 6.9	1 mL 5 % *v/v* EtOH **	60.7 ± 12.7	100
	10 mL EtOH + 10 mL H_2O	99.4	0.4 mL H_2O	93.8	1 mL 10 % *v/v* EtOH *	78.3	39.9

	10 mL EtOH + 10 mL H_2O (n = 6)	99.8 ± 0.1	0.4 mL PBS	94.9 ± 6.2	1 mL 5 % *v/v* EtOH **	83.5 ± 7.6	100

All listed purifications were performed once with known %RCP determined by HPLC analysis from crude reaction solution >95 %. %LA) the percentage of the total loaded radioactivity from the starting radioactivity with LA measure (MBq) on the cartridges after loading step pre and post-wash %EA) the percentage of the total recovered radioactivity from loaded cartridges radioactivity with EA measured (MBq) after the activity elution from cartridge post-wash**.** %RA) percentage of the total retained radioactivity on cartridges from the starting radioactivity with RA measured (MBq) after the activity elution (recovery) step. A A) tandem setup where cartridges were connected back-to-back. *) in water; **) PBS (pH7.4).

4.2.4 Appendix A.2.3. Confocal imaging

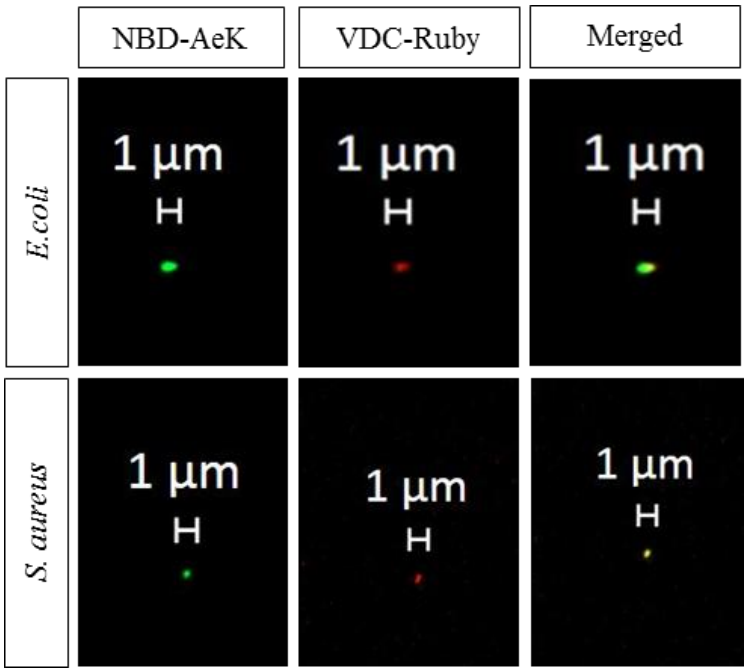

Figure A4: Representative confocal images of live *E. coli* and *S. aureus* cells labeled with NBD-AeK (green) and counterstained with the DNA stain VDC Ruby dye (red).

4.2.5 Appendix A.2.4. [^{68}Ga]Ga-DOTA-AeK- *ex vivo* biodistribution

Table A3: *Ex vivo* organ biodistribution (%ID/g) of [^{68}Ga]Ga-DOTA-AeK in a dual-mice model of infection (*E. coli* or *S. aureus)* and inflammation at Day 3 and 5 post-inoculation.

post-inoculation	*E. coli*			*S. aureus*		
	Day3 (n=4)	**Day5** (n=4)	***p*-value**	**Day3** (n=5)	**Day5** (n=3)	***p*-value**
Brain	0.1 ±0.0	0.2±0.2	0.344	0.1±0.0	0.2±0.0	0.030
Thyroid	1.0±0.7	0.7±0.3	0.497	0.9±0.5	1.9±0.3	0.020
Heart	0.8±0.4	1.6±1.3	0.299	1.2±0.3	3.7±0.5	0.000
Lungs	1.0±0.1	2.0±0.4	0.003	1.8±0.5	3.7±0.5	0.002
Liver	1.1±0.2	1.2±0.4	0.631	1.5±0.5	3.6±1.5	0.024
Spleen	0.7±0.3	0.7±0.1	0.986	1.4±1.6	1.6±0.6	0.801
Pancreas	0.6±0.3	0.8±0.4	0.450	0.7±0.3	2.3±0.2	0.000
Stomach	0.3±0.1	1.3±1.8	0.295	0.7±0.5	1.1±0.4	0.347
Intestines	0.4±0.2	1.1±1.2	0.356	1.2±1.9	1.8±0.8	0.653
Kidneys	3.8±1.6	2.9±0.7	0.374	5.6±3.4	7.0±0.1	0.512
Adipose	0.7±0.1	0.8±0.7	0.459	1.0±0.4	1.9±0.3	0.010
Femur	1.4±1.0	0.9±0.4	0.453	1.2±1.3	2.0±0.2	0.335
Muscle	0.7±0.4	0.6±0.2	0.632	0.4±0.4	1.1±0.5	0.041
Inflammation	0.9±0.0	0.9±0.1	0.987	1.1±0.5	2.6±0.6	0.010
Infection	0.4±0.1	0.4±0.0	0.398	0.8±0.6	0.9±0.3	0.781
Inflammation/muscle	2.0±1.6	1.8±0.8	0.492	7.1±9.9	2.1±0.3	0.064
Infection/muscle	0.8±0.5	0.8±0.3	0.771	3.0±0.2	0.8±0.1	0.559

*Unpaired t-tests were performed for comparison; $p < 0.05$ were considered statistically significant.

4.2.6 Appendix A.2.5. Histopathology

The H&E staining of both *E. coli* and *S. aureus* infection sites revealed variably mild to moderate inflammatory foci consisting of the infiltration of macrophages, neutrophils, and lymphocytes (granulomatous inflammation) (**Figure A5A,B**). Despite the inflammatory markers observed for both *E. coli* and *S. aureus* infection, the presence of bacteria intralesionally could not be confirmed for both *E. coli* and *S. aureus* infection via H&E and Gram staining (**Figure A5C,D**). As previously reported, this might have been due to the heterogeneous low-density bacterial distribution and phagocytosis of bacteria by macrophages [53]. As a study limitation, bacterial culturing, which is a more sensitive technique for verifying the presence of active infection, was not carried out [54].

The tissue responses to turpentine-induced severe intramuscular inflammation were mainly characterized by necrosis, edema, and neovascularization, and were similar in all mice at Day 3 and Day 5 post-induction. As expected, no positive bacteria staining was confirmed in the inflammation area (**Figure A6A,B**).

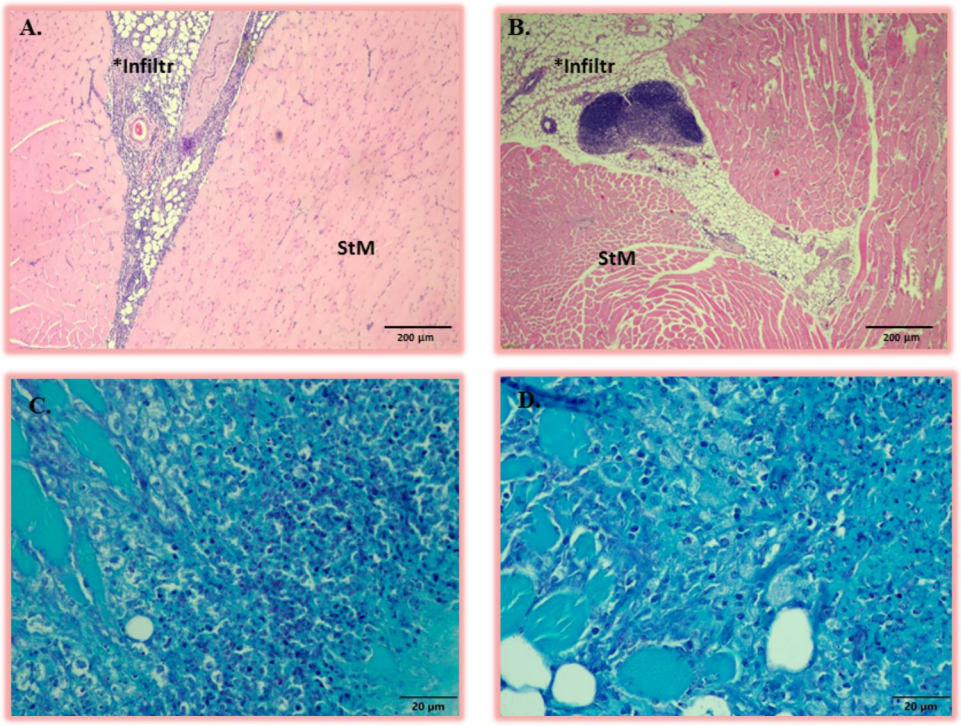

Figure A5: Representative histopathologic analysis of thigh muscular tissue at Day 3 and 5 post-inoculations with either (**A**) *E. coli* or (**B**) *S. aureus*. All the lesions induced by *E. coli* or *S. aureus* were identical and presented with moderate infiltration of neutrophils, macrophages, and lymphocytes (areas marked **Infiltr** *) within the adipose and striated muscle (**StM**). The corresponding Gram staining sections of (**C**) *E. coli* or (**D**) *S. aureus* post-inoculation in thigh muscular tissue at Days 3 and 5 are shown with no visualization of representative bacterial strains.

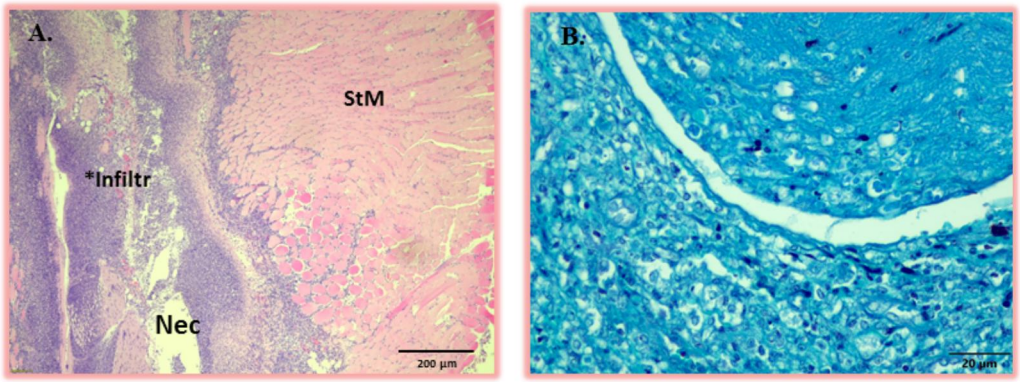

Figure A6: **(A)** Representative histopathology analysis of thigh muscular tissue showing inflammatory response to sterile turpentine oil injection at Day 3- and 5 post-inoculations. All the turpentine-induced tissue lesions were identical and presented with severe necrotic tissue areas (**Nec**) and infiltration of neutrophils and macrophages (area marked **Infiltr** *) within adipose and striated muscle (**StM**). **(B)** Corresponding Gram staining sections of thigh muscular tissue at Day 3 and 5 post-inoculation with turpentine oil showing the absence of bacterial strains.

4.3 REFERENCES

1. Laxminarayan R, Duse A, Wattal C, Zaidi AK, Wertheim HF, Sumpradit N, Vlieghe E, Hara GL, Gould IM, Goossens H. Antibiotic resistance—the need for global solutions. *Lancet Infect Dis*. *2013*;13(12):1057-98.

2. Laupland KB, Valiquette L. The changing culture of the microbiology laboratory. *Can J Infect Dis Med Microbiol*. *2013*;24(3):125-8.

3. Rak M, Barlič-Maganja D, Kavčič M, Trebše R, Cőr A. Comparison of molecular and culture method in diagnosis of prosthetic joint infection. *FEMS Microbiol Lett*. *2013*;343(1):42-8.

4. Kumar R, Basu S, Torigian D, Anand V, Zhuang H, Alavi A. Role of modern imaging techniques for diagnosis of infection in the era of ^{18}F-fluorodeoxyglucose positron emission tomography. *Clin Microbiol Rev*. *2008*;21(1):209-24.

5. Signore A, Glaudemans AWJM. The molecular imaging approach to image infections and inflammation by nuclear medicine techniques. *Ann Nucl Med*. *2011*;25(10):681-700.

6. Pijl JP, Kwee TC, Slart R, Glaudemans A. PET/CT Imaging for Personalized Management of Infectious Diseases. *J Pers Med*. *2021*;11(2):133.

7. Vos FJ, Bleeker-Rovers CP, Sturm PD, Krabbe PF, van Dijk AP, Cuijpers ML, Adang EM, Wanten GJ, Kullberg B-J, Oyen WJ. 18F-FDG PET/CT for detection of metastatic infection in gram-positive bacteremia. *J Nucl Med*. *2010*;51(8):1234-40.

8. Pijl JP, Nienhuis PH, Kwee TC, Glaudemans A, Slart R, Gormsen LC. Limitations and Pitfalls of FDG-PET/CT in Infection and Inflammation. *Semin Nucl Med*. *2021*;51(6):633-45.

9. Polvoy I, Seo Y, Parker M, Stewart M, Siddiqua K, Manacsa HS, Ravanfar V, Blecha J, Hope TA, Vanbrocklin H, Flavell RR, Barry J, Hansen E, Villanueva-Meyer JE, Engel J, Rosenberg OS, Wilson DM, Ohliger MA. Imaging joint infections using D-methyl-^{11}C-methionine PET/MRI: initial experience in humans. *Eur J Nucl Med Mol Imaging*. *2022*;49(11):3761-71.

10. Gemmel F, Dumarey N, Welling M, editors. Future diagnostic agents. Semin Nucl Med; 2009; Amsterdam, The Netherland: *Elsevier*. pp. 11-26.

11. Ordonez AA, Jain SK. Pathogen-Specific Bacterial Imaging in Nuclear Medicine. *Semin Nucl Med*. *2018*;48(2):182-94.

12. van Oosten M, Hahn M, Crane LMA, Pleijhuis RG, Francis KP, van Dijl JM, van Dam GM. Targeted imaging of bacterial infections: advances, hurdles and hopes. *FEMS Microbiol Rev*. *2015*;39(6):892-916.

13. Kleynhans J, Sathekge MM, Ebenhan T. Preclinical Research Highlighting Contemporary Targeting Mechanisms of Radiolabelled Compounds for PET Based Infection Imaging. *Semin Nucl Med*. *2023*.

14. Parker MFL, Flavell RR, Luu JM, Rosenberg OS, Ohliger MA, Wilson DM. Small Molecule Sensors Targeting the Bacterial Cell Wall. *ACS Infectious Diseases*. *2020*;6(7):1587-98.

15. Egan AJF, Errington J, Vollmer W. Regulation of peptidoglycan synthesis and remodelling. *Nat Rev Microbiol*. *2020*;18(8):446-60.

16. Hiron A, Borezée-Durant E, Piard JC, Juillard V. Only one of four oligopeptide transport systems mediates nitrogen nutrition in Staphylococcus aureus. *J Bacteriol*. *2007*;189(14):5119-29.

17. Vollmer W. Chapter 6 - Peptidoglycan. In: Tang Y-W, Sussman M, Liu D, Poxton I, Schwartzman J, editors. Molecular Medical Microbiology (Second Edition). Boston: *Academic Press*; 2015. p. 105-24.

18. Garai P, Chandra K, Chakravortty D. Bacterial peptide transporters: Messengers of nutrition to virulence. *Virulence*. *2017*;8(3):297-309.

19. Koatale PC, Welling MM, Ndlovu H, Kgatle M, Mdanda S, Mdlophane A, Okem A, Takyi-Williams J, Sathekge MM, Ebenhan T. Insights into Peptidoglycan-Targeting Radiotracers for Imaging Bacterial Infections: Updates, Challenges, and Future Perspectives. *ACS Infect Dis*. *2024*;10(2):270-86.

20. Kuru E, Radkov A, Meng X, Egan A, Alvarez L, Dowson A, Booher G, Breukink E, Roper DI, Cava F, Vollmer W, Brun Y, VanNieuwenhze MS. Mechanisms of Incorporation for D-Amino Acid Probes That Target Peptidoglycan Biosynthesis. *ACS Chem Biol*. *2019*;14(12):2745-56.

21. Radkov AD, Hsu Y-P, Booher G, VanNieuwenhze MS. Imaging Bacterial Cell Wall Biosynthesis. *Annu Rev Biochem*. *2018*;87:991-1014.

22. Neumann KD, Villanueva-Meyer JE, Mutch CA, Flavell RR, Blecha JE, Kwak T, Sriram R, VanBrocklin HF, Rosenberg OS, Ohliger MA, Wilson DM. Imaging Active Infection in vivo Using D-Amino Acid Derived PET Radiotracers. *Sci Rep*. *2017*;7(1):7903.

23. Mota F, Jain SK. Flagging Bacteria with Radiolabeled d-Amino Acids. *ACS Cent Sci*. *2020*;6(2):97-9.

24. Goodell EW. Recycling of murein by Escherichia coli. *J Bacteriol*. *1985*;163(1):305-10.

25. Olrichs NK, Aarsman MEG, Verheul J, Arnusch CJ, Martin NI, Hervé M, Vollmer W, de Kruijff B, Breukink E, den Blaauwen T. A novel in vivo cell-wall labeling approach sheds new light on peptidoglycan synthesis in Escherichia coli. *ChemBioChem*. *2011*;12(7):1124-33.

26. Ebenhan T, Chadwick N, Sathekge MM, Govender P, Govender T, Kruger HG, Marjanovic-Painter B, Zeevaart JR. Peptide synthesis, characterization and ^{68}Ga-radiolabeling of NOTA-conjugated ubiquicidin fragments for prospective infection imaging with PET/CT. *Nucl Med Biol*. *2014*;41(5):390-400.

27. Mokaleng BB, Ebenhan T, Ramesh S, Govender T, Kruger HG, Parboosing R, Hazari PP, Mishra AK, Marjanovic-Painter B, Zeevaart JR, Sathekge MM. Synthesis, 68Ga-radiolabeling,

and preliminary in vivo assessment of a depsipeptide-derived compound as a potential PET/CT infection imaging agent. *Biomed Res Int*. *2015*;2015:284354.

28. Lambidis E, Lumén D, Koskipahta E, Imlimthan S, Lopez BB, Sánchez AIF, Sarparanta M, Cheng RH, Airaksinen AJ. Synthesis and ex vivo biodistribution of two ^{68}Ga-labeled tetrazine tracers: Comparison of pharmacokinetics. *Nucl Med Biol*. *2022*;114-115:151-61.

29. Müller C, Farkas R, Borgna F, Schmid RM, Benešová M, Schibli R. Synthesis, Radiolabeling, and Characterization of Plasma Protein-Binding Ligands: Potential Tools for Modulation of the Pharmacokinetic Properties of (Radio)Pharmaceuticals. *Bioconjug Chem*. *2017*;28(9):2372-83.

30. Mandiwana V, Kalombo L, Lemmer Y, Labuschagne P, Semete-Makokotlela B, Sathekge M, Ebenhan T, Zeevaart JR. Preclinical assessment of ^{68}Ga-PSMA-617 entrapped in a microemulsion delivery system for applications in prostate cancer PET/CT imaging. *J Labelled Comp Radiopharm*. *2019*;62(7):332-45.

31. Ebenhan T, Schoeman I, Rossouw DD, Grobler A, Marjanovic-Painter B, Wagener J, Kruger HG, Sathekge MM, Zeevaart JR. Evaluation of a Flexible NOTA-RGD Kit Solution Using Gallium-68 from Different ^{68}Ge/^{68}Ga-Generators: Pharmacokinetics and Biodistribution in Nonhuman Primates and Demonstration of Solitary Pulmonary Nodule Imaging in Humans. *Mol Imaging Biol*. *2017*;19(3):469-82.

32. Suthiram J, Ebenhan T, Marjanovic-Painter B, Sathekge MM, Zeevaart JR. Towards Facile Radiolabeling and Preparation of Gallium-68-/Bismuth-213-DOTA-[Thi^{8}, Met$(O_2)^{11}$]-Substance P for Future Clinical Application: First Experiences. *Pharmaceutics*. *2021*;13(9):1326.

33. Mdlophane AH, Ebenhan T, Marjanovic-Painter B, Govender T, Sathekge MM, Zeevaart JR. Comparison of DOTA and NODAGA as chelates for ^{68}Ga-labelled CDP1 as novel infection PET imaging agents. *J Radioanal Nucl Chem*. *2019*;322(2):629-38.

34. Ebenhan T, Mokaleng BB, Venter JD, Kruger HG, Zeevaart JR, Sathekge M. Preclinical Assessment of a ^{68}Ga-DOTA-Functionalized Depsipeptide as a Radiodiagnostic Infection Imaging Agent. *Molecules*. *2017*;22(9):1403.

35. Kubíček V, Havlíčková J, Kotek J, Tircsó G, Hermann P, Tóth É, Lukeš I. Gallium(III) Complexes of DOTA and DOTA−Monoamide: Kinetic and Thermodynamic Studies. *Inorg Chem*. *2010*;49(23):10960-9.

36. Clarke ET, Martell AE. Stabilities of trivalent metal ion complexes of the tetraacetate derivatives of 12-, 13- and 14-membered tetraazamacrocycles. *Inorganica Chim Acta*. *1991*;190(1):37-46.

37. Zeglis BM, Lewis JS. A practical guide to the construction of radiometallated bioconjugates for positron emission tomography. *Dalton Trans*. *2011*;40(23):6168-95.

38. Velikyan I. Prospective of ^{68}Ga-radiopharmaceutical development. *Theranostics*. *2013*;4(1):47-80.

39. Tsionou MI, Knapp CE, Foley CA, Munteanu CR, Cakebread A, Imberti C, Eykyn TR, Young JD, Paterson BM, Blower PJ. Comparison of macrocyclic and acyclic chelators for gallium-68 radiolabelling. *RSC Adv*. *2017*;7(78):49586-99.

40. Sosabowski JK, Mather SJ. Conjugation of DOTA-like chelating agents to peptides and radiolabeling with trivalent metallic isotopes. *Nat Protoc*. *2006*;1(2):972-6.

41. Brom M, Franssen GM, Joosten L, Gotthardt M, Boerman OC. The effect of purification of Ga-68-labeled exendin on in vivo distribution. *EJNMMI Res*. *2016*;6(1):65.

42. Decristoforo C, Knopp R, von Guggenberg E, Rupprich M, Dreger T, Hess A, Virgolini I, Haubner R. A fully automated synthesis for the preparation of 68Ga-labelled peptides. *Nucl Med Commun*. *2007*;28(11):870-5.

43. Alhankawi AR, Al-Husseini JK, Spindler A, Baker C, Shoniwa TT, Ahmed M, Chiarelli PA, Johal MS. The Relationship between Hydrophobicity and Drug-Protein Binding in Human Serum Albumin: A Quartz Crystal Microbalance Study. *Biophysica*. *2022*;2(2):113-20.

44. Lever SZ, Fan KH, Lever JR. Tactics for preclinical validation of receptor-binding radiotracers. *Nucl Med Biol*. *2017*;44:4-30.

45. Coulson CJ, Smith VJ. Correlation of hydrophobicity with protein binding for clorobiocin analogs. *J Pharm Sci*. *1980*;69(7):799-801.

46. Autio A, Virtanen H, Tolvanen T, Liljenbäck H, Oikonen V, Saanijoki T, Siitonen R, Käkelä M, Schüssele A, Teräs M, Roivainen A. Absorption, distribution and excretion of intravenously injected 68Ge/68Ga generator eluate in healthy rats, and estimation of human radiation dosimetry. *EJNMMI Research*. *2015*;5(1):40.

47. Hacht B. Gallium (III) ion hydrolysis under physiological conditions. *Bulletin-Korean Chemical Society*. *2008*;29(2):372.

48. Hsu Y-P, Rittichier J, Kuru E, Yablonowski J, Pasciak E, Tekkam S, Hall E, Murphy B, Lee TK, Garner EC, Huang KC, Brun Yves V, VanNieuwenhze MS. Full color palette of fluorescent d-amino acids for in situ labeling of bacterial cell walls. *Chem Sci*. *2017*;8(9):6313-21.

49. Welling MM, de Korne CM, Spa SJ, van Willigen DM, Hensbergen AW, Bunschoten A, Duszenko N, Smits WK, Roestenberg M, van Leeuwen FWB. Multimodal Tracking of Controlled Staphylococcus aureus Infections in Mice. *ACS Infect Dis*. *2019*;5(7):1160-8.

50. Stewart MN, Parker MFL, Jivan S, Luu JM, Huynh TL, Schulte B, Seo Y, Blecha JE, Villanueva-Meyer JE, Flavell RR, VanBrocklin HF, Ohliger MA, Rosenberg O, Wilson DM. High Enantiomeric Excess In-Loop Synthesis of d-[methyl-^{11}C]Methionine for Use as a Diagnostic Positron Emission Tomography Radiotracer in Bacterial Infection. *ACS Infect Dis*. *2020*;6(1):43-9.

51. Parker MFL, Luu JM, Schulte B, Huynh TL, Stewart MN, Sriram R, Yu MA, Jivan S, Turnbaugh PJ, Flavell RR, Rosenberg OS, Ohliger MA, Wilson DM. Sensing Living Bacteria in Vivo Using d-Alanine-Derived ^{11}C Radiotracers. *ACS Cent Sci*. *2020*;6(2):155-65.

52. Renick PJ, Mulgaonkar A, Co CM, Wu C-Y, Zhou N, Velazquez A, Pennington J, Sherwood A, Dong H, Castellino L, Öz OK, Tang L, Sun X. Imaging of Actively Proliferating Bacterial Infections by Targeting the Bacterial Metabolic Footprint with d-[5-^{11}C]-Glutamine. *ACS Infect Dis*. *2021*;7(2):347-61.

53. Oyen WJG, Boerman OC, Corstens FHM. Animal models of infection and inflammation and their role in experimental nuclear medicine. *J Microbiol Methods*. *2001*;47(2):151-7.

54. Taddonio TE, Thomson PD, Tait MJ, Prasad JK, Feller I. Rapid quantification of bacterial and fungal growth in burn wounds: biopsy homogenate Gram stain versus microbial culture results. *Burns Incl Therm Inj*. *1988*;14(3):180-4.

CHAPTER 5GENERAL DISCUSSION AND FUTURE PERSPECTIVE

Bacteria have demonstrated capabilities to recycle and metabolically incorporate exogenous precursors for peptidoglycan synthesis. Interestingly, most peptidoglycan-based radioactive precursors reported (as reviewed in **Chapter 2**) performed remarkably in differentiating between infection and inflammation using PET/CT. However, whether they can be useful in a clinical setting remains ambiguous. Therefore **Chapter 3** comprises of the required systematic analyses to assess diagnostic accuracy, and clinical impact of developed radioactive peptidoglycan-based precursors that are of interest for infection imaging. A QUADAS analysis revealed that despite the marked potential in infection imaging, high background signal reported with most radiotracers remains a concern and may affect an efficient translation to routine clinical applications because of the risk for false-positive outcomes. As a result, the continuation to explore peptidoglycan as a promising cellular target of interest for optimal specificity and selectivity is justified. Therefore, developing and validating new radiotracers for more specific imaging of infection is a common goal to improve diagnosis and health care in patients. Recently, a comprehensive review was published including consensus results, expert opinion and recommendations regarding the current research standards aiming to improve radiotracers for infection imaging [1, 2]. Based on the inputs, several factors must be considered when developing radioactive probes for specific targeting, including the feasibility of synthesizing a precursor and/or its analogs, radiosynthesis strategy, and *in vitro* and *in vivo* validation strategy [3].

5.1 PRECURSOR DESIGN AND RADIOLABELING STRATEGY

The variety and types of targets presented on the bacterial cell envelope are often unique and therefore vastly different form those expressed in mammalian cells. This uniqueness is often

exploited in the development of antibiotics and other therapeutic agents, as targeting these bacterial-specific structures can help minimize harm to mammalian cells [4] . Tracking the peptidoglycan biosynthesis for bacterial targeting requires periplasmic or intracellular metabolism of precursors of interest by a series of enzymes for incorporation into the cell wall [5]. Therefore, structural changes such as choice of modification site, molecular size, conjugation of radioisotopes, linker length or geometry may affect the metabolic pathway and level of compound incorporation [6, 7].

Goodell [5] and co-workers, used L-Ala-γ-D-Glu-meso-[^{3}H]A2pm to decode the peptidoglycan recycling pathway. Using a similar approach, Olrichs et al. [8], fluorescently labeled the peptidoglycan using L-Ala-γ-D-Glu-L-Lys-NBD (AeK-NDB). The study further demonstrated that the replacement of m-DAP with L-lysine at the 3rd position of the tripeptide did not limit intracellular uptake of AeK-NBD necessary for metabolic incorporation into the peptidoglycan. This presented as an attractive approach for infection imaging using PET/CT, reported herewith for the first time. The radiometal-isotope Ga-68 which requires stable complexation; bifunctional chelators such as DOTA and NOTA directly conjugated with AeK to combine an ease of ^{68}Ga-activity production (daily supply via a radioisotope generator) with the optimal chemical and physical properties of DOTA [3, 9, 10]. In particular **Chapter 4** addresses the research required to develop a radiobeling and purification strategy for [^{68}Ga]Ga-DOTA-AeK as a potential radiotracer for bacterial infection imaging. Although the radiotracer demonstrated the required RCP ≥95% and physiochemical properties for an ideal radiotracer, bacterial uptake was negligible in both *in vitro* and *in vivo* investigations. As previously demonstrated, the intracellular uptake of AeK is required for ultimate metabolic integration into the peptidoglycan structure [5, 8]. Therefore, the lack of bacterial uptake seen with [^{68}Ga]Ga-DOTA-AeK (733 g/mol) *versus* AeK-NBD (509 g/mol) may be attributed to structural modifications with the bulkier DOTA chelator, and therefore hindering active transportation across the membrane.

Based on these findings, an ideal radiolabeling strategy in peptidoglycan biosynthesis targeting should preserve both the chemical structure and targeting moiety of the precursor [11]. In this case, direct labeling using radioisotopes with non-metallic radioisotopes, including ^{11}C and ^{18}F is recommended as it has shown minimal influence on metabolic uptake and incorporating the peptidoglycan-based precursors [12-14]. Consequently, these short-lived, radioisotopes can present challenges during radiosynthesis, including the use of harsh labeling conditions, which often result in unwanted by-products and compromise the stability of the precursor. Therefore,

the use of 'click' chemistry using different prosthetic groups may be an alternate radiosynthesis approach, especially applicable to ^{18}F or ^{123}I, however, this remained almost unexplored in comparison to ^{11}C [12, 15-17].

This procedure involves a two-step labeling strategy which requires pre-targeting of the peptidoglycan using endocyclic nitrone, alkyne, or azide-modified D-amino acids derivatives followed by subsequent visualization with a complementary fluorescent reporter using biorthogonal reactions [18, 19]. And is a promising approach for *in vivo* pre-targeting of infections and has been well demonstrated with optical imaging [20].

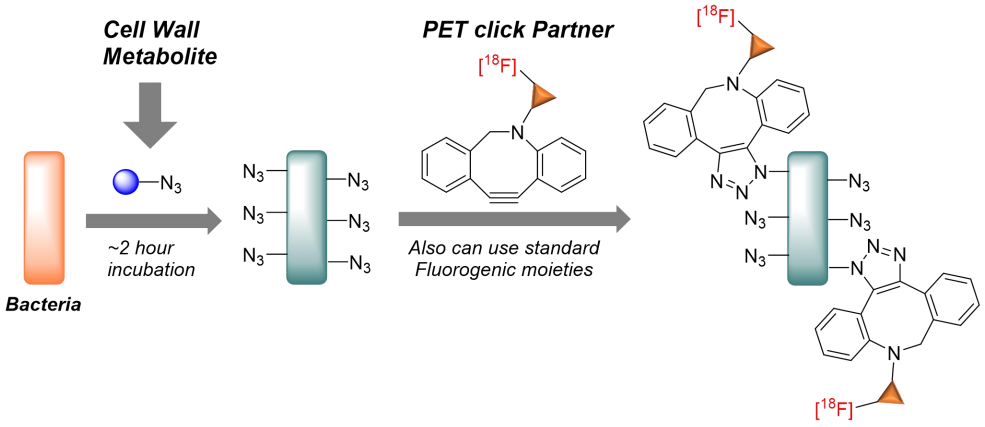

Figure 5-1: Click chemistry for pre-targeting radiolabeling approach of bacteria using D-azido-alanine (cell wall metabolite) followed [^{18}F]-cyclooctyne (PET 'click' partner). Reproduced with permission from Alanizi [21]. Copyright, Alanizi, 2021.

Interestingly, the Wilson group pioneered using ^{18}F-labeled click chemistry using the peptidoglycan-based targeting azide-modified D-alanine derivative for the first time (**Figure 6-1**). This promising metabolic targeting approach has set a footprint for applying click chemistry in PET imaging of infection [21] and beyond.

It is worth mentioning that the lengthy and complex chemical and chemo-enzymatic procedures during the synthesis of peptidoglycan-based precursors leave only little room for structural manipulations [22-24]. A plausible solution to mitigate these challenges and fast-track the development process requires the use of computational tools such as docking and high-throughput screening to create chemical libraries with diverse molecular adaptations that will predict how structural, chemical, physical, and physicochemical properties of molecules can alter the net cellular uptake through interaction with target enzymes and the pharmacokinetic profiling [7, 10, 25-27].

5.2 *IN VITRO* TESTING

Further testing of candidate radiotracers should be carried out to investigate the effect of precursor modifications and radioisotope on pharmacokinetics and cell wall incorporation. *In vitro,* bacterial uptake studies using the live bacteria cultures *versus* their heat-inactivated cultures were used as a standard approach in the current study and for several of the reviewed peptidoglycan precursors. However, uptake does not necessarily prove binding selectivity and accurate representation of the peptidoglycan biosynthesis' status. Therefore, competition studies with an unlabeled compound are required as the standard test in most *in vitro* studies [20]. The latter might not be sensitive enough to elucidate the proposed mechanism of integration since bacteria can use most precursors, including the D-amino acids and glycan's, as building blocks in other structures (proteins, lipopolysaccharides, teichoic acids, and nucleic acids) or as a source of energy [28, 29]. Therefore, using radioisotopes with a long half-life, i.e., ^{3}H or ^{14}C can be very beneficial for the *in vitro* evaluation of various precursors with different structural modifications. This setting will require the integration of advanced techniques with high sensitivity such as polyacrylamide high-pressure liquid chromatography (HPLC), polyacrylamide gel electrophoresis, autoradiography, mass spectrometry, and nuclear magnetic resonance (NMR) [24, 30-33]. Once potential derivatives specific to the peptidoglycan metabolism have been identified, they should be further tailored towards the conditions required for ^{18}F- or ^{11}C-radiosynthesis, followed by *in vitro* uptake - also using mutated bacterial strains with altered enzyme expression that are involved in the metabolic process of interest (as negative controls). This can be achieved through genetic manipulation or targeted peptidoglycan inhibitors, such as antibiotics [20, 34, 35]. In addition, for specific *in vitro* tests, the radioactive compounds should

also be evaluated using planktonic bacterial cultures, as in the clinical setting, persistent or treatment-resistant bacteria are often re-associated within biofilms. This will improve the likeliness of translating results from pre-clinical evaluations further into the clinics [36].

5.3 *IN VIVO* EVALUATION

Imaging complex infectious processes and discriminating them from sterile inflammation is still a challenge in diagnostic imaging [1]. Our results demonstrate significantly higher distribution of [68Ga]Ga-DOTA-AeK with the site of sterile muscular inflammation in comparison to the infectious foci ($p \leq 0.05$); however, as to whether this finding can limit the specificity of AeK as a potential infection radiotracer needs to be further explored. The presence of bacterial strains could not be confirmed using tissue histopathology despite the signs of inflammatory markers indicative of infection. This inconsistency could be due to several factors, including the use of non-pathogenic bacterial strains, low number of colonies inoculated, immunocompetent mice, or beyond the 24-hr imaging time point chosen post-infection. In addition, absence of viable bacteria confirmed using both histopathology and microbiology analyses was mainly to attributed to the division of the abscess tissue and heterogeneous bacterial distribution in a previous study [37]. To mitigate the problem, all the tissue samples of animals that underwent PET imaging were analysed by microbiological culture, which was a limitation in the current study.

The variability in the choice of animal model and study design has been observed across different studies, which might pose a challenge to data interpretation and reproducibility. Therefore, to successfully provide valid preclinical data for clinical translation, the animal model should be standardized and ideally reflect the same pathogenesis patterns as the infectious disease in humans. Thus, further harmonizing the design and animal study requirements is recommended [38, 39]. In addition, it should be considered that targeting bacteria with low metabolic activity will probably not render sufficient tracer ‘load’ to allow for its visualization. Therefore, the correct window to employ imaging to detect or monitor infection should be explored [40]. Of note, antibiotics can also drastically interfere with bacterial cell wall synthesis and hamper the uptake of these tracers. Inherently challenging will be detecting infections

caused by targeting intracellular bacteria such as *Mycobacterium tuberculosis, Salmonella typhimurium, Listeria monocytogenes*, and *Legionella pneumophila* [41].

5.4 CONCLUSION AND FUTURE DIRECTIONS

Enzymatic studies and functional fluorescence-based imaging have shed a bright light on peptidoglycan biosynthesis and led to innovative translation of peptidoglycan-based drugs or precursors for molecular imaging. However, despite the constant novelty of fluorescence imaging, research efforts into developing and translating radiolabeled peptidoglycan precursors remains a major undertaking with several limitations. The latter hinges on complex chemical procedures involved in synthesizing molecules of interest, which can restrict radiotracer design and its adaptation with various modifications. Given the strict peptidoglycan assembly processes which is the target for possible incorporation, the described precursors, including the herein studied AeK tripeptide, may be limited to radiochemistry involving covalent ^{18}F- or ^{11}C-substitution only, i.e., radioactive tagging with short-lived isotopes that requires complex chemistry and a cyclotron. As a result, due to progressive limitations and the complexity of the involved infrastructure, most research laboratories, may have slowed down investigations into furthering development and subsequent clinical translation of such radiotracers for nuclear imaging of bacterial infections. Therefore, strategies to address these challenges should include technological innovation in molecular biology, organic chemistry, and radiochemistry, which can be fostered through solid collaboration and advocating multidisciplinary research.

5.5 REFERENCES

1. Signore A, Artiko V, Conserva M, Ferro-Flores G, Welling MM, Jain SK, Hess S, Sathekge M. Imaging Bacteria with Radiolabelled Probes: Is It Feasible? Journal of Clinical Medicine. 2020;9(8):2372.

2. Alberto S, Ordonez AA, Arjun C, Aulakh GK, Beziere N, Dadachova E, Ebenhan T, Granados U, Korde A, Amirreza J, Lestari W, Mukherjee A, Petrik M, Sakr T, Cuevas CLS, Welling MM, Zeevaart JR, Jain SK, Wilson DM. The Development and Validation of Radiopharmaceuticals Targeting Bacterial Infection. Journal of nuclear medicine. 2023:jnumed.123.265906.

3. Fani M, Maecke HR. Radiopharmaceutical development of radiolabelled peptides. European journal of nuclear medicine and molecular imaging. 2012;39(1):11-30.

4. Miethke M, Pieroni M, Weber T, Brönstrup M, Hammann P, Halby L, Arimondo PB, Glaser P, Aigle B, Bode HB, Moreira R, Li Y, Luzhetskyy A, Medema MH, Pernodet J-L, Stadler M, Tormo JR, Genilloud O, Truman AW, Weissman KJ, Takano E, Sabatini S, Stegmann E, Brötz-Oesterhelt H, Wohlleben W, Seemann M, Empting M, Hirsch AKH, Loretz B, Lehr C-M, Titz A, Herrmann J, Jaeger T, Alt S, Hesterkamp T, Winterhalter M, Schiefer A, Pfarr K, Hoerauf A, Graz H, Graz M, Lindvall M, Ramurthy S, Karlén A, van Dongen M, Petkovic H, Keller A, Peyrane F, Donadio S, Fraisse L, Piddock LJV, Gilbert IH, Moser HE, Müller R. Towards the sustainable discovery and development of new antibiotics. Nature Reviews Chemistry. 2021;5(10):726-49.

5. Goodell EW. Recycling of murein by Escherichia coli. Journal of Bacteriology. 1985;163(1):305-10.

6. Fura JM, Kearns D, Pires MM. D-Amino Acid Probes for Penicillin Binding Protein-based Bacterial Surface Labeling. J Biol Chem. 2015;290(51):30540-50.

7. Chaturvedi S, Mishra AK. Small Molecule Radiopharmaceuticals – A Review of Current Approaches. Frontiers in Medicine. 2016;3.

8. Olrichs NK, Aarsman MEG, Verheul J, Arnusch CJ, Martin NI, Hervé M, Vollmer W, de Kruijff B, Breukink E, den Blaauwen T. A novel in vivo cell-wall labeling approach sheds new light on peptidoglycan synthesis in Escherichia coli. ChemBioChem. 2011;12(7):1124-33.

9. Pekošak A, Filp U, Poot AJ, Windhorst AD. From Carbon-11-Labeled Amino Acids to Peptides in Positron Emission Tomography: the Synthesis and Clinical Application. Molecular imaging and biology. 2018;20(4):510-32.

10. Charron C, Hickey J, Nsiama T, Cruickshank D, Turnbull W, Luyt L. Molecular imaging probes derived from natural peptides. Natural product reports. 2016;33(6):761-800.

11. Pekošak A, Rotstein BH, Collier TL, Windhorst AD, Vasdev N, Poot AJ. Stereoselective 11C Labeling of a “Native” Tetrapeptide by Using Asymmetric Phase-Transfer Catalyzed Alkylation Reactions. European Journal of Organic Chemistry. 2017;2017(5):1019-24.

12. Ermert J, Coenen HH. Methods for 11C- and 18F-labelling of amino acids and derivatives for positron emission tomography imaging. Journal of Labelled Compounds and Radiopharmaceuticals. 2013;56(3-4):225-36.

13. Kwak TS. Evaluation of D-Amino Acids as Probes for Molecular Imaging of Bacterial Infections [Msc Thesis]: University of California, San Francisco; 2015.

14. Filp U, Pekošak A, Poot AJ, Windhorst AD. Stereocontrolled [11C]Alkylation of N-Terminal Glycine Schiff Bases To Obtain Dipeptides. European Journal of Organic Chemistry. 2017;2017(37):5592-6.

15. Walsh JC, Kolb HC. Applications of click chemistry in radiopharmaceutical development. Chimia. 2010;64(1-2):29-.

16. Wangler C, Schirrmacher R, Bartenstein P, Wangler B. Click-chemistry reactions in radiopharmaceutical chemistry: fast & easy introduction of radiolabels into biomolecules for in vivo imaging. Current medicinal chemistry. 2010;17(11):1092-116.

17. Bauer D, Sarrett SM, Lewis JS, Zeglis BM. Click chemistry: a transformative technology in nuclear medicine. Nature protocols. 2023.

18. MacKenzie DA, Sherratt AR, Chigrinova M, Kell AJ, Pezacki JP. Bioorthogonal labelling of living bacteria using unnatural amino acids containing nitrones and a nitrone derivative of vancomycin. Chemical Communications. 2015;51(62):12501-4.

19. Siegrist MS, Whiteside S, Jewett JC, Aditham A, Cava F, Bertozzi CR. d-Amino Acid Chemical Reporters Reveal Peptidoglycan Dynamics of an Intracellular Pathogen. ACS Chemical Biology. 2013;8(3):500-5.

20. Banahene N, Kavunja HW, Swarts BM. Chemical Reporters for Bacterial Glycans: Development and Applications. Chemical Reviews. 2022;122(3):3336-413.

21. Alanizi A. Targeting Peptidoglycan using Radiolabeled Click Chemistry for PET Infection Imaging [Msc Thesis]. San Francisco: University of California; 2021.

22. Dumbre S, Derouaux A, Lescrinier E, Piette A, Joris B, Terrak M, Herdewijn P. Synthesis of Modified Peptidoglycan Precursor Analogues for the Inhibition of Glycosyltransferase. Journal of the American Chemical Society. 2012;134(22):9343-51.

23. Higashi Y, Strominger JL, Sweeley CC. Structure of a lipid intermediate in cell wall peptidoglycan synthesis: a derivative of a C55 isoprenoid alcohol. Proceedings of the National Academy of Sciences. 1967;57(6):1878-84.

24. Gale RT, Brown ED. New chemical tools to probe cell wall biosynthesis in bacteria. Current Opinion in Microbiology. 2015;27:69-77.

25. Emine Selin D, Emre O, Meliha E, Evren Atlihan G, Derya İlem Ö, Makbule A. Computational Study of Radiopharmaceuticals. In: Amalia S, editor. Molecular Docking and Molecular Dynamics. London: IntechOpen; 2019. p. 79.

421 26. Kilbourn MR. Targeted Diagnostic Radiopharmaceuticals: Design Options for Small-
422 Molecule Radiotracers. In: Peter Scott MK, editor. Handbook of Radiopharmaceuticals. 2nd
423 ed2020. p. 1-21.

424 27. Ataeinia B, Heidari P. Artificial Intelligence and the Future of Diagnostic and
425 Therapeutic Radiopharmaceutical Development:: In Silico Smart Molecular Design. PET Clin.
426 2021;16(4):513-23.

427 28. Aliashkevich A, Alvarez L, Cava F. New Insights Into the Mechanisms and Biological
428 Roles of D-Amino Acids in Complex Eco-Systems. Frontiers in Microbiology. 2018;9.

429 29. Bonnet M, Lagier JC, Raoult D, Khelaifia S. Bacterial culture through selective and non-
430 selective conditions: the evolution of culture media in clinical microbiology. New microbes and
431 new infections. 2020;34:100622.

432 30. Brown AR, Gordon RA, Hyland SN, Siegrist MS, Grimes CL. Chemical Biology Tools
433 for Examining the Bacterial Cell Wall. Cell Chem Biol. 2020;27(8):1052-62.

434 31. Romaniuk JAH, Cegelski L. Bacterial cell wall composition and the influence of
435 antibiotics by cell-wall and whole-cell NMR. Philosophical Transactions of the Royal Society B:
436 Biological Sciences. 2015;370(1679):20150024.

437 32. Schaefer K, Owens TW, Kahne D, Walker S. Substrate preferences establish the order of
438 cell wall assembly in Staphylococcus aureus. Journal of the American Chemical Society.
439 2018;140(7):2442-5.

440 33. Born P, Breukink E, Vollmer W. In Vitro Synthesis of Cross-linked Murein and Its
441 Attachment to Sacculi by PBP1A from Escherichia coli. Journal of Biological Chemistry.
442 2006;281(37):26985-93.

443 34. Kuru E, Radkov A, Meng X, Egan A, Alvarez L, Dowson A, Booher G, Breukink E,
444 Roper DI, Cava F, Vollmer W, Brun Y, VanNieuwenhze MS. Mechanisms of Incorporation for
445 D-Amino Acid Probes That Target Peptidoglycan Biosynthesis. ACS Chemical Biology.
446 2019;14(12):2745-56.

447 35. Barreteau H, Kovač A, Boniface A, Sova M, Gobec S, Blanot D. Cytoplasmic steps of
448 peptidoglycan biosynthesis. FEMS Microbiology reviews. 2008;32(2):168-207.

449 36. Welling MM, Warbroek K, Khurshid C, van Oosterom MN, Rietbergen DDD, de Boer
450 MGJ, Nelissen R, van Leeuwen FWB, Pijls BG, Buckle T. A radio- and fluorescently labelled
451 tracer for imaging and quantification of bacterial infection on orthopaedic prostheses : a proof of
452 principle study. Bone Joint Research. 2023;12(1):72-9.

453 37. Nielsen KM, Jørgensen NP, Kyneb MH, Borghammer P, Meyer RL, Thomsen TR,
454 Bender D, Jensen SB, Nielsen OL, Alstrup AKO. Preclinical evaluation of potential infection-
455 imaging probe [68Ga]Ga-DOTA-K-A9 in sterile and infectious inflammation. Journal of
456 Labelled Compounds and Radiopharmaceuticals. 2018;61(10):780-95.

457 38. Alstrup AKO, Jensen SB, Nielsen OL, Jødal L, Afzelius P. Preclinical Testing of
458 Radiopharmaceuticals for the Detection and Characterization of Osteomyelitis: Experiences from
459 a Porcine Model. Molecules. 2021;26(14):4221.

460 39. Chen X, Gallagher F, Sellmyer MA, Ordonez AA, Kjaer A, Ohliger M, Wilson DM, Jain
461 SK. Visualizing Bacterial Infections With Novel Targeted Molecular Imaging Approaches. The
462 Journal of Infectious Diseases. 2023;228(Supplement_4):S249-S58.

463 40. Muranaka Y, Matsue M, Mizutani A, Kobayashi M, Sato K, Kondo A, Nishiyama Y,
464 Ohata S, Nishi K, Yamazaki K, Nishii R, Shikano N, Okamoto S, Kawai K. Evaluation of L-
465 Alanine Metabolism in Bacteria and Whole-Body Distribution with Bacterial Infection Model
466 Mice. International journal of molecular sciences. 2023;24(5):4775.

467 41. Thakur A, Mikkelsen H, Jungersen G. Intracellular Pathogens: Host Immunity and
468 Microbial Persistence Strategies. Journal of Immunology Research. 2019;2019:1356540.

469

470

ANNEXURE A: LIST OF PUBLICATIONS

Koatale, P.C; Welling, M.M.; Mdanda, S.; Mdlophane, A.; Takyi-Williams, J.; Durandt, C.; van den Bout, I.; Cleeren, F.; Sathekge, M.M.; Ebenhan, T. Evaluation of [^{68}Ga]Ga-DOTA-AeK as a Potential Imaging Tool for PET Imaging of Cell Wall Synthesis in Bacterial Infections. *Pharmaceuticals* 2024, *17*, 1150. https://doi.org/10.3390/ph17091150

Koatale PC, Welling MM, Ndlovu H, Kgatle M, Mdanda S, Mdlophane A, Okem A, Takyi-Williams J, Sathekge MM, Ebenhan T. Insights into Peptidoglycan-Targeting Radiotracers for Imaging Bacterial Infections: Updates, Challenges, and Future Perspectives. ACS Infect Dis. 2024 Feb 9;10(2):270-286. doi: 10.1021/acsinfecdis.3c00443.

Kgatle MM, Lawal IO, Mashabela G, Boshomane TMG, **Koatale PC**, Mahasha PW, Ndlovu H, Vorster M, Rodrigues HG, Zeevaart JR, Gordon S, Moura-Alves P, Sathekge MM. COVID-19 Is a Multi-Organ Aggressor: Epigenetic and Clinical Marks. Front Immunol. 2021 Oct 8;12:752380. doi: 10.3389/fimmu.2021.752380.

ANNEXURE B: UNIVERSITY OF PRETORIA HEALTH SCIENCE RESEARCH ETHICS APPROVAL

UNIVERSITEIT VAN PRETORIA
UNIVERSITY OF PRETORIA
YUNIBESITHI YA PRETORIA

Faculty of Veterinary Science
Animal Ethics Committee

12 July 2024

Approval Certificate
Amendment 2

AEC Reference No.: 435/2020 Line 3

Title: Developing PET Infection Imaging Agent for Visualizing Bacterial Peptidoglycan Assembly

Researcher: Ms PC Koatale

Student's Supervisor: Prof MM Sathekge

Dr T Ebenhan

Dear Ms PC Koatale,

The **Amendment** as supported by documents received between 2024-06-14 and 2024-07-09 for your research, was approved by the Animal Ethics Committee on its quorate meeting of 2024-07-09.

Please note the following about your ethics approval:

1. The change of the title is approved:

   New Title: Developing PET Infection Imaging Agent for Visualizing Bacterial Peptidoglycan Assembly

   Methodology change (There are challenges with the sourcing and the synthesis of Mycobactin T (MBT) compound. As a results, no work has been done to date on [68Ga]Ga –MBT and the protocol was amended to exclude work related to MBT compound.)

Room 6-13, Arnold Theiler Building, Onderstepoort
Private Bag X04, Onderstepoort 0110, South Africa
Tel +27 12 529 8434
Fax +27 12 529 8321
Email: marleze.rheeder@up.ac.za

2. Please note that the approved date(s) from the original application certificate / annual renewal certificate will be applicable to this amendment.

3. Please remember to use your protocol number (435/2020) on any documents or correspondence with the AEC regarding your research.

4. Please note that the AEC may ask further questions, seek additional information, require further modification, monitor the conduct of your research, or suspend or withdraw ethics approval.

5. **All incidents** must be reported by the PI by email to Ms Marleze Rheeder (AEC Coordinator) within 3 days, and must be subsequently submitted electronically on the application system within 14 days.

6. The committee also requests that you record major procedures undertaken during your study for own- archiving, using any available digital recording system that captures in adequate quality, as it may be required if the committee needs to evaluate a complaint. However, if the committee has monitored the procedure previously or if it is generally can be considered routine, such recording will not be required.

Ethics approval is subject to the following:

- The ethics approval is conditional on the research being conducted as stipulated by the details of all documents submitted to the Committee. In the event that a further need arises to change who the investigators are, the methods or any other aspect, such changes must be submitted as an Amendment for approval by the Committee.

We wish you the best with your research. Yours sincerely

CHAIRMAN: UP-Animal Ethics Committee

Room 6-13, Arnold Theiler Building, Onderstepoort
Private Bag X04, Onderstepoort 0110, South Africa
Tel +27 12 529 8434
Fax +27 12 529 8321
Email: marleze.rheeder@up.ac.za